Lawrence Berkeley Laboratory
UNIVERSITY OF CALIFORNIA

Materials & Molecular Research Division

DESIGN OF DUAL PHASE Fe/Mn/C STEEL FOR LOW TEMPERATURE APPLICATION

Nack-Joon Kim
(Ph.D. thesis)

September 1981

Prepared for the U.S. Department of Energy under Contract W-7405-ENG-48

DISCLAIMER

DESIGN OF DUAL PHASE Fe/Mn/C STEEL FOR LOW TEMPERATURE APPLICATION

by

Nack-Joon Kim

(Ph.D. Thesis)

September 1981

Department of Materials Science and Mineral Engineering

Materials and Molecular Research Division

Lawrence Berkeley Laboratory

University of California

Berkeley, CA 94720

This work was supported by the Director, Office of Energy Research, Office of Basic Energy Sciences, Division of Materials Sciences of the U.S. Department of Energy under Contract No. DE-AC03-76SF00098.

Design of Dual Phase Fe/Mn/C Steel for Low Temperature Application

Nack-Joon Kim

Ph.D. Materials Science &

Sponsor: U.S. Department of Energy Mineral Engineering

Gareth Thomas
Chairman of Committee

ABSTRACT

An investigation has been made to improve the impact properties of a dual phase Fe/1.5Mn/.06C steel for potential low temperature application. The research involved establishing the microstructure-property relationships, especially with regard to the morphology of the constituents. Dual phase processing was done in two ways, viz., controlled rolling and intercritical annealing of the as-hot-rolled structure.

Controlled rolling of a Fe/1.5Mn/.06C alloy produced a microstructure which consists mainly of ferrite and upper bainite. The microstructure and mechanical properties of this as-hot-rolled ferritic-bainitic structure were strongly influenced by the processing variables. There was a simultaneous improvement in tensile and impact properties with a decrease in the finish rolling temperature and an increase in the amount of deformation. This was due to refinement of the ferrite grain size.

The as-hot-rolled ferritic-bainitic structure has superior impact properties to the intercritically annealed ferritic-martensitic structure when compared at the same tensile strength level. The superiority of the

former is attributed to its favorable morphology in that the relatively coarse second phase is uniformly dispersed within fine ferrite grains. This research also showed that the initial structure of the alloy before intercritical annealing had a strong influence on the impact properties of the ferritic-martensitic structure. The dual phase structure developed from the martensitic-bainitic structure had a higher transition temperature than that developed from the ferritic-bainitic structure, while they showed similar tensile properties. This behavior was due to the difference in the "effective grain size", which was the prior austenite grain size in the former, and the ferrite grain size in the latter. Changing the volume fraction of martensite does not affect the transition temperature of this dual phase steel.

The mechanical properties attained in the as-hot-rolled ferritic-bainitic steel were shown to be quite attractive for low temperature line pipe application. The properties already exceed those specified for Arctic line pipe in the as-hot-rolled state. Moreover, pipe forming causes a large increase in yield strength with only a small increase in transition temperature.

DESIGN OF DUAL PHASE Fe/Mn/C STEEL FOR LOW TEMPERATURE APPLICATION

Table of Contents

I. INTRODUCTION

The simultaneous attainment of high strength, ductility and toughness is one of the perpetual aims of physical metallurgists. In the past twenty years, man's ever increasing demands for energy conservation stimulated extensive research efforts to produce high strength steels in grades covering both structural and automotive applications, e.g., cost-effective steels for pipelines and power plants to produce energy, and optimized steel for energy efficient transportation systems, etc. The basic difficulty was that these properties are to a large extent incompatible in steels having conventional microstructures.

The introduction of so-called dual phase steels[1,2,3] sparked a tremendous amount of research activity throughout the world in the past decade because of their characteristic mechanical properties. These dual phase steels consist mainly of ferrite and martensite with small amounts of retained austenite and/or bainite depending on alloy content and processing. Compared with conventional high strength low alloy (HSLA) steels, the incorporation of the strong second phase of martensite in the soft ferrite matrix results in a composite which has highly desirable tensile properties, such as continuous yielding from a low yield strength, high initial strain hardening rates and excellent combinations of ultimate tensile strength and ductility. Such characteristics have led dual phase steels to be regarded as an attractive material for the automotive industry which requires lighter weight vehicles for improved gas mileage. Hence, research on dual phase steels have been mainly concentrated on their stress-strain behavior[4,5,6] to exploit new alloy chemistry and processing techniques for optimum

combinations of strength and ductility, while the other important mechanical property such as impact toughness has not been well characterized. It has been shown that the morphology (size, shape, distribution) of the constituents has a great effect on the tensile fracture behavior and the ductility of dual phase steels.[7,8] The strength increases and the ductility decreases with an increase in the volume fraction of the second phase.[3,7,9-14] Exceptions[15-17] occur when fine precipitates are present in the ferrite matrix.

Although dual phase steels are progressively replacing conventional high strength low alloy (HSLA) steels in the automotive industry, their potential for structural applications was not considered. The conventional ferritic-pearlitic HSLA steels for structural applications obtain their strength mainly from the fine alloy precipitates which have adverse effects on the toughness.[19,20] Also, there is a loss in strength during shape forming because of the discontinuous yielding behavior and Bauschinger effect.[21-26] In fact, the stress-strain characteristics of dual phase steels (continuous yielding, high initial work hardening rate, and excellent combinations of strength and ductility) are also of great merit for other structural applications such as pressure vessels and pipelines which also need high strength, high ductility and low cost in addition to a low ductile-brittle transition temperature and a high resistance to low energy ductile fracture. The main drawback to their structural application might be, from the observation of initial research, that although dual phase steels have excellent combinations of strength and ductility, they have rather disappointingly poor impact

properties. However, little research was done specifically on the impact properties of dual phase steels.[27,28] Koo[27] pointed out that the impact energy of dual phase steels are largely influenced by the connectivity, carbon concentration, and volume fraction of martensite, but the origin of their brittleness has been given little attention.

The current research was, therefore, designed to increase the understanding of the role of microstructural factors which have a significant influence on the impact properties of dual phase steels, and from this to improve the low temperature mechanical properties of dual phase steels for low temperature structural applications.

II. APPROACH

The adopted approach to obtaining good combinations of impact toughness, strength, and ductility is primarily that of microstructural control by thermomechanical treatment, alloying or combinations of both. The basic concept underlying this research is that good impact toughness can be obtained primarily by grain size control, while utilizing dual phase microstructures to simultaneously obtain good combinations of strength and ductility.

1. Controlled Rolling

In low alloy steels, grain size control is very important since a reduction in grain size simultaneously improves both the yield strength and the ductile-brittle transition temperature.[29,30] Controlled rolling is one of the processing methods that can effectively decrease the grain size. Optimum grain size can only be obtained by careful control of processing variables, especially the deformation and temperature conditions.[31]

Work on controlled rolling is based on the premise that a fine austenite grain size is a prerequisite for a fine ferrite grain size. The austenite grain size prior to transformation is influenced by both 1) the rate of recrystallization, which is raised by increasing deformation and temperature but is retarded by solutes or fine precipitate particles, and 2) the rate of grain growth, which is increased by increasing temperature but is retarded by precipitate particles. The grain size of the ferrite formed during the transformation of the austenite depends on 1) the transformation temperature, being smaller with decreasing transformation temperature, 2) the prior austenite grain size, because

ferrite nucleates at the prior austenite grain boundaries, 3) the morphology of the austenite grains which may control the impingements of the ferrite grains formed during transformation, and 4) the deformation substructure and precipitates which may nucleate ferrite.[32]

Controlled rolling can be divided into three stages:

A. 1st Stage: simultaneous deformation and recrystallization above the recrystallization temperature.

In the high temperature range, the austenite grain size is refined to a limiting value by recrystallization. This can be attained by using deformation above the critical amount required for completion for recrystallization. Below the critical amount of deformation, partial recrystallization and strain induced grain boundary migration takes place.[33] In consequence, a small amount of deformation is apt to cause grain coarsening instead of grain refining.

B. 2nd Stage: low temperature austenite deformation.

The second stage deformation produces elongated grains, deformation bands, and possibly strain induced precipitation. Since austenite grain boundaries are the preferred nucleation sites for ferrite nucleation, the elongation of austenite grains by deformation inhibits the grain growth of ferrite. Deformation bands also provide nucleation sites. With increasing amounts of deformation, the number of deformation bands increases, and their distribution becomes uniform, giving rise to fine and uniform ferrite grains.[34]

C. 3rd Stage: deformation in the ($\alpha + \gamma$) phase region.

In this temperature range, the newly formed ferrite is deformed giving rise to the formation of subgrains. Several investigations have shown that subgrains contribute considerable strengthening when they are formed by the deformation of ferrite within the ($\alpha + \gamma$). However, their effect on the impact properties are still unknown.

2. Alloy Chemistry

Increasing the carbon content of steel is by far the most effective and economical way of raising the strength of steel. However, these significant gains in strength are generally accompanied by deterioration of the toughness.[25] In martensitic structure, a high carbon content (> 0.35 w/o) causes the formation of microstructural twinning.[36-38] Hence, the average carbon content in the initial alloy should be kept sufficiently low to maintain a carbon level of about 0.3 pct. in the austenite, resulting in dislocated martensite.

Among the substitutional alloying elements, only manganese[39] and nickel[40] have been reported to significantly lower the transition temperature. Mn is most beneficial. It not only lowers the transition temperature, but it raises the shelf energy. Mn prevents the formation of carbide films at grain boundaries and lowers the dislocation locking strength of carbon.[44] These behaviors lead to a lowering of transition temperature and an increase in shelf energy. Also, Mn lowers the ferrite transformation temperature,[42] thus providing a wider range of temperatures at which rolling can be performed.

Boron addition has been made mainly to obtain the martensitic-bainitic structure in the as-hot-rolled state so as to study its mechanical

behavior and the effects of boron on the final dual phase (ferritic-martensitic) structure. A boron content of 20 ppm was added since this content has been known to have a great affect on increasing the hardenability.[43-45]

III. EXPERIMENTAL PROCEDURES

1. Material Preparation

The materials used in this investigation were obtained from the Foote Mineral Company in the form of 75 lb. ingots. The alloys were air-melted. The ingots were sand-blasted, homogenized at 1200°C in vacuum for 24 hours and subsequently furnace cooled. They were then upset-cross-forged at 1100°C into 1.2" x 2.5" slabs. The compositions of alloys are listed in Table 1.

2. Thermomechanical Treatment

The heat treatments used in this investigation are controlled rolling and intercritical annealing of as-hot-rolled structures.

A. Controlled Rolling: In order to determine the proper rolling schedule, the 35% strain-induced recrystallization temperature was measured by an optical microscopy study of the specimens deformed 35% at different temperatures. Controlled rolling employed in this research was two-step rolling which involved rolling above the recrystallization temperature, and rolling below the recrystallization temperature.

The 1.2" x 2.5" x 3" slabs were soaked at 1100°C for 45 minutes and hot rolled 35% in one pass at 1000°C and then rolled 30% and 50% in one pass in the temperature range of 750°C to 950°C and directly quenched into water. The temperature was monitored by thermocouples inserted at the midpoint of the plate thickness.

B. ($\alpha + \gamma$) Phase Annealing: To compare the as-hot-rolled structures with the conventional dual phase structures (i.e., ferrite-martensite), specimens finish rolled at 850°C were intercritically annealed for 30 minutes and water quenched.

Typical thermomechanical treatments used in this research are illustrated schematically in Figures 1 and 2.

3. Phase Transformation Measurements

A Theta Dilatronic IIR dilatometer was used to measure phase transformation temperatures. A drawing of a specimen used in this experiment is shown in Figure 3. Each specimen was heated to 1100°C and held for 5 minutes before quenching to room temperature. Since the pressure of the specimen chambers was maintained below 10^{-5} torr, the specimen surface was well protected from oxidation. A programmed linear heating rate of 440°C/min. was used and the quenching rate of approximately 70°C/sec. was caused by a jet stream of He gas. Transformation temperatures were determined as first deviation points from linearity on dilation and temperature versus time charts. The experiment was repeated on the same specimen until consistent data was obtained.

4. Mechanical Testing

A. Tensile Testing: Cylindrical tensile specimens of 12.7 mm gauge length and 3 mm gauge diameter, as shown in Figure 4, were used. The loading direction was kept consistent with the rolling direction of the original plate. Tests were conducted at room temperature in an Instron machine. A strain rate of 0.04/min. was employed. The engineering yield stress was determined as the 0.2% offset value. Elongation and reduction in the area was observed by a travelling microscope with an accuracy of ± 0.01 nm. Uniform elongation was measured on the chart as the elongation obtained until the ultimate tensile strength was reached.

B. Charpy Impact Test: The standard and $^3/_4$ subsize Charpy V-notch

specimens[88] were used for the Charpy tests (Figure 5). Tests were done in both longitudinal and transverse directions. Low temperature tests were performed following the ASTM-23-72 specifications.[88] Subzero temperatures were obtained using a MULTI-COOL machine, and also using a mixture of isopentane and liquid nitrogen.

5. Microscopy

A. Optical Microscopy: Specimens for optical microscopy studies were cut from broken Charpy bars along a longitudinal direction to reveal the microstructure below the fracture surface. They were mounted in Koldmount and ground on successive emery papers up to 600 grade under flood cooling. Polishing was performed on 1 μm diamond paste wheel. The specimens were etched with 5% Nital solution, and the microstructures were examined with a Carl Zeiss metallograph. The volume percent of the second phase was determined by standard quantitative metallography using the intercept method.

B. Transmission Electron Microscopy: Thin slices of about 12 mils thick were cut from broken Charpy specimens. Specimens used for revealing the microstructure below the fracture surfaces were prepared similarly to the optical microscopic specimens. The sliced specimens were chemically thinned to about 5 mils in a solution of 3 ml HF + 100 ml H_2O_2, spark cut to 3 mm discs and sanded down to about 2 mils in thickness. These thin foils were finally electropolished in a twin jet electropolishing apparatus at room temperature using a solution of 400 ml CH_3COOH, 75 g CrO_3, and 21 ml H_2O. The polishing voltage varied from 35 to 45 volts. Thin foils so obtained were examined in Philips EM 301 electron microscopes at an operating voltage of 100 kV.

C. Scanning Electron Microscopy and Energy Dispersive Analysis of X-rays: Surfaces of the broken Charpy specimens were subjected to a fractographic study with an AMR-1000 Scanning electron microscope operated at 20 kV. For the investigations of crack propagation, the broken Charpy specimens were mounted in Koldmount and cut along the direction of the crack propagation. (The cross sections of the fracture surfaces were ground, polished and etched in a 5% Nital solution. These cross sectional areas were coated with evaporated gold for electrical conduction and examined using an AMR-1000 scanning electron microscope). An energy dispersive analysis of X-ray spectrometer (EDAX), attached to the microscope, permitted quantitative chemical analysis of precipitates on the fracture surface.

D. Scanning Transmission Electron Microscopy: The composition of the constituents in the final structures were studied with a Philips 400 scanning transmission electron microscope using an operating voltage of 100 kV. The procedure of preparing thin foils for STEM was the same as that described for TEM thin foils. Chemical analyses of elements whose atomic numbers are higher than 11 were performed with an EDAX unit attached to the microscope. Count rate data for X-ray intensities of each element from the EDAX equipment was converted to a weight percentage of chemical concentration by the method suggested by Russ and Duncumb.[89]

IV. EXPERIMENTAL RESULTS

1. Transformation Temperature

The martensite transformation temperatures M_s and M_f and the austenite formation temperatures obtained by dilatometry are tabulated in Table 2. The temperature intervals between A_s and A_f allow a rough assessment of the boundaries of the $(\alpha + \gamma)$ phase field. Extensive isothermal experiments were conducted to determine the A_{r3} temperature, solution treatment temperature, and $(\alpha + \gamma)$ phase annealing temperature. The austenization temperature was determined to be 1100°C and the A_{r3} temperature was about 750°C. The addition of boron does not measurably affect the transformation temperature.

2. Controlled Rolling

A. Fe/1.5Mn/.06C:

1. Grain Size and Microstructure

The structure just prior to rolling, obtained by quenching after solution treatment (1100°C, 45 minutes), is shown in Figure 6(a). The prior austenite grain size of this structure was about 250 μm. After rolling of the 35% reduction at 1000°C, the austenite grain size was decreased to ~ 100 μm (Figure 6 (b)). Complete recrystallization of the austenite is evident. Rolling below this recrystallization temperature causes the austenite grains to be elongated as shown in Figure 7. The change in the microstructure due to different amounts of deformation at a finish rolling temperature of 850°C is shown in Figure 8. This shows increased amounts of deformation cause a decrease in the ferrite grain size. The volume fraction of the second phase was constant and was about 25%. Figure 9 shows the microstructures of the steels

which were hot rolled 35% at 1000°C and then rolled 50% at various finish rolling temperatures. Lowering the finish rolling temperature produced a finer ferrite grain size and a gradual but small decrease in the volume fraction of the second phase (also accompanied by a decrease in its size). However, the distribution of the second phase was not changed.

The general microstructural features of these steels were blocky second phase particles surrounded by fine ferrite grains. Transmission electron microscopy studies revealed that the nature of the second phase in the as-hot-rolled state was mainly upper bainite. Figure 10(a) shows the upper bainitic structure developed in the specimen finish rolled at 850°C. Dark field imaging of interlath carbides is shown in Figure 10(b). This structure and morphology resembles that of high carbon upper bainite.[47] Changing the finish rolling temperature and amount of reduction produced no significant change in the nature of the second phase except that a small amount of acircular ferrite was found in the specimens finish rolled above 900°C (Figure 11). The substructure of the ferrite was similar in all cases. A significant feature was interphase carbide precipitation which was located only in the immediate vicinity of the ferrite/bainite interfaces, as shown in Figure 12. These carbides have been recognized as a new eutectoid transformation product in a variety of steels.[47-50] Due to the complexity of the carbide diffraction spots, the carbides could not be positively identified. However, they are most likely the M_7C_6 type according to the suggestion reported by Campbell and Honeycombe.[48] Another type of carbide was observed in the ferrite matrix which was located far away from the bainitic region (Figure 13). These carbides

were identified as cementite. The association of cementite with dislocations suggests that these precipitates came from the supersaturated ferrite. Another interesting feature encountered in these structures is the presence of retained austenite, as shown in Figure 14. This type of retained austenite is often found in steels with the microalloying elements (Nb,V)[18,51,52] or highly alloyed steel.[53] However, there was no evidence of presence of interlath retained austenite which is often encountered in other alloy systems.[27,37]

2. Mechanical Properties

The mechanical properties of these as-hot-rolled ferritic-bainitic steels are summarized in Table 3, and are plotted in Figure 15 as a function of the finish rolling temperature. All of the tensile tests were done at room temperature. The general trends are classical in that the strength increases with no appreciable change in elongation, and the ductile-brittle transition temperature decreases with decreasing finish rolling temperatures and/or increasing amounts of reduction. However, the rate of change in mechanical properties becomes small when the finish rolling temperature is lowered. One notes that larger amounts of deformation at the lower finish rolling temperature give better properties than the other rolling schedules. These mechanical properties can be correlated with the ferrite grain size (Figure 16). As the ferrite grain size decreases, the strength increases and the ductile-brittle transition temperature decreases.

Charpy impact energy values for the longitudinal direction were

measured at various temperatures and are plotted in Figure 7. The upper shelf energy increases with decreasing finish rolling temperatures. Also, a comparison of impact shelf energy between the longitudinal and transverse directions was made for the specimen finish rolled at 750°C (Figure 18), and it showed that there was a difference in the upper shelf energy values. This might be due to the elongation of MnS along the rolling direction during the controlled rolling process.

Since all Charpy impact tests were done with $^3/_4$ subsize specimens (because of the plate thickness < 10 mm) an evaluation of the validity of impact toughness was necessary. A comparison between full size and $^3/_4$ subsize specimens was made and the result is shown in Figure 19. It shows that the full size specimen (plane strain condition) has a higher shelf energy and higher transition temperature (~ 5°C) than the $^3/_4$ subsize specimens.

3. Effects of Cold Working on Mechanical Properties

Since this investigation is intended for the application of dual phase steels for low temperature use such as pipeline, and the literature has shown[21-26] that there are differences in mechanical behavior before and after pipe formation, it is necessary to study the effect of cold working on the mechanical properties of this alloy. In this investigation, cold working is done in the form of cold rolling. Figure 20 shows the variation of mechanical properties with the amount of cold reduction. There is a sharp increase in yield strength with cold work. This is because of the high initial work hardening rate of the dual phase structure. However, ductility and tensile strength change only gradually with increasing amounts of cold reduction. One

thing to note is that the DBTT increases rather slowly while there is a sharp increase in yield strength with increasing amounts of cold reduction. The amount of strain which is needed to form pipe by UOE process is about 1 ~ 3% strain.[21-26] When we assume that this amount of strain is equivalent to the amount of cold reduction, we can estimate what the mechanical properties of pipe made from this material might be. The mechanical properties of ferritic-bainitic structures are compared with the property specification for Arctic pipeline[90] in Table 4. This shows that this ferritic-bainitic structure exceeds the property specification in the as-hot-rolled state and also after 1 ~ 3% deformation.

B. Fe/1.5Mn/.06C/.002B:

1. Microstructure

When this alloy was soaked at 1100°C for 45 minutes, it developed a prior austenite grain size of 250 μm. After hot rolling 35% at 1000°C, the austenite was fully recrystallized. The variation of the microstructure with the finish rolling temperature is shown in Figure 21. This steel has somewhat different characteristics from the base Fe/1.5Mn/.06C alloy. This structure clearly shows the elongated austenite which was formed during final rolling. Since there was essentiallly no nucleation of ferrite upon quenching after the final rolling, the shape of the prior austenite grains is clearly visible. When finish rolled at 950°C, the austenite was fully recrystallized, but with finish rolling below 950°C, the austenite was not recrystallized. Rather, it was deformed to an elongated shape.

Figure 22 is a transmission electron micrograph of as-hot-rolled boron treated alloy finish rolled at 850°C and water quenched. It shows that the structure consists mainly of lath martensite and upper bainite. The dark field image in Figure 22(b) shows the interlath retained austenite which is often observed in as-quenched martensitic structures. Figure 22(c) shows an image of interlath carbide in upper bainite. Changing the finish rolling temperature between 850-950°C caused no appreciable changes in substructure. However, a small amount of ferrite was found when finish rolled at 800°C.

2. Mechanical Properties

Mechanical properties of these as-hot-rolled martensitic-bainitic structures are summarized in Table 5. They are plotted as a function of the finish rolling temperature in Figure 23. There was no apparent variation in the tensile properties between the finish rolling temperature of 850°C and 950°C. Also, the impact properties do not change with changes in finish rolling temperature (Figure 24). The plate which was finish rolled at 800°C showed some decrease in strength and transition temperature.

3. ($\alpha + \gamma$) Phase Annealing

A. Fe/1.5Mn/.06C (Type I)*

1. Microstructure

As the as-hot-rolled ferritic-bainitic structures are

---

*For the author's convenience, the Fe/1.5Mn/.06C ferritic-martensitic steel is denoted as the Type I dual phase steel and the boron modified steel as the Type II dual phase steel.

intercritically annealed and quenched, typical dual phase ferritic-martensitic structures result (Figure 25). At a low ($\alpha + \gamma$) annealing temperature, martensite particles exhibit a continuous network along the ferrite grain boundaries (Figure 25(a)). However, at a higher ($\alpha + \gamma$) annealing temperature (larger volume fraction of martensite), the microstructure has a resemblance to that of the as-hot-rolled state (Figure 25(c)). It shows the continuous network of martensite and some globular martensite embedded in certain areas of the ferrite matrix, which is believed to be the area previously occupied by the bainite in the as-hot-rolled state. This indicates that during annealing in the ($\alpha + \gamma$) region, formation of austenite from the initial ferrite-bainite structure begins at the ferrite grain boundaries and also, at the ferrite/carbide interfaces. The austenite then grows into the carbide enriched phase (i.e., bainite region in the as-hot-rolled state) with increasing temperature.

Figure 26 shows a typical region of martensite embedded in the ferrite matrix. A dark field image shows the retained austenite surrounding the martensite particles. Diffraction analysis shows that there is a Kurdjumov-Sachs orientation relationship, $[111]_{\alpha}//[110]_{\gamma}$ between martensite and austenite. The substructure of the martensite exhibited a high density of twinning and it was noted that the amount of twinning decreased with an increasing volume fraction of martensite for a given annealing time in the ($\alpha + \gamma$) region. Figure 27 shows a typical twinned

area in the base alloy with about 20% martensite. Dark field imaging of a twin spot superimposed on a matrix spot is shown in Figure 27(b). In most cases, they were internal microtwins typical of high carbon martensite.

The ferrite regions have undergone some substructural changes during the (α + γ) phase annealing as shown in Figure 28. The ferrite is the matrix which does not undergo structural transformation during heat treatment in the (α + γ) region. During the annealing process, a high density of dislocations is inherited from the initial structure which undergoes recovery, recrystallization and grain growth. The result is a fine subgrain distribution in the ferrite areas. In addition, subsequent quenching from the (α + γ) region results in the generation of a high density of fresh dislocations in the ferrite region due to the accomodation of strain caused by the austenite-martensite transformation. The ferrite grain size was constant (~ 7 μm) for a given two phase annealing temperature and the subgrain size varied from 0.3 μm to 1 μm.

2. Mechanical Properties

The mechanical properties of these (α + γ) phase annealed dual phase structures are summarized in Table 6, and are plotted in Figure 29 as a function of the reheating temperature. The general trends shown in this figure are that the strength increases, the elongation decreases, and the ductile-brittle transition temperature remains relatively unchanged with an increase in the reheating temperature. Particularly, the strength and elongation relationship obeys the two-phase mixture rule in the range of martensite volume fractions investigated as demonstrated

in many dual phase systems.[9-14]

Charpy impact energy values for the longitudinal direction were measured at various temperatures and are plotted in Figure 30. It shows that the upper shelf energy values increase gradually as the volume fraction of martensite decreases, but ductile-brittle transition temperatures remain relatively unchanged. There were differences between the Charpy energy values tested in the longitudinal direction and those tested in the transverse (Figure 18). This behavior might be due to the occurence of the texture upon ($\alpha + \gamma$) annealing, and the presence of elongated MnS inherited from the initial as-hot-rolled structure.

B. Fe/1.5Mn/.06C/.002B (Type II):

1. Microstructure

Two phase ($\alpha + \gamma$) annealing of the boron-treated alloy resulted in a different morphology from that of the base alloy. As can be seen in Figure 31, the martensite particles exhibit a mixture of needle-like and globular morphology. Since the initial structure prior to ($\alpha + \gamma$) phase annealing in this case was a two phase martensitic-bainitic structure, the kinetics of austenite nucleation might be different from those of the base alloy. A needle-like morphology was adopted for the formation of austenite at martensite lath boundaries and at ferrite/carbide interfaces from the martensite region and the bainite region, respectively. Hot rolling below the recrystallization temperature introduces lattice defects in the as-hot-rolled structure. These structural instabilities might be responsible for the fine, uniform distribution of globular martensite particles. Although there were morphological

differences between the base alloy and the boron-treated alloy, the substructure of the boron-treated alloy was essentially the same as that of the base alloy. The martensite particles contain a large amount of microtwins as shown in Figure 32. Ferrite subgrain formation was also found in this alloy (Figure 33).

2. Mechanical Properties

The mechanical properties of the boron-treated dual phase structures are summarized in Table 7, and plotted in Figure 34 as a function of the (α + γ) phase annealing temperature. Figure 35 shows the Charpy impact energy at various testing temperatures for different (α + γ) phase annealing temperatures. The boron-treated steel shows similar behavior to that of the base alloy. The strength increases, the ductility decreases, and the ductile-brittle transition temperature remains relatively unchanged with increased reheating temperature (i.e., increased volume fraction of martensite). Also, the upper shelf energy decreases with an increasing volume fraction of martensite.

4. Mn Distribution by Thermomechanical Treatment

Investigation of the alloying element partitioning within phases is of great importance with respect to understanding the resulting microstructure-mechanical property relationships, as demonstrated by Koo, et al.[87] The results of the STEM X-ray microanalysis for the manganese distribution is shown in Table 8. It shows that there was no segregation of Mn in the as-hot-rolled structures. However, upon (α + γ) phase annealing, redistribution of Mn occurred such that martensite (austenite) was enriched with Mn. On an average, the Mn concentration in martensite was about 0.3-0.5 w/o higher than that in ferrite.

5. Overall Comparison

As shown previously, the mechanical properties of these duplex alloys (ferrite-bainite, ferrite-martensite, or martensite-bainite) are quite sensitive to their microstructures, i.e., nature and morphology of the constituents.

In understanding the process of plastic deformation of the duplex alloys, a study of the characteristic stress-strain behavior is useful. The actual load-elongation properties of these duplex alloys are shown in Figure 36. Also shown in this figure, for comparison, is the engineering stress-strain curves for the 100% martensite. Note that the martensitic-bainitic structure has similar characteristics to those of the fully martensitic structure. They have a high yield stress to ultimate stress ratio and a small uniform elongation to total elongation ratio. Duplex ferritic-bainitic and ferritic-martensitic structures have relatively low yield strengths, high initial work hardening rates, low yield/ultimate tensile strength ratios and good values of elongation to necking. However, the ferritic-bainitic structure has a higher yield strength and ductility than the conventional dual phase (ferrite-martensite) structure at the same tensile strength level.

Microstructure also affects Charpy impact toughness (Figure 37). The impact toughness of ferritic-martensitic structure is generally inferior to that of the ferritic-bainitic structure. At the same tensile strength, the latter has a lower DBTT and an even higher shelf energy than the former. This is somewhat surprising because it is generally believed that upper bainite is inferior to martensite in terms of mechanical properties. Although comparison of the impact toughness between

the martensitic-bainitic structure and the ferritic-bainitic structure is essentially irrelevant because of the great difference in strength level, the impact toughness of the martensitic-bainitic structure is quite inferior to that of the ferritic-bainitic structure. However, the martensitic-bainitic structure is quite equivalent to the boron-treated ferritic-martensitic structure (Type II) in terms of ductile-brittle transition temperature, in spite of the great difference in strength level.

From the above analysis, one notes that the as-hot-rolled ferritic-bainitic structure exhibits a superior combination of strength and impact toughness. This is best illustrated in the plot of yield strength (0.2% offset) against DBTT as shown in Figure 38.

6. Fracture Behavior

The fracture morphology of broken tensile and Charpy impact specimens was examined in a scanning electron microscope. The general fracture appearance of the fractured tensile specimens was remarkably similar for all the duplex steels. The fracture surfaces were randomly fibrous, which indicates that crack propagation occurred by fracture predominantly from microvoid coalescence (Figure 39). Fracture surfaces of the room temperature-tested Charpy specimens show the same ductile fracture mode, regardless of their microstructural constituents (Figure 40). One notes that each dimple is usually associated with an inclusion, which was identified as MnS. However, scanning electron micrographs of cross section show that the void was nucleated because of decohesion at the matrix/second phase interfaces (Figure 41), not necessarily because of the MnS inclusions. As the testing temperature is lowered to -196°C there is a change in

fracture mode from ductile dimple mode to brittle cleavage mode. Figure 42 shows the fracture surface of Charpy impact specimens tested at -196°C. One clearly sees that the martensitic-bainitic and ferritic-martensitic (Type II) structures (Figure 42(c,d,)) have a larger cleavage facet size than the ferritic-bainitic and ferritic-martensitic (Type I) structures (Figure 42(a,b)).

It has been shown[7] that during the tensile loading of the ferritic-martensitic structures, fracture occurs by crack initiation and propagation within the ferrite matrix, not in the martensite particles. Therefore, it is interesting to investigate the fracture behavior in various duplex structures tested with high strain rates such as occurs in a Charpy impact test. Figure 43 shows the 5% Nital etched fracture surface of the ferritic-bainitic Charpy impact specimen tested at -196°C. Since the fracture surface is smooth, after etching it behaves so as to show the nature of constituents directly on the fracture surface. One easily sees that the secondary cracks lie within the ferrite. SEM of a cross section of the broken Charpy specimen clearly shows the microcrack developed in the ferrite matrix (Figure 44(a)). This behavior was also observed in the ferritic-martensitic structures as shown in Figure 44(b,d)). However, it is somewhat difficult to observe crack initiation in the martensitic-bainitic structures since they are indistinguishable by scanning electron microscopy. In this case, the microcrack lies in the prior austenite grain (Figure 44(c)).

Cross sectional areas of fracture surfaces of various duplex structures are shown in Figure 45. With this technique, the fracture surface and the microstructure can be directly correlated so that the unit crack

size can be measured. The ferritic-bainitic structure (Figure 45(a)) has the same unit crack size as the Type I ferritic-martensitic structure (Figure 45(b)), which is of the order of ferrite grain size. It should be noted that in the ferritic-martensitic alloy, most of the martensite particles do not have any effect in changing the direction of crack propagation, i.e., reducing the unit crack size. This might be due to the memory effect of martensitic transformation. One notes that the Type II ferritic-martensitic structure (Figure 45(d)) and the martensitic-bainitic structure (Figure 45(c)) have the same unit crack size which is of the order of the prior austenite grain size. This is because the martensite and bainite laths which nucleated from the same austenite grain have the same crystallographic orientation. Thus, once initiated, the crack propagates without changing its direction until it meets the prior austenite grain boundaries. The big difference in the unit crack size between the Type I and Type II ferritic-martensitic structures clearly shows the importance of the initial structure for dual phase processing.

V. DISCUSSION

1. Influence of Processing Variables on Microstructure and Mechanical Properties

A. Controlled Rolling

1. Fe/1.5Mn/.06C Alloy

*Recrystallization of Deformed Austenite

As pointed out previously, the importance of recrystallized austenite grain size to obtain fine ferrite grain size cannot be underestimated. For recrystallized austenite of a particular steel, the degree of austenite grain refinement is determined by the effective finishing temperature, provided the conditions for successive recrystallization and critical deformation are met. In a plain carbon steel, such as Fe/1.5Mn/.06C, which does not contain microalloying elements (Nb,V), recrystallized austenite grains are relatively coarse and grow coarser with time due to the absence of fine precipitates to inhibit growth in the stable austenite range. The relationship between the deformation temperature and the critical amount of deformation required for the completion of recrystallization in this alloy was diverse. Recrystallization was complete within a few seconds after the rolling. The recrystallized austenite grain size decreased rapidly as the amount of deformation increased. Beyond 35% reduction, however, the rate of decrease diminished, and the grain size reached a limiting value of about 80 μm (Figure 8(b)). Sekine, et al.,[54] postulated that grain refinement in high temperatures was attributed to dynamic recrystallization, and at intermediate temperatures was believed to be caused by static recrystallization. In dynamic recrystallization, the recrystallized grain size was reported not to have been influenced by the initial grain size. The conditions which favor dynamic recrystallization are rolling at high temperatures and large reductions.

However, in static recrystallization, the number of recrystallization nuclei depends on the grain boundary area per unit volume and the amount of deformation. Once enough deformation to cause static recrystallization takes place, the recrystallization process is complete in a matter of seconds.[55] It seems this situation is true for all the steels studied in this work.

*Effect of Amount of Deformation and Finish Rolling Temperature

Microstructural changes in recrystallized austenite due to rolling below its recrystallization temperature are other important phenomena which must be carefully understood so as to obtain the optimum microstructure. As austenite is deformed below its recrystallization temperature, another phenomenon occurs in addition to elongation of austenite grains. This involves the introduction of deformation bands into the grains.[55,56] Although the exact nature of the deformation bands is not known, they generally exist in closely spaced pairs of parallel lines which often terminate within a grain, creating a twin-like pattern in a heterogeneous distribution[55] (Figure 7). As austenite grain boundaries are the preferred nucleation sites for austenite-to-ferrite transformation,[57] the elongation of austenite grains inhibits grain growth of ferrite. Deformation bands also provide nucleation sites. It was found that increasing the amount of reduction decreases the ferrite grain size as shown in Figure 8. This is because increasing the amount of deformation increases the grain-aspect ratio (measure of grain elongation) and the number of deformation bands and their distribution becomes uniform, giving rise to fine and uniform ferrite grains.[58,59] Grain size also decreases with decreasing finish rolling temperature as shown in

Figure 9. However, the kinetics of grain refining by changing the deformation temperature are different from those caused by changing the amount of deformation. Significant refinement, which was obtained by reducing the deformation temperature, corresponds to the transformation of a strain-hardened structure. Decreasing the deformation temperature results in more stored energy available to nucleate the ferrite grains. Also, after deformation at a relatively high temperature, there might be partial recrystallization and insufficient nucleation sites which leads to heterogeneous transformation (Figure 9(d)). Lowering the deformation temperature reduces the tendency for partial recrystallization, and eventually nonrecrystallization will occur. The above two factors govern the changes in the kinetics of grain refinement that occur with changes in the deformation temperature. However, even at the lowest deformation temperature (750°C), the microstructure consists of fine ferrite grains with a coarse second phase suggesting the occurrence of heterogeneous transformation. I. Kozasu, et al.[55], claimed that not all deformation bands have the same ferrite nucleation potential and some bands have a poor nucleation capability. Also, M. Fukada, et al.[60], found that even with a very large amount of deformation it was impossible to produce a uniform distribution of deformation bands, and thus, there existed a region which has a poor nucleation capability. Upon fast cooling, those regions transform to other phases, i.e., martensite or bainite depending on their hardenability. In this alloy system, the transformation is to upper bainite as shown in Figure 10.

By consideration of a CCT diagram for a suitable steel, a general

understanding of the transformations taking place during quenching treatment could be obtained. A complete CCT diagram for the alloy investigated was not available and Figure 46 (taken from reference 61) shows the CCT diagram for a 0.13% C-0.56% Mn steel. For lower carbon steels the ferrite transformation "start" curve would be displaced even closer to the vertical axis. The higher Mn content also affects the transformation characteristics. As a result of these factors, it is almost impossible to obtain martensite as a second phase in this alloy, even with the highest possible cooling rate because of low martensite hardenability. However, there is a relatively wide range of cooling rates that will give upper bainite as a second phase. The volume fraction of the second phase shows small variations with changes in the finish rolling temperature. This might be because of the rise in the starting temperature of ferrite nucleation by deformation which has been pointed out by many researchers.[62-63] The change in the critical temperature signifies a transition from nonpolygonal to polygonal structures. This temperature change is independent of the deformation temperature.[55] The above effects give rise to the large amount of polygonal ferrite transformation during quenching. Thus, the increase in quenching temperature produces only a small increase in the volume fraction of the second phase, and this is accompanied by an increase in the size of the second phase, without a change in its distribution.

*Mechanical Properties

Ferrite grain size plays the predominant role since grain refinement is the only means by which both the yield strength and the

fracture strength can be increased with a simultaneous lowering of the transition temperature. The mechanical properties of this alloy are enhanced by increasing the amount of deformation and/or decreasing the finish rolling temperature as shown in Figure 15.

As discussed previously, the main structural change that occurred by increasing the amount of deformation and decreasing the finish rolling temperature was to refine the ferrite grain size. The effect of the ferrite grain size on the yield stress of a material is generally described by the Hall-Petch equation[64-65]

$$\sigma_y = \sigma_i + K_y d^{-1/2}$$

where σ_y is the yield strength, and σ_i is the internal friction. K_y is the Hall-Petch slope representing the resistance to slip propagation across a grain boundary and d is grain size. Also, it has been shown that the fracture strength increases[29,30] and the transition temperature decreases[66] with refining the grain size. The refinement of grain size from 10 μm to approximately 4 μm resulted in a suppression of DBTT by 30°C. For each unit increment in $d^{-1/2}(mm^{-1/2})$, the transition temperature is decreased by 5°C (Figure 16(b)). This is lower than the value of $11.5°C/d^{-1/2}(mm^{-1/2})$ reported by Petch.[67]

Aside from transition temperature, the impact energy is influenced by other factors such as amount and shape of the second phase, cleanliness, and the absence of interstitials. Figure 17 shows the variation of impact energy with testing temperature. It shows that upper shelf energy increases consistently, although slightly, with decreases in the deformation temperature. This behavior might be due to the decreased amount and size of the second phase. Also, the variation of impact

energy between the longitudinal and transverse directions are shown in Figure 18. It shows that the direction of impact testing does not affect the transition temperature. However, there is a small but noticeable change in impact energy with testing direction. This might be due to the influence of inclusions and/or texture even though no attempt is made here to analyze this effect quantitatively.

2. Fe/1.5Mn/.06C/.002B

*Microstructure

The deformation of austenite in this system is the same as in the base alloy system, but, unlike the base alloy, polygonal ferrite nucleation did not occur. Thus, the shape of prior austenite grain was clearly shown in the final structure (Figure 20). Boron has been known to be a very potent element in increasing the hardenability of steel. A mechanism of the boron hardenability effect has been proposed to be due to the surface absorption of boron onto the prior austenite grain boundaries.[68-71] It is, therefore, possible that boron contributes to the hardenability of steel by a reduction in the interfacial energy of austenite grain boundaries and therefore retards ferrite nucleation on these sites. Thus, the effect of boron on the CCT diagram is to move the ferrite nucleation "start" curve to the right side as shown in Figure 46. Although the effect of boron on hardenability of plain carbon and low alloy steels has been well established[43,44,45], and utilized in commercial practice, its influence on the hot working behavior is not clear. The experimental evidence observed here shows that boron has no effect on the kinetics of deformation and recrystallization of austenite. The boron-treated

steel behavior similar to that of the base alloy. When it was deformed at 950°C, the austenite recrystallized to the finer grain size (Figure 20(c)), but did not recrystallize when deformed below this temperature.

Figure 22 shows that this structure consists mainly of lath martensite and upper bainite. Figure 22(b) is a dark field image of retained austenite and Figure 22(c) is a dark field image of interlath carbide. Smith and Mehl[72] claimed that bainitic formation is similar in its crystallographic features to that of martensite. This micrograph shows that the bainitic ferrite has the same orientation as the martensite lath.

*Mechanical Properties

In this alloy system, the structural change caused by changing the finish rolling temperature is not as significant as in the case of the base alloy. The only observable change is the nonrecrystallization of deformed austenite, thus preserving the elongated grains when finish rolled below 900°C. When finish rolled between 850-950°C, no appreciable changes in mechanical properties were found (Figure 23). Since there was no ferrite nucleation in this alloy, there are some ambiguities in the definition of the grain size. Some experimental results show that prior austenite grain sizes in martensitic alloys can be used as an "effective grain size". One easily notes that this prior austenite grain size is almost the same along the direction of crack propagation (transverse) whether or not the austenite is recrystallized. This fact may account for the constant mechanical properties with changing finish rolling temperature. The decrease in strength and transition temperature when finish rolled at 800°C might be due to presence of a small amount of ferrite.

B. ($\alpha + \gamma$) Phase Annealing

*Microstructure

($\alpha + \gamma$) phase annealing has received much attention in recent years because of its beneficial effect on the microstructure and resultant mechanical properties.[53,73,74-76] This intercritical annealing is often regarded as a prerequisite for dual phase steels[3,4] which need ferrite and martensite as their major constituents. Many investigators have studied the formation of austenite from ferrite-pearlite[78,79,80] and from martensite[77,81], but the formation of austenite from ferrite-bainite has been studied in less detail.

Formation of austenite is initially highly preferential[78,82], starting from defects in the crystal structure, concentration fluctuations and at interfaces between ferrite and carbides. In the present study, the preferential precipitation of austenite on reheating was along the ferrite grain boundaries which are high angle boundaries of high energy (Figure 25(a)). However, at a higher ($\alpha + \gamma$) annealing temperature (Figure 25(c)), austenite also nucleated along the ferrite-carbide interfaces (bainitic lath boundaries) and grew to form the cluster-like austenite at the region which was believed to be the carbon-rich bainite of the initial as-hot-rolled structure. This suggests that lattice imperfections (ferrite grain boundaries) are the preferential site for austenite nucleation at the lower temperatures, while at higher temperatures, concentration fluctuations are also responsible for austenite nucleation and growth in this system. The dominating influence of the boundaries in the austenite nucleation process arises from the additional surface energy available at the interfaces as given by classical

nucleation theory.[82] For austenite growth, diffusion of carbon into the nucleated austenite is needed.

Previous studies[77,78] showed that when the initial structure consists of martensite, austenite nucleates preferentially at the martensite lath boundaries. However, this was not observed in the ($\alpha + \gamma$) annealing of the as-hot-rolled martensitic-bainitic structure in the present work (Figure 31). Miller, et al.[83], reported that heavy cold working was an effective means of destroying the memory effect. Destruction of the memory effect in martensite by introducing heavy cold work seems to be due to increased numbers of possible nucleation sites through the introduction of structural instabilities involving strain energy. The increase in the number of nucleation sites seems to be obtained also by controlled rolling if the finish rolling temperature is below the recrystallization temperature. This ferritic-martensitic structure (Type II) has a finer appearance than the Type I ferritic-martensitic structure. Martensite of high dislocation density has, of course, many more nucleation sites than stable ferrite and, thus, we can expect a finer grain size than that resulting from a ferrite phase.

*Mechanical Properties

The mechanical behavior of this ferritic-martensitic structure is generally well characterized. It has been shown by numerous investigations[8-14] that the strength increases and ductility decreases with increasing volume fraction of martensite (i.e., increasing the annealing temperature), except in cases[15-17] where strong carbide formers are included as an alloying element. Figures 29 and 34 show that the results

of this investigation were not an exception to the above rule.

The impact properties are interesting. There was no variation in the transition temperature with different volume fractions of martensite. However, there was an increase in the upper shelf energy with decreasing volume fractions of martensite. As pointed out earlier, the transition temperature is controlled mainly by the "effective grain size". The introduction of martensite does not seem to have any effect on decreasing the "effective grain size". This might be due to the memory effect of the martensitic transformation such that the austenite transforms to the martensite whose crystallographic orientation is the same as that of ferrite matrix. Thus, the "effective grain size" in Type I ferritic-martensitic structure is the ferrite grain size of the initial as-hot-rolled ferritic-bainitic structure which does not change considerably with increasing annealing temperatures, while the prior austenite grain size or packet size is the "effective grain size" in Type II ferritic-martensitic structure. However, a higher shelf energy can be obtained in the lower volume fraction of martensite since this gives less constraint to the surrounding ferrite, i.e., more freedom to deform plastically in addition to more of the soft ferrite matrix.

2. Correlation of Microstructure with Mechanical Properties

Two phase microstructure with constituents of comparable size occur in many technologically important alloys. Some of the important constituents in ferrous alloys are ferrite, pearlite, martensite, bainite, and austenite. When these constituents coexist in a simple alloy system, the resulting mechanical behavior is entirely different from that of each

constituent existing as a single constituent. There are many factors which affect the mechanical behavior of duplex structures, that is: 1) morphology (size, shape, distribution) of each constituent, 2) volume fraction of the second constituent, and 3) properties of each constituent. The alloying element and the thermomechanical treatment control these main structural and resultant mechanical properties.

A. Tensile Behavior: Figure 36 shows the variation in the stress-strain behavior of several different duplex structures with change in the microstructural constituents. Both the ferritic-bainitic and the ferritic-martensitic structures show high tensile/yield strength ratios and a high rate of work hardening in the early stage of plastic deformation. However, the ferritic-bainitic structure has a lower work hardening rate and higher yield strength than the ferritic-martensitic structure at the same tensile strength level. In the early stage of plastic deformation, the deformation is largely confined to the soft ferrite matrix. The plastic deformation in the ferrite is constrained by the adjacent second phase. This constrained deformation of the ferrite causes the rate of dislocation multiplication to be accentuated, resulting in a high work hardening rate. Thus, the work hardening rate depends on the property of the constraining second phase, i.e., the severity of constraint. Since the yield strength of martensite is generally higher than that of upper bainite, martensite will provide more constraint and thus a higher work hardening rate than upper bainite. This is in agreement with the result of Fischmeister, et al.[84], who observed an increase in the work hardening rate with an increase in the ratio of the hardness (or yield strength) of the constituents. The morphology of martensite

which more or less surrounds the ferrite might also increase the severity of constraint.

The tensile behavior of upper bainite and low carbon martensite are known to be similar in nature except for magnitude.[72] Within a prior austenite grain, they have the same orientation as shown in Figure 22. Thus, this mixture of martensite and upper bainite can be thought of as an ideal system which satisfies the mixture rule. There might be no complications which occur from the differences in morphology, and it shows similar stress-strain behavior to that of a fully martensitic structure.

B. Impact Properties and Fracture Behavior: In general, the results of impact testing are often divided into two terms: 1) shelf energy, and 2) ductile-brittle transition temperature. These depend on different factors as will be described below.

1. Shelf Energy

Figure 37 shows the typical variation of shelf energy with testing temperature for various duplex structures. The highest upper shelf energy was obtained in the ferritic-bainitic structure followed by the ferritic-martensitic and then martensitic-bainitic structure. Fracture surfaces of these structures tested at room temperature show that the fracture mode was entirely dimpled rupture and that the void was often associated with MnS inclusions (Figure 40).

The shelf energy at ductile fracture is known to decrease with: 1) decreasing cleanliness of matrix, 2) increasing volume fraction of second phase, 3) increasing strength level, and 4) decreasing strain hardening rate. An interesting observation was that the ferritic-

bainitic structure which has a higher volume fraction of second phase and higher yield strength has a higher upper shelf energy than the ferritic-martensitic structure at the same tensile strength level. This observation was not in agreement with the above mentioned factors. The metallographic evidence shown in Figure 41 indicates that void initiation occurs at both sulfide inclusions and at the interphase boundaries in both cases. The uniform distribution of fine martensite around the ferrite matrix in the ferritic-martensitic structure will have more interphase boundaries, and thus a higher probability of void initiation than the ferritic-bainitic structures in which relatively coarse bainite regions are separated by several fine ferrite grains. After void initiation, void coalescence by shear might be easier in the ferritic-martensitic structure which has a smaller spacing between martensite particles than the ferritic-bainitic structure. Thus, the above observations indicate the overwhelming role of the morphology of second phase in determining the Charpy shelf energy for duplex structure of relatively similar mechanical behavior. When the structure consists of martensite and bainite, the other factors become important since there is no morphological difference between the matrix and the second phase in this structure. A high yield strength and a low work hardening rate promote low energy ductile fracture.

2. Ductile-Brittle Transition Temperatures

The transition temperature is governed by differerent factors. Even though grain size is the major factor, other factors may dominate in some cases. As shown in Figure 37, Type II ferritic-martensitic structure has a similar transition temperature to that of the martensitic-bainitic structure and a higher transition temperature than

the Type I ferritic-bainitic structure. Careful studies of the cross section of the fracture surface show that the higher DBTT is associated with the larger unit crack size (Figure 45). Also, it is reflected on the fracture surfaces in terms of cleavage facet size (Figure 42). The prior austenite grain size, which is the "effective grain size" for crack propagation in the martensitic-bainitic structure, is also the "effective grain size" in the Type II ferritic-martensitic structure in which the initial structure is martensite-bainite as discussed previously. Thus, this results in the same DBTT for these two structures despite the differences in their constituents and morphologies. However, when the initial structure prior to ($\alpha + \gamma$) phase annealing consists of ferrite and bainite, the "effective grain size" in the resulting ferritic-martensitic (Type I) structure is the ferrite grain size which is much smaller than the prior austenite grain size. This refinement in the "effective grain size" in the Type I ferritic-martensitic structure causes an abrupt decrease in the transition temperature from that of Type II ferritic-martensitic structure although they show essentially the same tensile behavior. This point illustrates the importance of the initial structure for dual phase structures when good impact property is required. Similar behavior was observed in the Fe/2Si/.1C system.[85]

Another important observation is that the ferritic-bainitic structure has a lower transition temperature than Type I ferritic-martensitic structure even though they have the same "effective grain size" as shown in Figure 45(a,b). Many investigators[18,21,23] claimed that upper bainite should be avoided in the final structure to obtain optimum strength-

touhgness combinations because of the following characteristics. In upper bainite, large interlath carbides crack to form super-critical defects. The cleavage crack, once initiated, is not obstructed by the low angle bainitic ferrite boundaries, but only by bainite packet boundaries or prior austenite grain boundaries. Thus, the crack propagates rapidly. However, the above point is certainly not an important factor in duplex structures since the crack nucleates in the polygonal ferrite matrix without fracturing the second phase (Figure 44). The "effective grain size" of these structures is essentially the same, being of the order of the ferrite grain size, since martensite in the ferritic-martensitic structure does not have any effect on the crack propagation as discussed previously. Thus, it appears that nucleation of cracks is more important than their propagation across boundaries in determining the transition temperature for these structures. Kunio, et al.[86], observed that the connected ferritic-martensitic steels deform in such a manner that the slip system was confined to (110) [111], thus the probability of cleavage crack nucleation in the ferrite matrix is higher than for other morphologies at a given testing temperature. However, in the ferritic-bainitic structure where relatively coarse upper bainite particles are dispersed in the fine ferrite matrix, the possibility of cleavage crack nucleation in the ferrite will be depressed since constraint of ferrite by upper bainite is less than when the second phase is stronger martensite and/or when the second phase more or less forms a continuous network around the ferrite matrix. This morphological advantage of the as-hot-rolled ferritic-bainitic structure coupled with other factors (work hardening rate, etc.) results in a lower DBTT than that

in the ferritic-martensitic structure.

3. Characteristics of As-Hot-Rolled Ferritic-Bainitic Structure

Figure 38 shows the relation between yield strength and transition temperature of the various duplex structures. One can easily see the superior combinations of yield strength and transition temperature in the as-hot-rolled ferritic-bainitic structures. This is due mainly to the favorable morphology of upper bainite in a ferrite matrix. This structure is quite attractive for low temperature applications such as line pipe in which one needs high strength, good weldability, high resistance to brittle cleavage and low energy ductile fractures as well as a low transition temperature. This Fe/1.5Mn/.06C steel with the ferritic-bainitic structure easily surpasses the mechanical property specification for the Artic line pipe and is superior or equal to other line pipe steels which contain rather expensive Nb and V as essential alloying elements.

Another advantage of these ferritic-bainitic steels is the continuous stress-strain behavior and high work hardening rate. There will be an additional increase in yield strength in the duplex ferritic-bainitic structure during pipe forming, whereas pipe made from conventional ferritic-pearlitic structures[21-26] experience a 10 to 15% loss in yield strength because of the yield point elongation coupled with the Bauschinger effect. Figure 20 shows the response of mechanical properties with cold reduction. When pipe is formed by the UOE process[21,22], the yield strength cannot be estimated directly from the stress-strain curve of uniaxial tensile tests because the deformation of material by bending and expansion is mostly under plane strain condition. Thus, the above result might

only be used to give a rough estimation of the mechanical properties of the pipe formed by the UOE process. One notes that the transition temperature increases very little, while there is an abrupt increase in yield strength with small amounts of cold deformation. The amount of strain needed to form pipe by the UOE process is about 1-3%.[21-26] The mechanical properties of ferritic-bainitic structure after 2% cold reduction are shown in Table 4 along with the property specification for Arctic line pipe. This clearly demonstrates the potential of as-hot-rolled Fe/1.5Mn/.06C ferritic-bainitic structure for the pipe application.

SUMMARY AND CONCLUSIONS

The following conclusions may be drawn from the present investigation:

1. The main objectives of this research have been met, viz., to design dual phase steels with superior mechanical properties, particularly with low temperature toughness.

2. When a Fe/1.5Mn/.06C alloy is controlled rolled followed by direct quenching, it exhibits a duplex ferritic-bainitic structure. Both a decrease in the finish rolling temperature and an increase in the amount of deformation refine the ferrite grain size and thus improve the resulting mechanical properties of ferritic-bainitic structure, i.e., increase the strength, and lower the ductile-brittle transition temperature.

3. An addition of boron does not affect the hot working characteristics of the base alloy. It does, however, affect the transformation behavior of the hot-worked austenite such that duplex martensitic-bainitic structure is obtained after direct quenching. Decreasing the finish rolling temperature does not produce any appreciable change in the mechanical properties of as-hot-rolled martensitic-bainitic structure.

4. In conventional dual phase (ferritic-martensitic) steels, increasing the volume fraction of martensite does not produce any changes in ductile-brittle transition temperature, while it increases the strength and decreases the ductility in the usual way.

5. It has been shown that cleavage cracks are initiated in the ferrite matrix in both the ferritic-bainitic and ferritic-martensitic structures.

6. Ductile-brittle transition temperatures are determined by the

"effective grain size" which also depends on the structure and the transformation path.

a. The "effective grain size" of as-hot-rolled ferritic-bainitic structure is the ferrite grain size, while that of the martensitic-bainitic structure is the prior austenite grain size.

b. The "effective grain size" of ferritic-martensitic structure is determined by its initial structure, since the martensitic particles do not refine the "effective grain size". This clearly suggests the importance of the initial structure prior to ($\alpha + \gamma$) phase annealing for dual phase steels when good impact property is required. Thus, further improvement in the impact property of dual phase steel is possible by careful choice of the initial structure and the carbon content to ensure a fine "effective grain size" and the formation of lath martensite.

7. The superior mechanical properties of steels with the as-hot-rolled ferritic-bainitic structure compared to those with ($\alpha + \gamma$) phase annealed ferritic-martensitic structure are attributed to the former's favorable morphology such that relatively coarse bainite regions are uniformly separated by several fine ferrite grains.

8. The mechanical behavior of steels with the as-hot-rolled ferritic-bainitic structure is shown to be attractive for line pipe application. Present results already exceed the property specifications for Artic line pipe in the as-hot-rolled condition, and moreover, there is a large increase in yield strength (25 ksi) with small increase in transition temperature (5°C) by cold working (pipe forming).

ACKNOWLEDGEMENTS

The author would like to express his deepest gratitude to Professor Gareth Thomas for his guidance, encouragement and support throughout this investigation. He is also grateful to Professor J. W. Morris, Jr. and Professor D. A. Dornfeld for their reviews of this manuscript. Thanks are also due to Drs. Jayoung Koo, Jungihl Kim and Cholkyl Syn for their advice and encouragement.

The author acknowledges the assistance provided by the support staff of the Materials and Molecular Research Division of Lawrence Berkeley Laboratory. Appreciation is also extended to Kathy Brusse, Helen Johnson and Madeline Moore for typing this manuscript.

Dr. P. Mangonon and Foote Mineral Company graciously supplied the alloys used in this research. Special thanks are extended to the author's colleagues, especially to Hyung Jai Lee and Hee Jin Kim, who made my stay at Berkeley so enjoyable. The author is also grateful to Alvin Nakagawa and James Wasynczuk for editorial assistance.

Finally, I am greatly indebted to my family, especially to my parents and wife, Miji, who showed a rare love and patience which made this work possible.

This work was supported by the Director, Office of Energy Research, Office of Basic Energy Sciences, Division of Materials Sciences of the U. S. Department of Energy under Contract No. DE-AC03-76SF00098.

References

1. T. Katsuoka and K. Yamamori, Met. Trans. 6A, 1613 (1975).
2. S. Hayami and T. Furukawa, Micro-Alloying 75, Washington, D. C. October 1975; Union Carbide Corporation, N. Y., 1977, p. 311.
3. J. Y. Koo and G. Thomas, Mat. Sci. and Engr. 24, 187 (1976).
4. A. T. Davenport, ed., Formable HSLA and Dual-Phase Steels, AIME, New York, N. Y. 1979.
5. R. A. Kot and J. W. Morris, eds., Structure and Properties of Dual-Phase Steels, AIME, New York, N. Y. 1979.
6. R. A. Kot and B. L. Bramfitt, eds., Fundamentals of Dual-Phase Steels, AIME, New York, N. Y. 1981.
7. N. J. Kim and G. Thomas, Met. Trans. 12A, 483 (1981).
8. G. Thomas and J. Y. Koo, Structure and Properties of Dual-Phase Steels, R. A. Kot and J. W. Morris, eds., AIME, New York, N. Y. 1979, p. 183.
9. J. W. Morrow and G. Tither, J. Met., December 1978, p. 20.
10. G. R. Spetch and R. L. Miller, Structure and Properties of Dual-Phase Steels, R. A. Kot and J. W. Morris, eds., AIME, New York, N. Y. 1979, p. 145.
11. R. G. Davies, Met. Trans. 9A, 41 (1978).
12. R. G. Davies, Ibid., p. 451.
13. R. G. Davies, Ibid., p. 671.
14. J. Y. Koo and G. Thomas, Met. Trans. 8A, 525 (1977).
15. T. O'Neil, M. S. Thesis, University of California, Berkeley 1979 (LBL-9047)
16. P. K. Costello, M. S. Thesis, University of California, Berkeley 1978 (LBL-8628).

17. J. S. Gau, J. Y. Koo, A. H. Nakagawa and G. Thomas, Fundamentals of Dual-Phase Steels, R. A. Kot and B. L. Bramfitt, eds., AIME, New York, N. Y. 1981.

18. J. M. Rigsbee, J. K. Abraham, A. T. Davenport, J. E. Franklin and J. W. Pickens, Structure and Properties of Dual Phase Steels, R. A. Kot and J. W. Morris eds., AIME, New York, N. Y. 1979, p. 304.

19. R. R. Preston, J. Met., 1977, 29, No. 1, 9.

20. F. B. Pickering, Micro-Alloying 75, Union Carbide Corporation, N. Y. 1977, 1, p. 3.

21. T. Tanaka, Micro-Alloying 75, Line Pipe, Union Carbide Corporation, N. Y. 1977, 3, p. 38.

22. Y. Takada and E. Sugie, Kawasaki Steel Technical Report, 1974, vol. 6, p. 502.

23. T. Yamaguchi, T. Osuka, T. Taira and N. Iwasaki, Micro-Alloying 75, Line Pipe, Union Carbide Corporation, N. Y., 3, p. 49.

24. I. Kozasu and T. Osuka, Processing and Properties of Low Carbon Steel, AIME, 1973, p. 47.

25. H. Matsubara, T. Osuka, I.Kozasu and K. Tsukada, Trans. I. S. I., Japan 12, 435 (1972).

26. I. Kozasu, T. Shimizu and K. Tsukada, ibid., p. 305.

27. J. Y. Koo, Ph.D. Thesis, University of California, Berkeley, 1977 (BL-6657).

28. T. Greday, H. Mathy and P. Messien, Structure and Properties of Dual-Phase Steels, R. A. Kot and J. W. Morris, eds., AIME, New York, 1979, p. 260.

29. A. H. Cottrell, Trans. AIME 212, 192 (1958).

30. N. J. Petch, Phil. Mat. 3, 1089 (1958).

31. Micro-Alloying 75, Washington, D. C., October 1975, Union Carbide Corporation, N. Y. 1977.

32. J. H. Woodhead and P. Webster, J.I.S.I., 207, 51 (1969).

33. T. Tanaka, N. Tabata and C. Shiga, Micro-Alloying 75, Washington, D. C., 1975, Union Carbide Corporation, N. Y. 1977, p. 88.

34. T. Gladman, D. Dulten and I. D. McIvor, Ibid., p. 25.

35. T. Gladman, I. D. McIvor and F. B. Pickering, J.I.S.I. 210, 916 (1972).

36. J. McMahon and G. Thomas, Proc. 3rd Internat. Conf. on Strength of Metals and Alloys, Inst. of Metals, London 1973, p. 180.

37. B. V. N. Rao, Ph.D. Thesis, University of California, Berkeley 1978 (LBL-7361).

38. S. K. Das and G. Thomas, Met. Trans. 1, 325 (1970).

39. N. P. Allen, W. P. Ress and H. R. Tipler, J.I.S.I. 174, 108 (1953).

40. M. Gensamer, Trans. AIME, 2, 215 (1959).

41. N. P. Allen, Iron and Its Dilute Solid Solutions, Interscience, N. Y., 1963, p. 271.

42. E. C. Bain and H. W. Paxton, Alloying Elements in Steel, ASM, 1966, p. 113.

43. P. T. Llewellyn and W. T. Cook, Metals Tech. 1, 517 (1974).

44. R. A. Grange and J. B. Mitchell, Trans. ASM, 53, 157 (1961).

45. R. A. Grange and T. M. Garvey, Trans. ASM, 37, 136 (1946).

46. F. B. Pickering, Transformation and Hardenability in Steels, Symp. Climax Molybdenum Co., Michigan 1977, p. 109.

47. A. T. Davenport, F. G. Berry and R. W. K. Honeycombe, Metal. Sci. 2, 104 (1968).

48. K. Campbell and R. W. K. Honeycombe, Metal. Sci. 8, 197 (1974).

49. W. B. Morrison, J.I.S.I. 201, 317 (1963).

50. M. Tanino and K. Aoki, Trans. I.S.I. Japan 8, 339 (1968).

51. J. M. Rigsbee and P. J. Vander Arend, Formable HSLA and Dual-Phase Steels, A. T. Davenport, ed., AIME, New York, N. Y. 1979, p. 58.

52. K. Nakaoka, Y. Hosoya, M. Ohmura and A. Nishimoto, Structure and Properties of Dual-Phase Steels, R. A. Kot and J. W. Morris, eds., AIME, New York, N. Y. 1979, p. 330.

53. J. I. Kim, Ph.D. Thesis, University of California, Berkeley, 1979 (LBL-9956).

54. H. Sekme and T. Maruyama, The Microstructure and Design of Alloys, Cambridge, 1973, p. 85.

55. I. Kozasu, C. Ouch, T. Sampei and T. Okita, Micro-Alloying 75, Washington, D. C., October 1975, Union Carbide Corporation, New York, N. Y. 1977, 1, p. 120.

56. H. Sekine and T. Maruyama, Tetsu-to-Hagane 58, 1044 (1972).

57. A. G. Guy, Introduction of Materials Science, McGraw-Hill, Inc. N. Y., 1972, p. 66.

58. H. Kaji, M. Katsumata, M. Machida and S. Kinoshita, Tetsu-to-Hagane 60, 295 (1974).

59. H. Sekine, T. Maruyama and Y. Kawashima, Ibid., p. 557.

60. M. Fukuda, T. Hashimoto and K. Kunishige, Micro-Alloying 75, Washington, D. C. 1975, Union Carbide Co., New York, N. Y. 1977, 1, p. 120

61. N. P. Allen and R. Priestner, Heat Treatment of Metals, ISI Spec. Rep. 95, 1966, p. 1.

62. Y. E. Smith and C. A. Seibert, Met. Trans. 2, 1171 (1971).

63. S. Sekino, N. Mori and S. Tamukai, Tetsu-to-Hagane 59, 1418 (1973).

64. E. O. Hall, Proc. Phys. Soc. B64, 727 (1951).

65. N. J. Petch, J.I.S.I. 174, 25 (1953).

66. N. S. Stoloff, Fracture, vol. 6, H. Leibowitz, ed., Academic Press, N. Y. 1969, p. 7.

67. N. J. Petch, Proc. Swampscott Conf., MIT Press, 1959, p. 54.

68. C. R. Simcor, A. R. Elsea and G. K. Manning, Trans. AIME 203, 193 (1955).

69. A. M. Adair, J. W. Spretnak and R. Speiser, Ibid., p. 353.

70. J. W. Spretnak and R. Speiser, Trans. AIME 197, 445 (1953).

71. J. C. Fisher, Trans. AIME 200, 1146 (1954).

72. G. V. Smith and R. F. Mehl, Trans. AIME 150, 211 (1942).

73. S. Yano, H. Sakurai, H. Mimura, N. Wakita, T. Ozawa and K. Aori, Trans. I.S.I.J. 13, 133 (1973).

74. C. K. Syn, S. Jin and J. W. Morris, Jr., Met. Trans. 7A, 1827 (1976).

75. M. Enomoto and E. Furubayashi, Mat. Sci. Eng. 24, 123 (1976).

76. J. T. Plewes, Met. Trans. 6A, 537 (1975).

77. M. R. Plichta and H. I. Aaronson, Met. Trans. 5, 2611 (1974).

78. G. R. Speich and A. Szirmae, Trans. AIME 245, 1063 (1969).

79. G. A. Roberts and R. F. Mehl, Trans. ASM 31, 613 (1943).

80. R. R. Judd and H. W. Paxton, Trans. AIME, 242, 206 (1968).

81. A. E. Nehrenberg, Trans. AIME 188, 162 (1950).

82. J. W. Christian, The Theory of Transformations in Metals and Alloys, Pergamon Press, New York, 1965.

83. R. L. Miller, Met. Trans. 3, 905 (1972).

84. H. Fischmeister, J. O. Hjalmered, B. Karlsson, G. Linden, and B. Sundstrom, The Microstructure and Design of Alloys, Proc. 3rd Internat. Conf. on Strength of Metals and Alloys,Inst. of Metals and Iron Steel Inst., London, 1973, p. 621.

85. N. J. Kim, unpublished work.

86. T. Kunio, M. Shimizu, K. Yamada and H. Suzuki, Eng. Fracture Mechanics 7, 411 (1975).

87. J. Y. Koo, M. Raghavan and G. Thomas, Met. Trans. 11A, 351 (1980).

88. Annual Book of ASTM Standards, Designation E23-72, 1973, p. 277.

89. J. Russ, EDAX Editor 1, 8 (1973).

90. P. A. Tichauer, WRC Bulletin 201, 1 (1974).

Table 1. Alloy Composition (wt. pct.)

Alloy	Fe	C	Mn	Si	P	S	B
Fe/1.5Mn/.06C	Bal.	.06	1.51	.05	.06	.05	---
Fe/1.5Mn/.06C/.002B	Bal.	.06	1.48	.04	.07	.06	.002

Table 2. Phase Transformation Temperatures (°C)

Alloy No.	M_s	M_f	A_s	A_f
1	440	342	745	890
2	436	340	742	890

Table 3. Mechanical Properties of the As-Hot-Rolled Fe/1.5Mn/.06C Steel with Finish Rolling Temperature

Finish rolling temp. (°C)	DBTT (°C)	YS (ksi)	UTS (ksi)	e_u (%)	e_T (%)
750	-122	65.0	93.2	17.2	30.9
800	-110	65.1	92.8	17.5	31.2
850	-109	64.4	91.0	17.0	30.8
900	-98	61.6	86.6	16.5	30.1
950	-90	55.6	80.0	17.8	31.5

Table 4. Property Specifications for Arctic Pipeline and Typical Mechanical Properties of the As-Hot-Rolled Fe/1.5Mn/.06C Steel With and Without Cold Working

	σ_Y (ksi)	σ_{UTS} (ksi)	Charpy shelf energy	
			Transverse	Longitudinal
Arctic Pipeline[90]	75	85	68 ft-lb at -60°C	100-125 ft-lb at -60°C
Fe/1.5Mn/.06C (as hot-rolled)	65	93.2	110 ft-lb up to -100°C	135 ft-lb up to -100°C
Fe/1.5Mn/.06C (with 2% cold reduction)	86	94.2	95 ft-lb up to -100°C	125 ft-lb up to -150°C

Table 5. Mechanical Properties of the As-Hot-Rolled Fe/1.5Mn/.06C/.002B Alloy with Finish Rolling Temperature

Finish rolling temp. (°C)	DBTT (°C)	Y.S. (ksi)	U.T.S. (ksi)	e_u (%)	e_T (%)
800	-48	97.8	120.2	5.2	21.8
850	-35	108.5	128.7	3.7	17.5
900	-32	110.1	128.0	3.9	18.4
950	-35	108.4	127.5	3.9	18.2

Table 6. Mechanical Properties of Type I Ferritic-Martensitic Steel

Annealing temp (°C)	% Ms	σ_Y (ksi)	σ_{UTS} (ksi)	e_u (%)	e_T (%)	DBTT (°C)
750	10	47.2	80.5	18.3	37.5	-81
820	20	58.8	84.8	15.2	29.8	-84
855	40	68.9	99.8	13.6	26.7	-80

Table 7. Mechanical Properties of Type II Ferritic Martensitic Steel

Annealing temp (°C)	% Ms	σ_Y (ksi)	σ_{UTS} (ksi)	e_u (%)	e_T (%)	DBTT (°C)
820	25	58.9	90.1	15.4	30.1	-42
855	45	69.7	98.7	13.6	26.5	-41

Table 8. Chemical Composition of the Constituents of Various Duplex Structures

Duplex Structure	Constituent	Fe (w/o)	Mn (w/o)
Ferrite-bainite	Ferrite	98.48	1.44
	Bainite	98.40	1.52
Martensite-bainite	Martensite	98.41	1.51
	Bainite	98.41	1.45
Ferrite-martensite (I)	Ferrite	98.62	1.30
	Martensite	98.26	1.66
Ferrite-martensite (II)	Ferrite	98.66	1.26
	Martensite	98.22	1.70

Figure Captions

Fig. 1. Schematic diagram of thermomechanical treatment for the Fe/1.5Mn/.06C alloy.

Fig. 2. Schematic diagram of thermomechanical treatment for the Fe/1.5Mn/.06C/.002B alloy.

Fig. 3. Dilatometry specimen for measuring phase transformation temperatures.

Fig. 4. Standard Charpy impact test specimen.

Fig. 5. Subsize cylindrical tensile test specimen.

Fig. 6. Optical micrographs of the prior austenite grain (a) just before rolling; (b) after 35% deformation at 1000°C.

Fig. 7. Optical micrograph of the as-hot-rolled specimen showing elongated grains.

Fig. 8. Optical micrographs of the ferrite-bainite structure finish rolled at 850°C with (a) 30% reduction; (b) 50% reduction.

Fig. 9. Optical micrographs of the ferrite-bainite structure for different finish rolling temperatures: 1000°C, 35% → T°C, 50%, (a) 750°C, (b) 800°C, (c) 850°C, (d) 900°C.

Fig. 10. TEM of the upper bainite region (a) bright field, (b) dark field of interlath carbide.

Fig. 11. Acicular ferrite developed in the specimen finish rolled at 900°C.

Fig. 12. Morphology of the interphase carbide precipitation in the vicinity of the ferrite/bainite interface.

Fig. 13. Bright field (a) and dark field (b) of cementite precipitation in the ferrite matrix.

Fig. 14. Bright field (a) and dark field (b) of retained austenite in association with ferrite.

Fig. 15. Variation of the mechanical properties of the as-hot-rolled ferrite-bainite structure with finish rolling temperature. 35%, 1000°C → 50%, T°C.

Fig. 16. Mechanical properties of as-hot-rolled ferrite-bainite structure as a function of the ferrite grain size.

Fig. 17. Ductile-brittle transition curves of as-hot-rolled ferrite-bainite structure with various finish rolling temperatures.

Fig. 18. Ductile-brittle transition curves of Fe/1.5Mn/.06C alloy for different testing direction.

Fig. 19. Effect of specimen geometry on the ductile-brittle transition curves of the as-hot-rolled ferrite-bainite structure (finish rolled at 800°C).

Fig. 20. Variation of mechanical properties of the as-hot-rolled ferrite-bainite structure with cold reduction.

Fig. 21. Optical micrographs of the as-hot-rolled boron treated alloy with various finish rolling temperatures. 1000°C, 35% → T°C, 50% (a) 800°C, (b) 850°C, (c) 900°C.

Fig. 22. TEM of the as-hot-rolled boron treated alloy showing martensite and upper bainite (finish rolled at 850°C). (a) bright field, (b) dark field of interlath retained austenite in martensite, (c) dark field of interlath carbide in upper bainite.

Fig. 23. Mechanical properties of the as-hot-rolled martensitic-bainitic structure with finish rolling temperature. 35%, 1000°C → 50% T°C.

Fig. 24. Ductile-brittle transition curves of the as-hot-rolled martensitic-bainitic structure with various finish rolling temperatures.

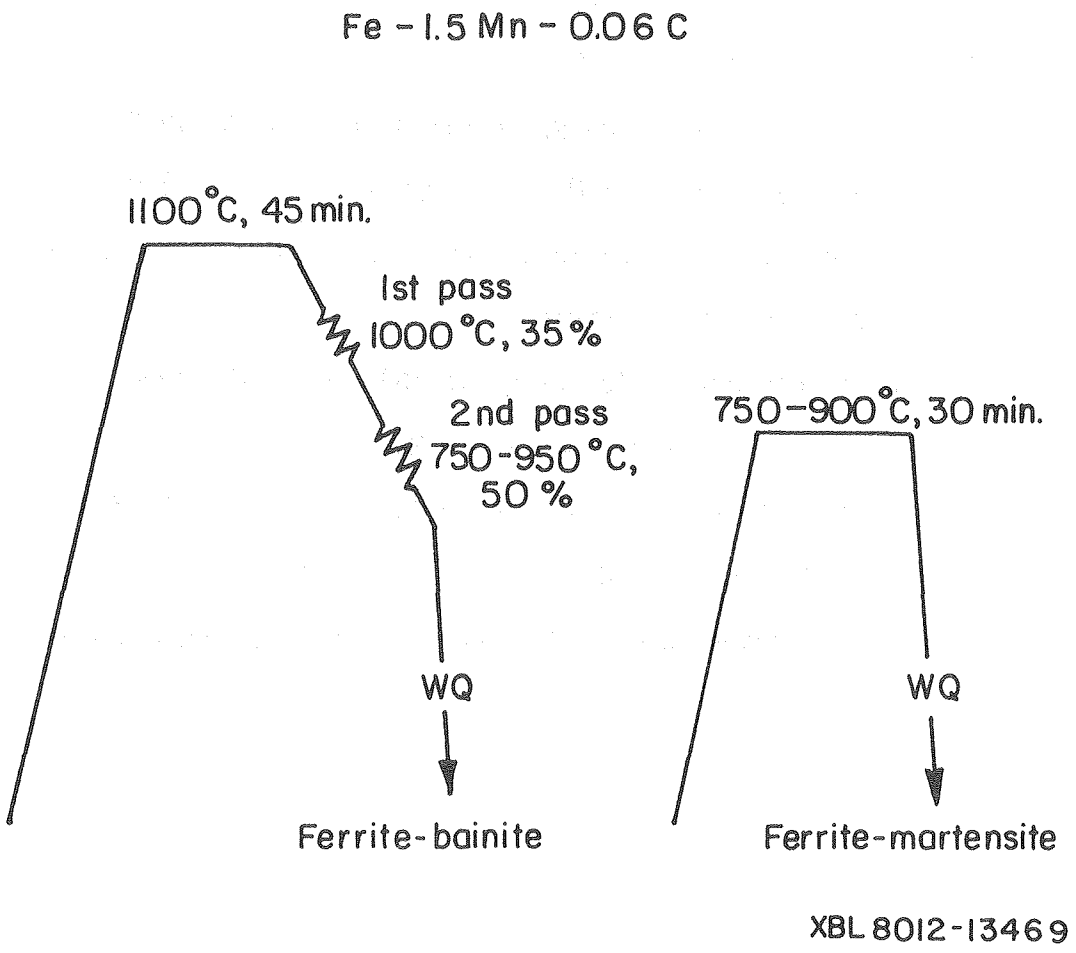
Fe - 1.5 Mn - 0.06 C
1100°C, 45 min.
1st pass
1000°C, 35%
2nd pass
750-950°C,
50%
WQ
Ferrite-bainite
750-900°C, 30 min.
WQ
Ferrite-martensite
XBL 8012-13469

Fig. 1

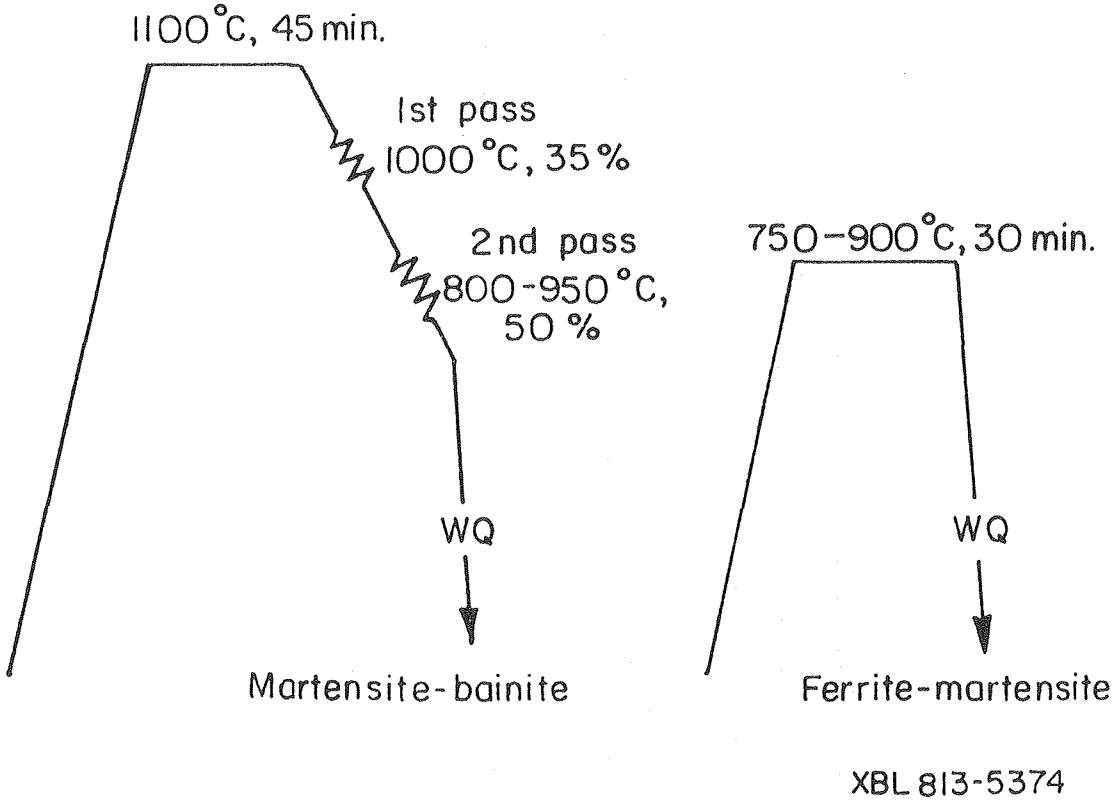
Fe - 1.5 Mn - 0.06 C - 0.002 B
1100°C, 45 min.
1st pass
1000°C, 35%
2nd pass
800-950°C,
50%
WQ
Martensite-bainite
750-900°C, 30 min.
WQ
Ferrite-martensite
XBL 813-5374

Fig. 2

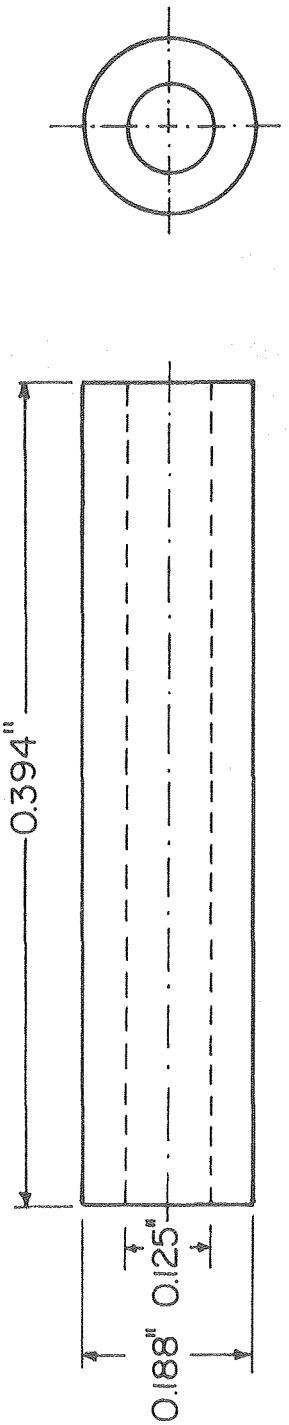

XBL 7910-7192

Fig. 3

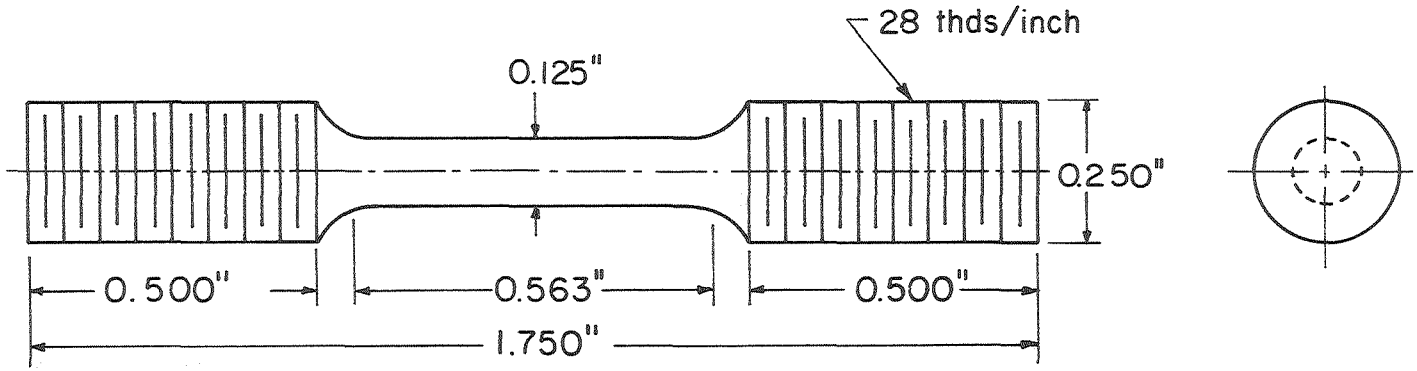

XBL 774-5354

Fig. 4

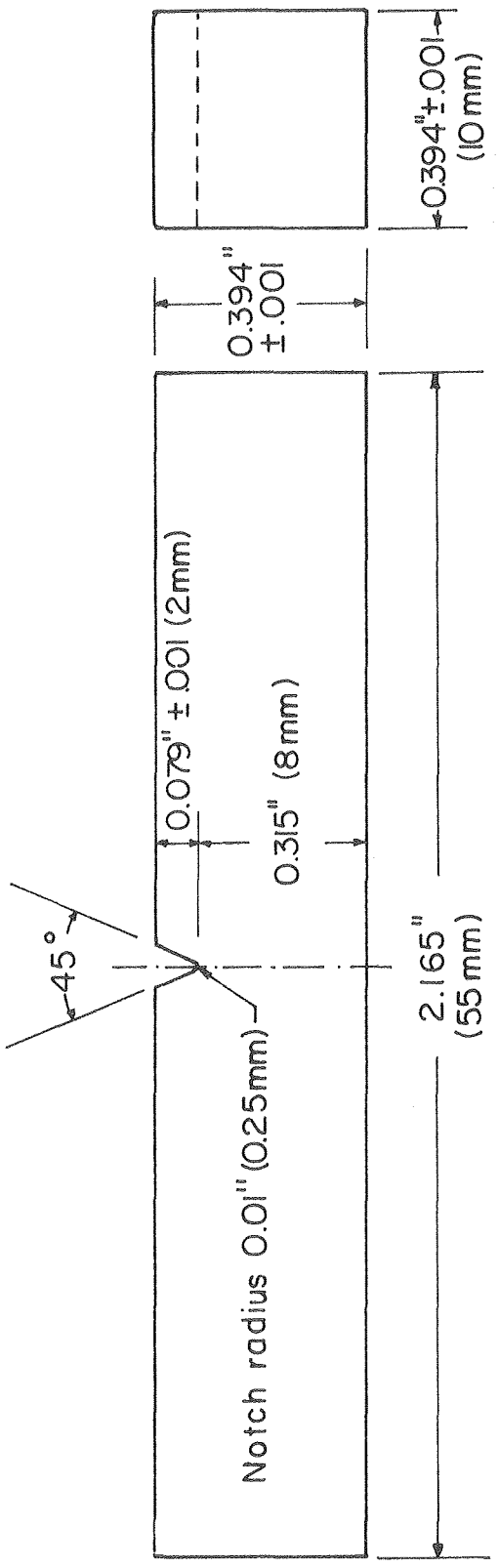

XBL 7910-7195

Fig. 5

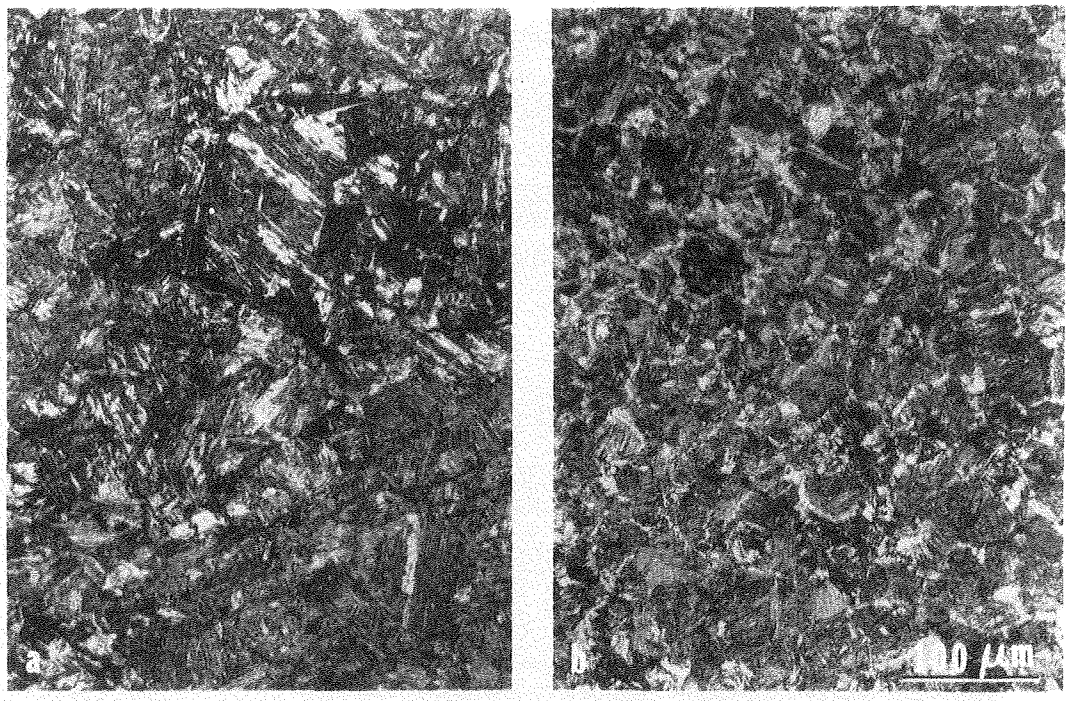

XBB 814-3213

Fig. 6

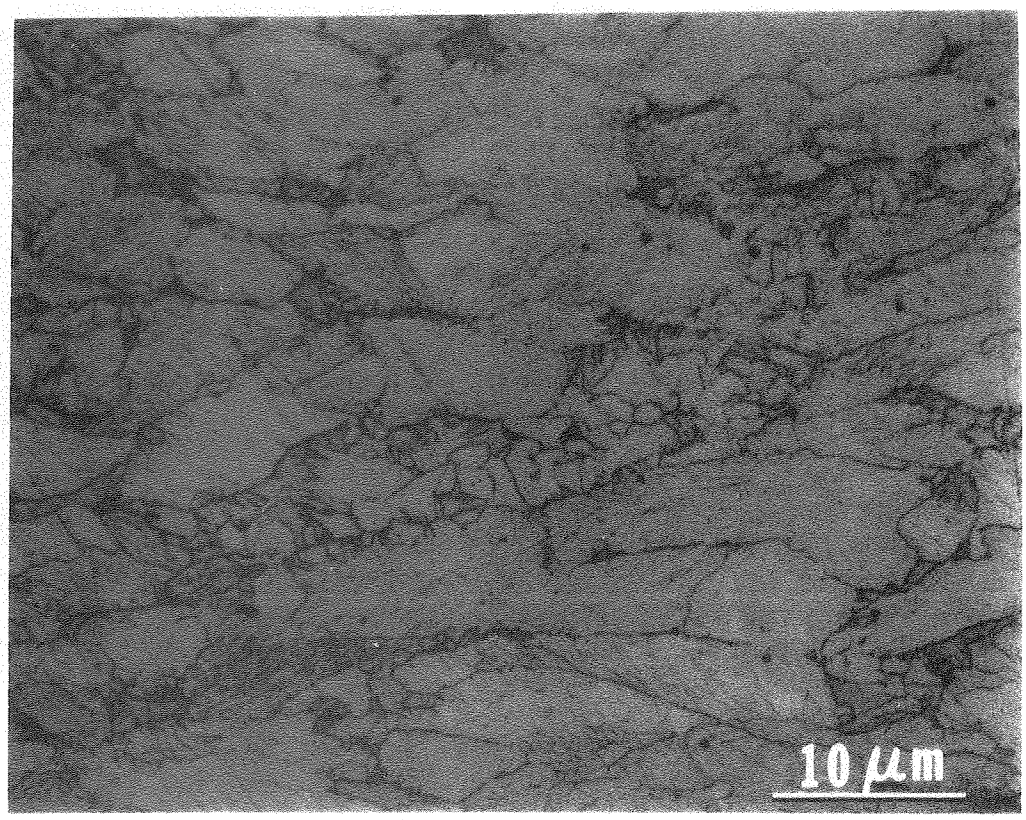

XBB 814-3886

Fig. 7

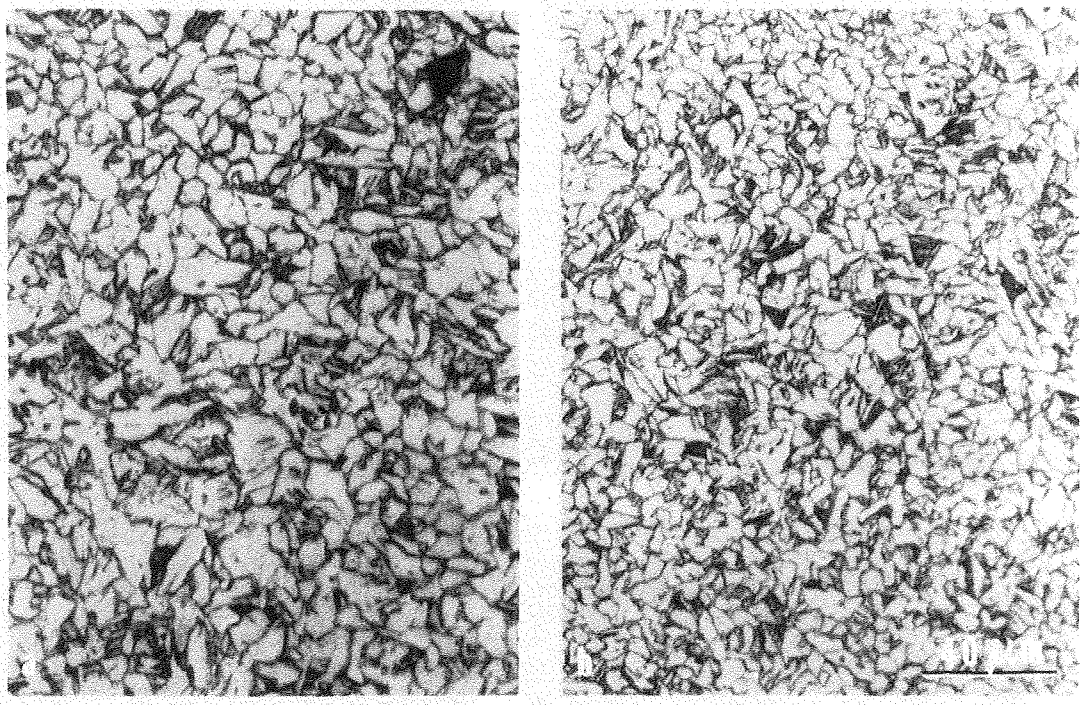

XBB 814-3217

Fig. 8

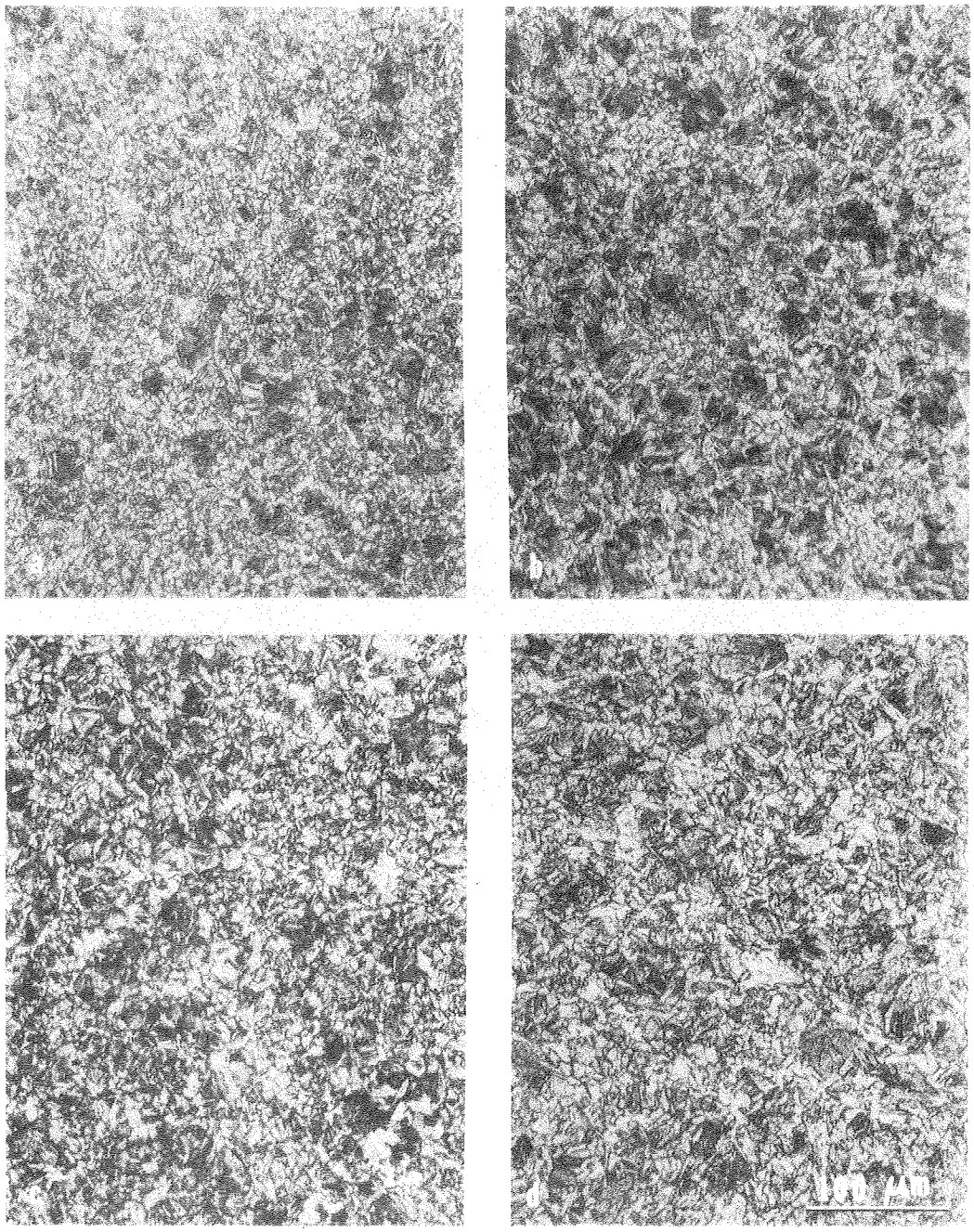

XBB 814-3218

Fig. 9

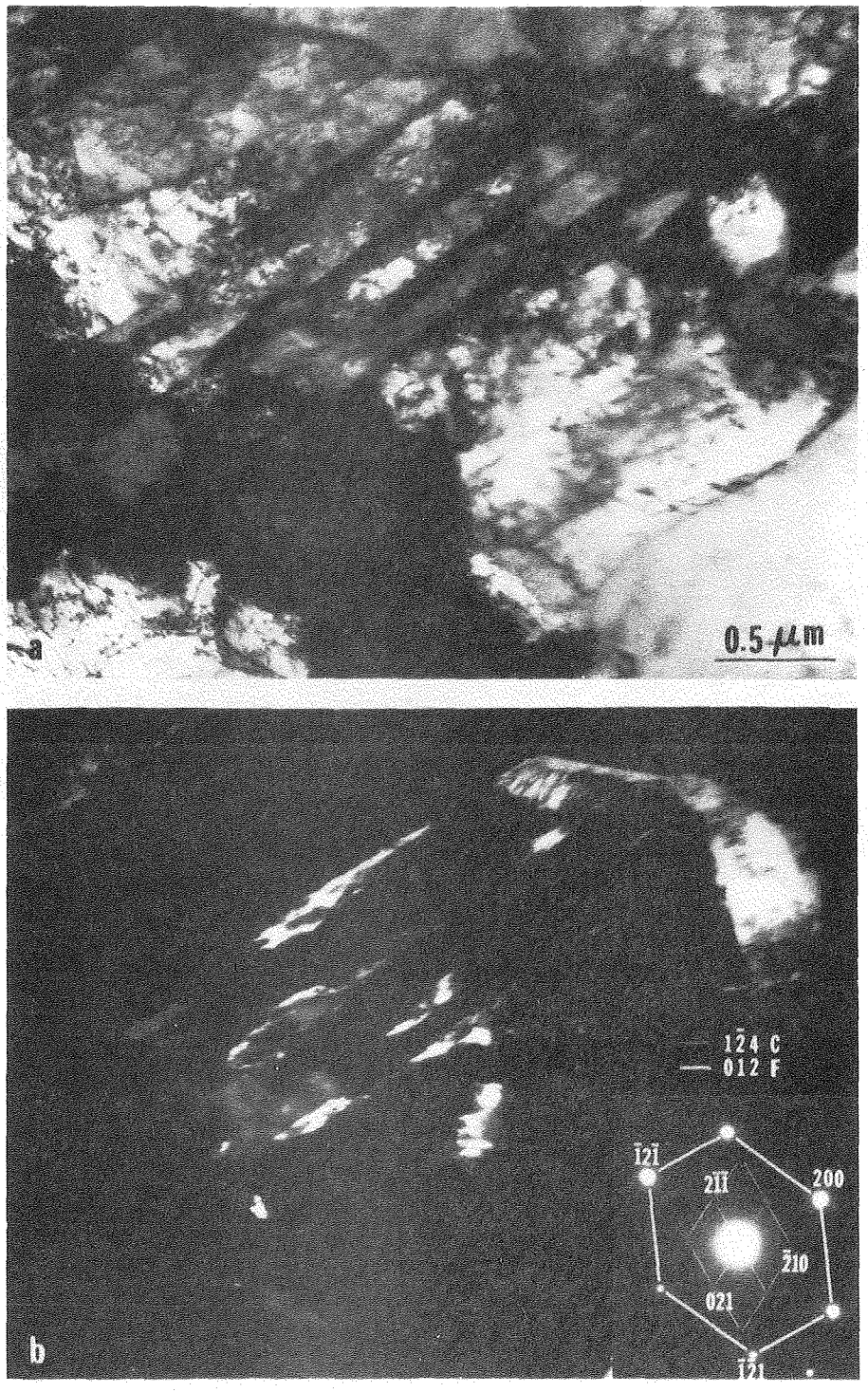

XBB 814-3203

Fig. 10

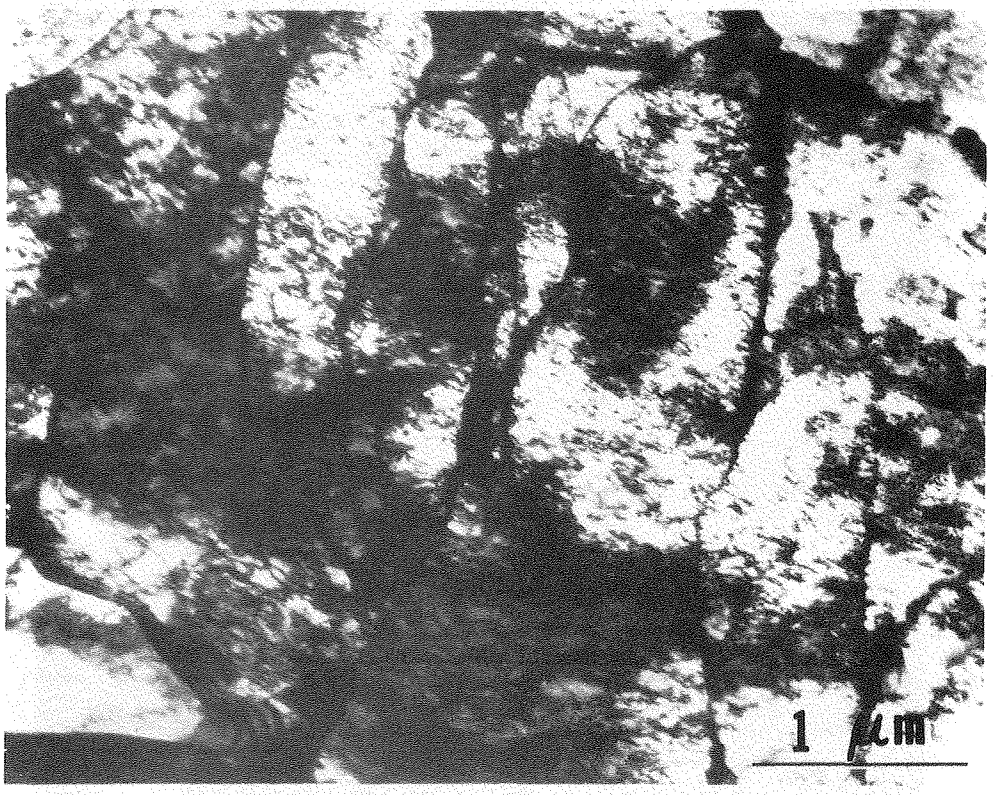

XBB 814-3204

Fig. 11

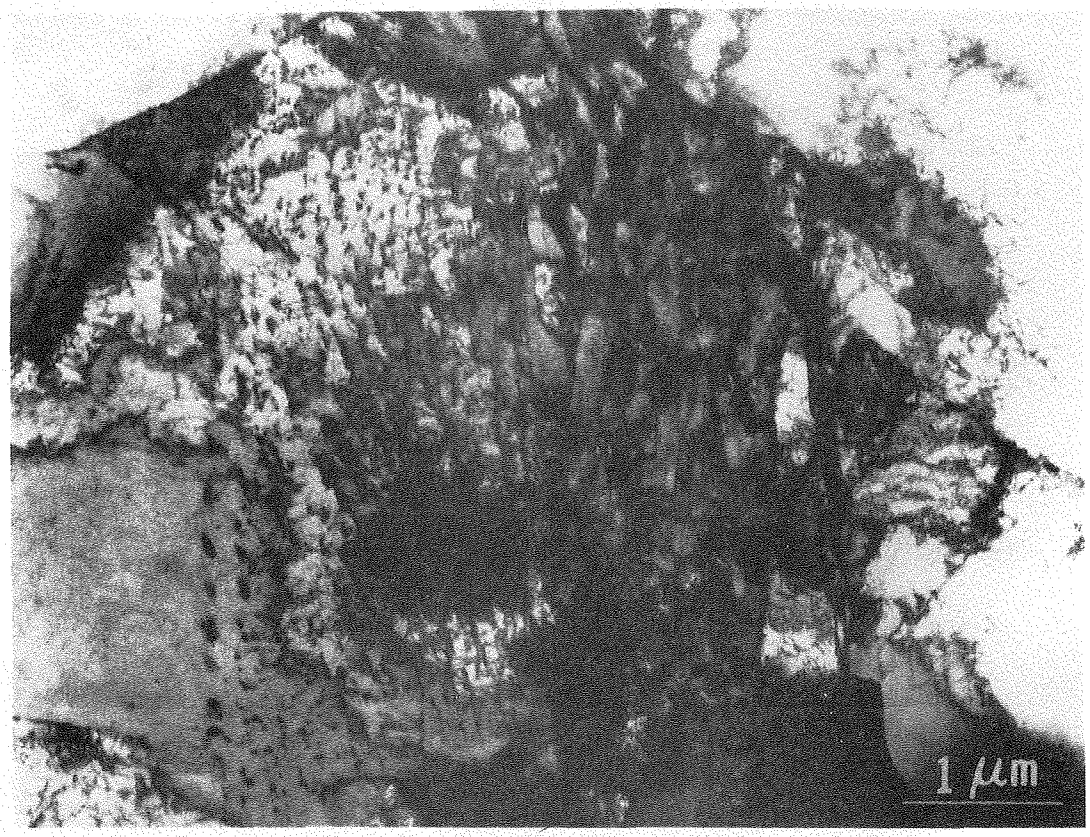

XBB 814-3216

Fig. 12

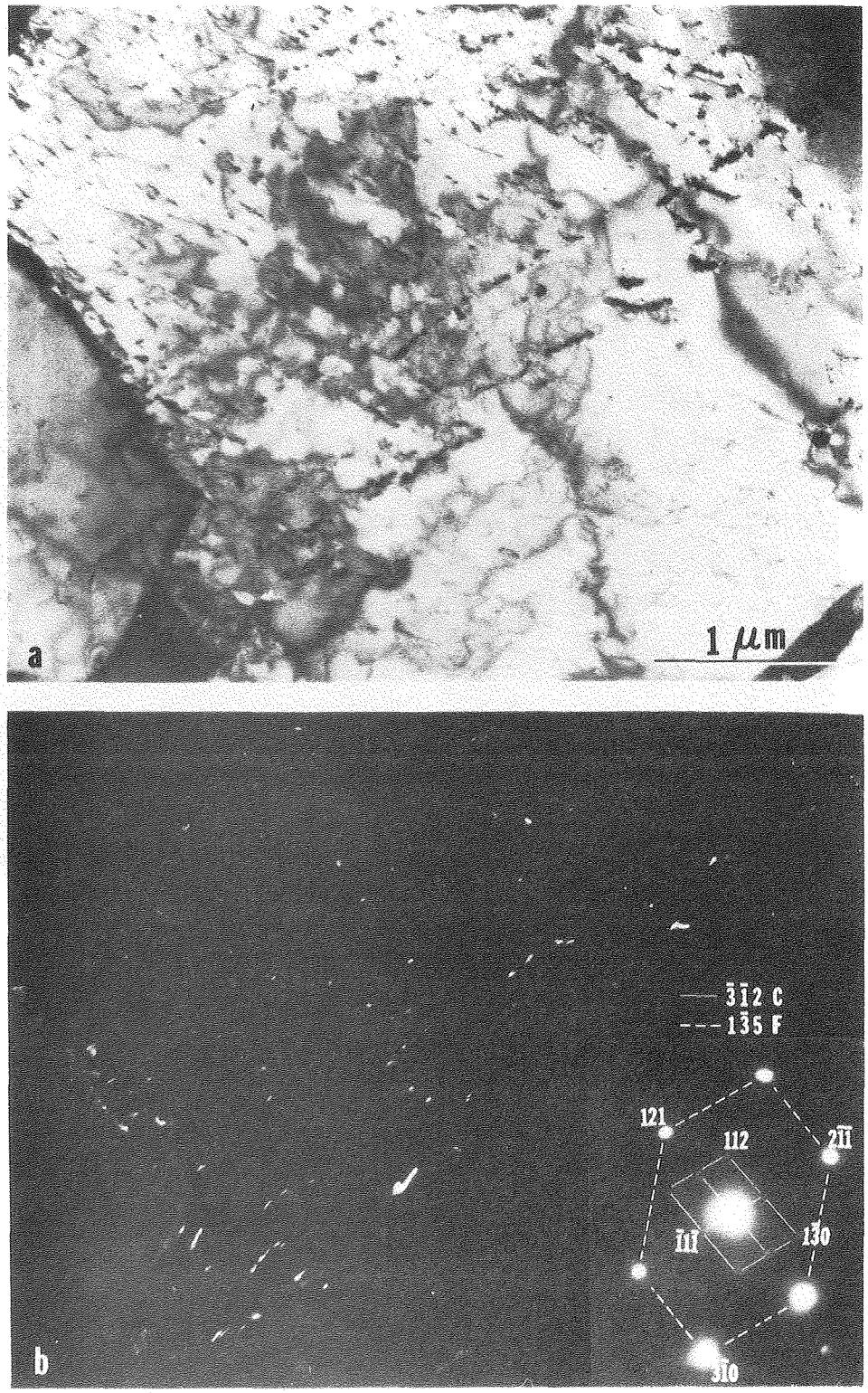

XBB 809-11370

Fig. 13

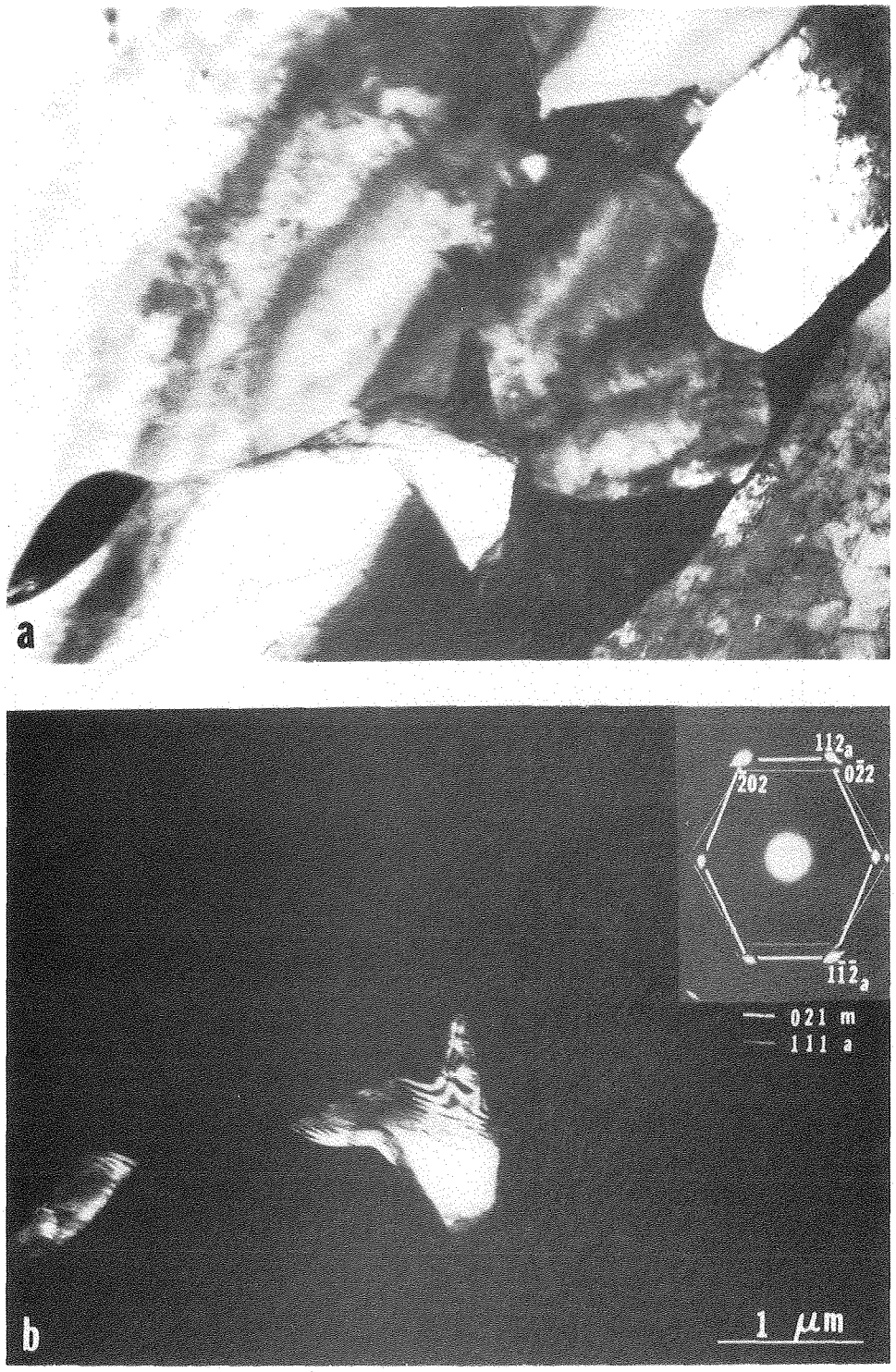

XBB 814-3205

Fig. 14

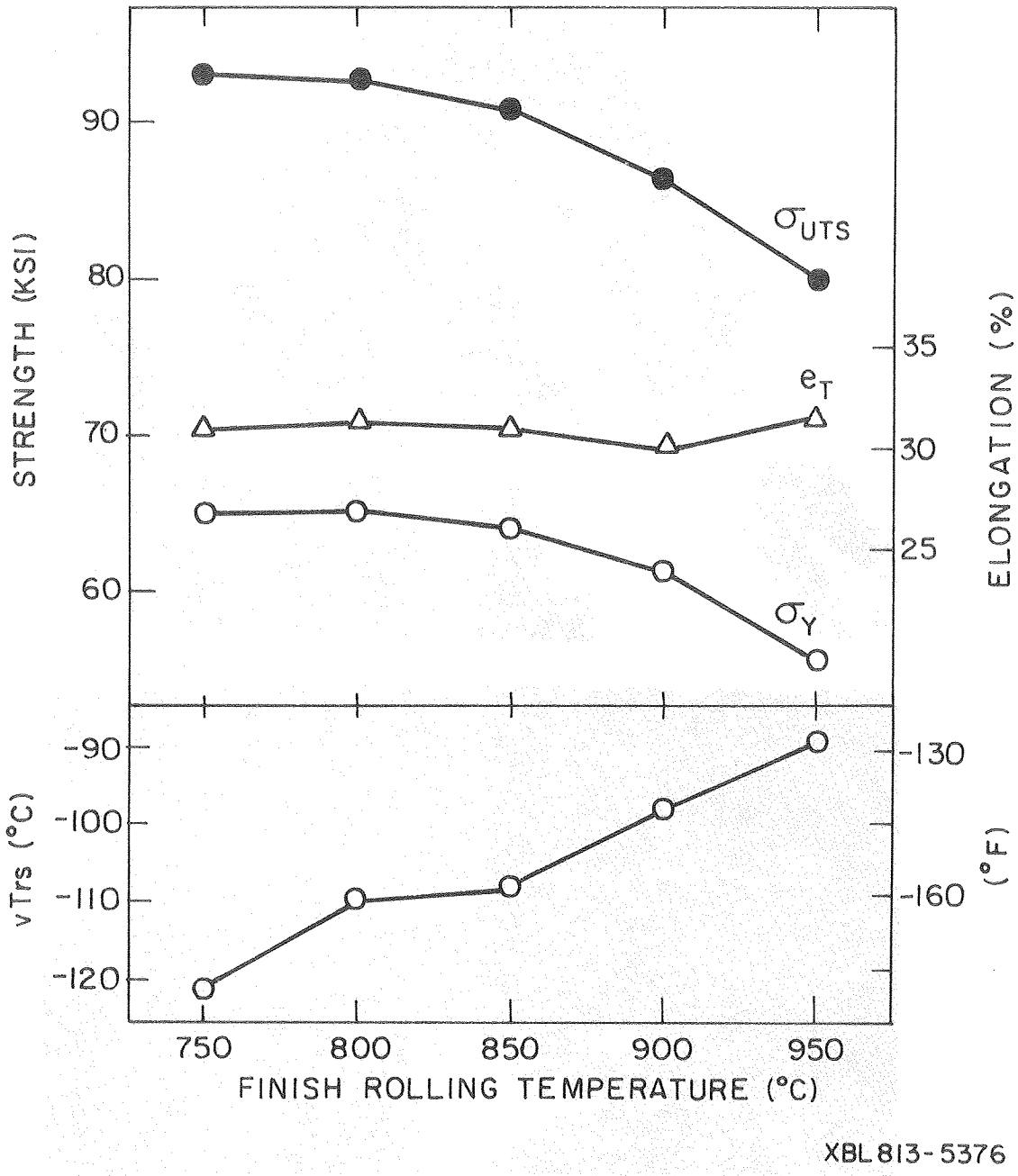
STRENGTH (KSI)
90
80
70
60
σ_{UTS}
e_T
σ_Y
35
30
25
ELONGATION (%)
vTrs (°C)
-90
-100
-110
-120
-130
-160
(°F)
750
800
850
900
950
FINISH ROLLING TEMPERATURE (°C)
XBL813-5376

Fig. 15

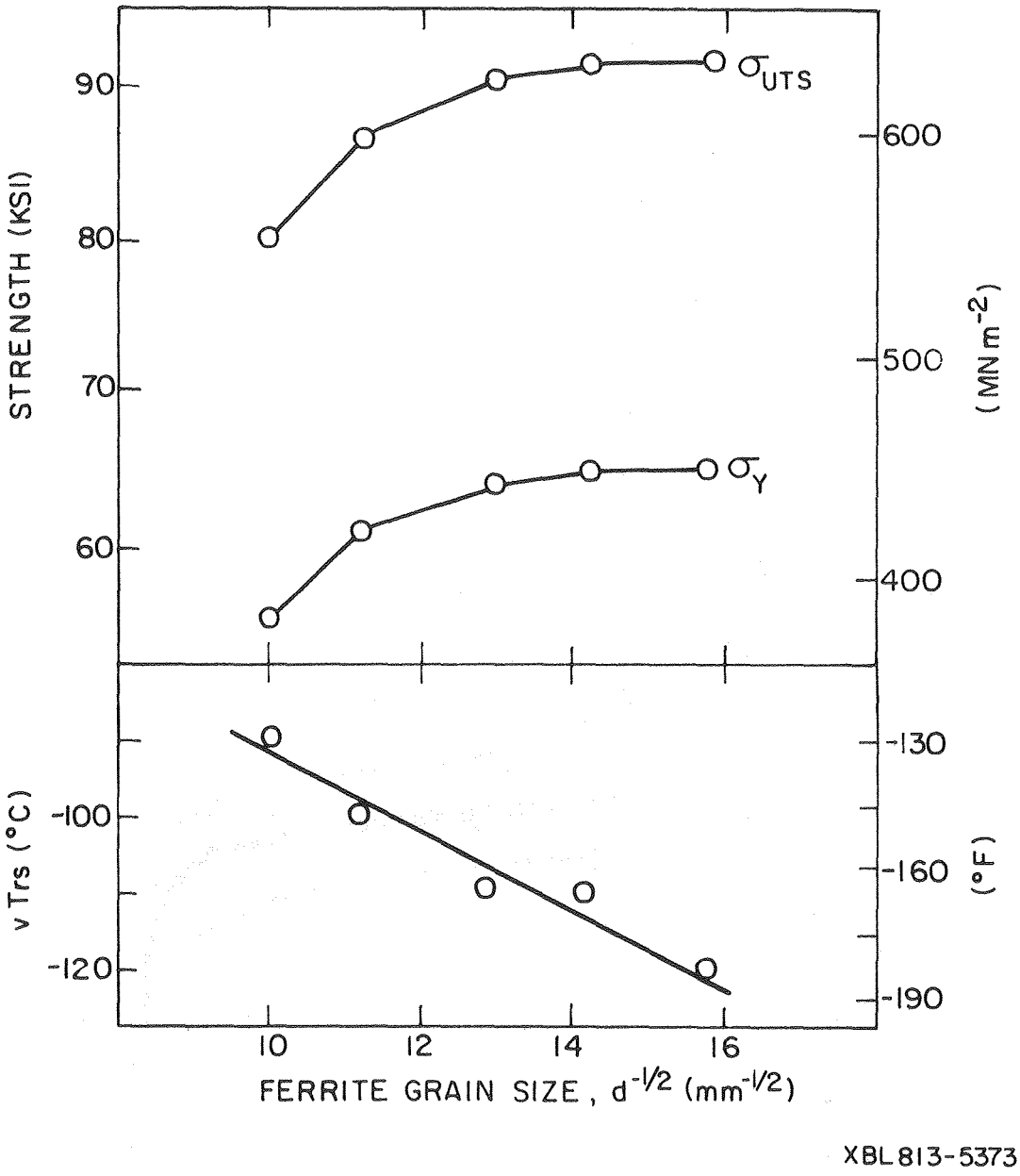
STRENGTH (KSI)
90
80
70
60
σ_{UTS}
σ_Y
600
500
400
(MN m^{-2})
v Trs (°C)
-100
-120
-130
-160
-190
(°F)
10
12
14
16
FERRITE GRAIN SIZE, d$^{-1/2}$ (mm$^{-1/2}$)
XBL813-5373

Fig. 16

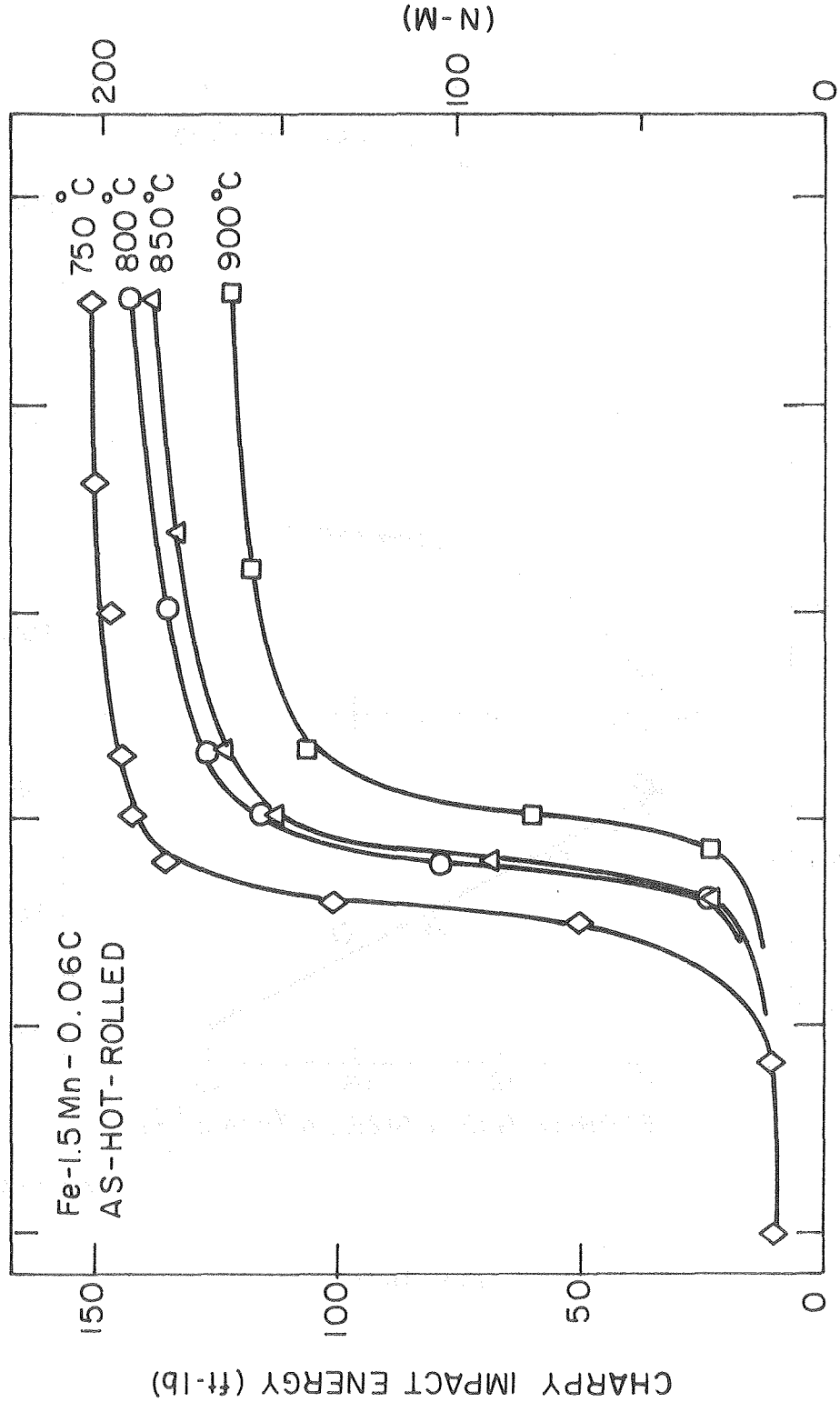
CHARPY IMPACT ENERGY (ft-lb)
150
100
50
0
200
100
0
(N-M)
0
-100
-200
T (°C)
Fe-1.5 Mn-0.06C
AS-HOT-ROLLED
750 °C
800 °C
850 °C
900 °C
XBL813-5381

Fig. 17

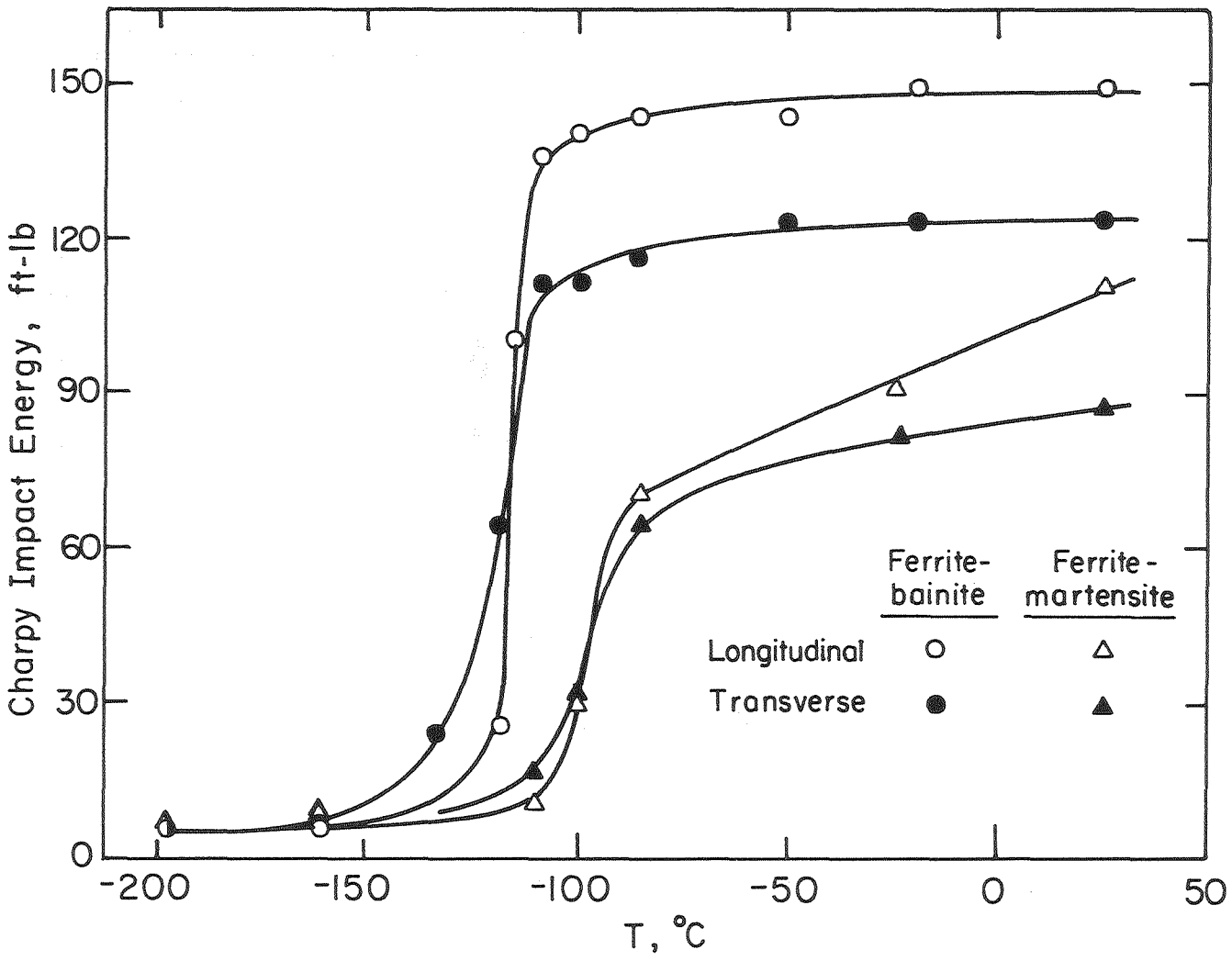
Charpy Impact Energy, ft-lb
150
120
90
60
30
0
-200
-150
-100
-50
0
50
T, °C
Ferrite-bainite
Ferrite-martensite
Longitudinal
Transverse
XBL 8012-13468

Fig. 18

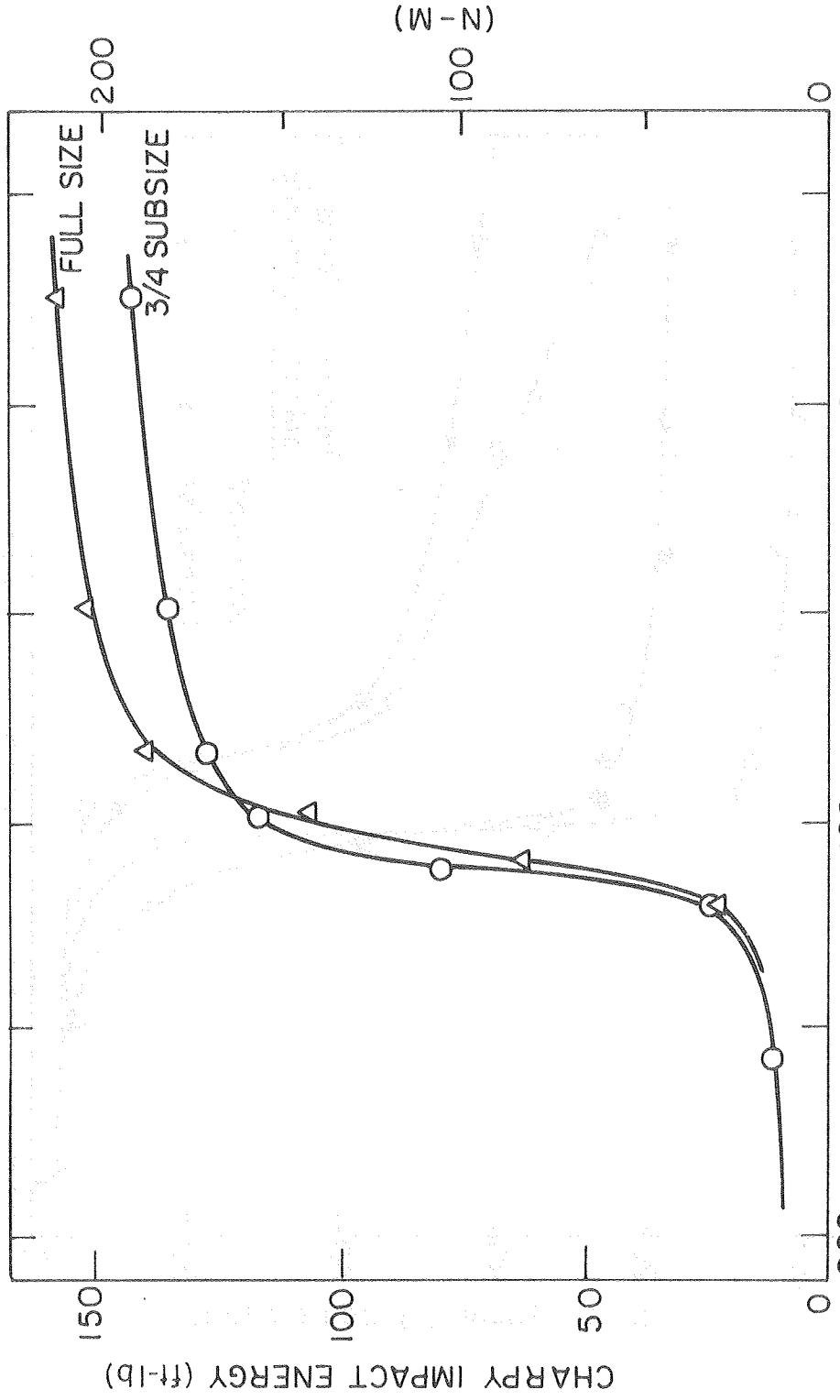

XBL813-5412

Fig. 19

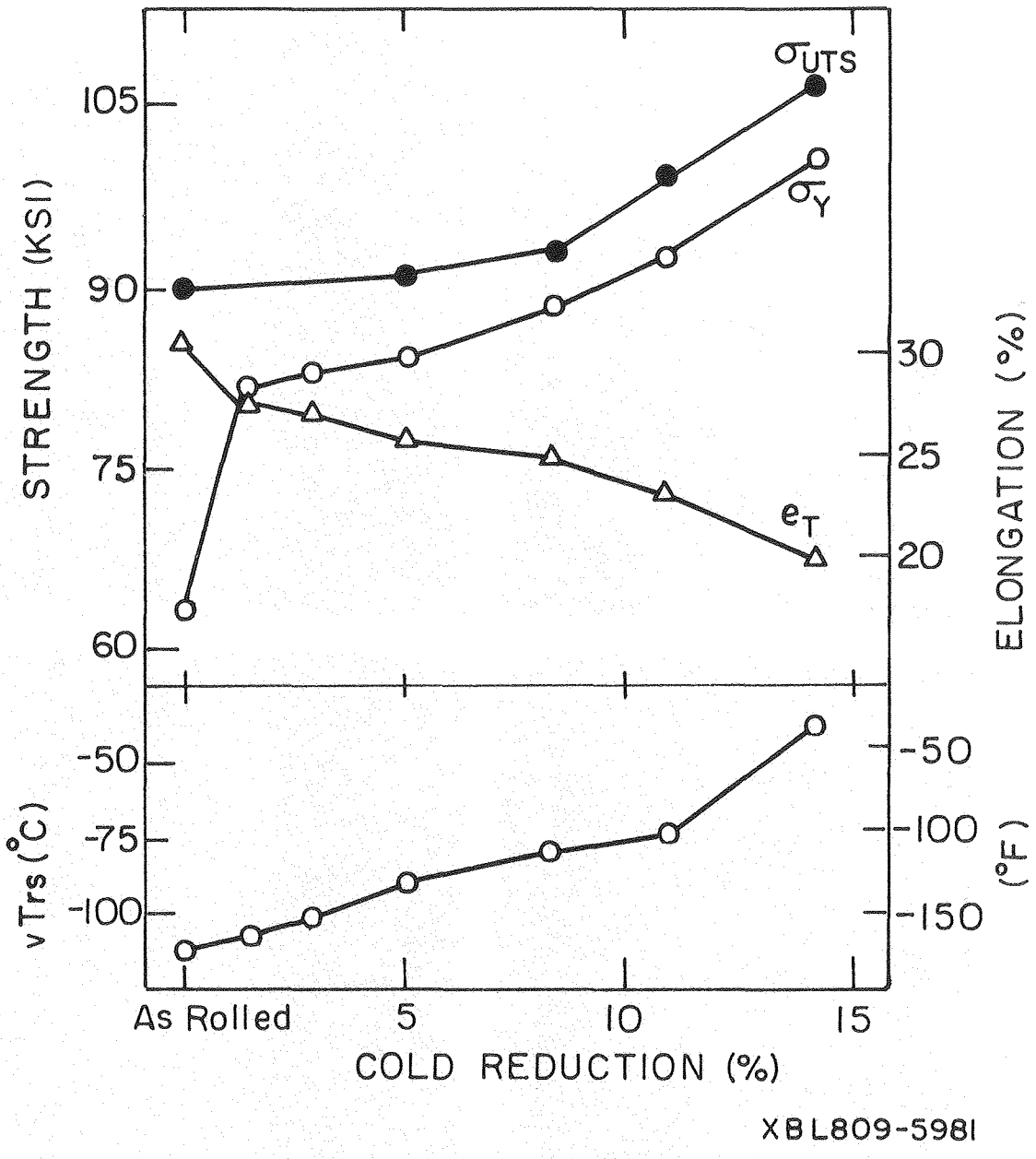
σ_{UTS}
σ_Y
e_T
105
90
75
60
STRENGTH (KSI)
30
25
20
ELONGATION (%)
-50
-75
-100
vTrs (°C)
-50
-100
-150
(°F)
As Rolled
5
10
15
COLD REDUCTION (%)
XBL809-5981

Fig. 20

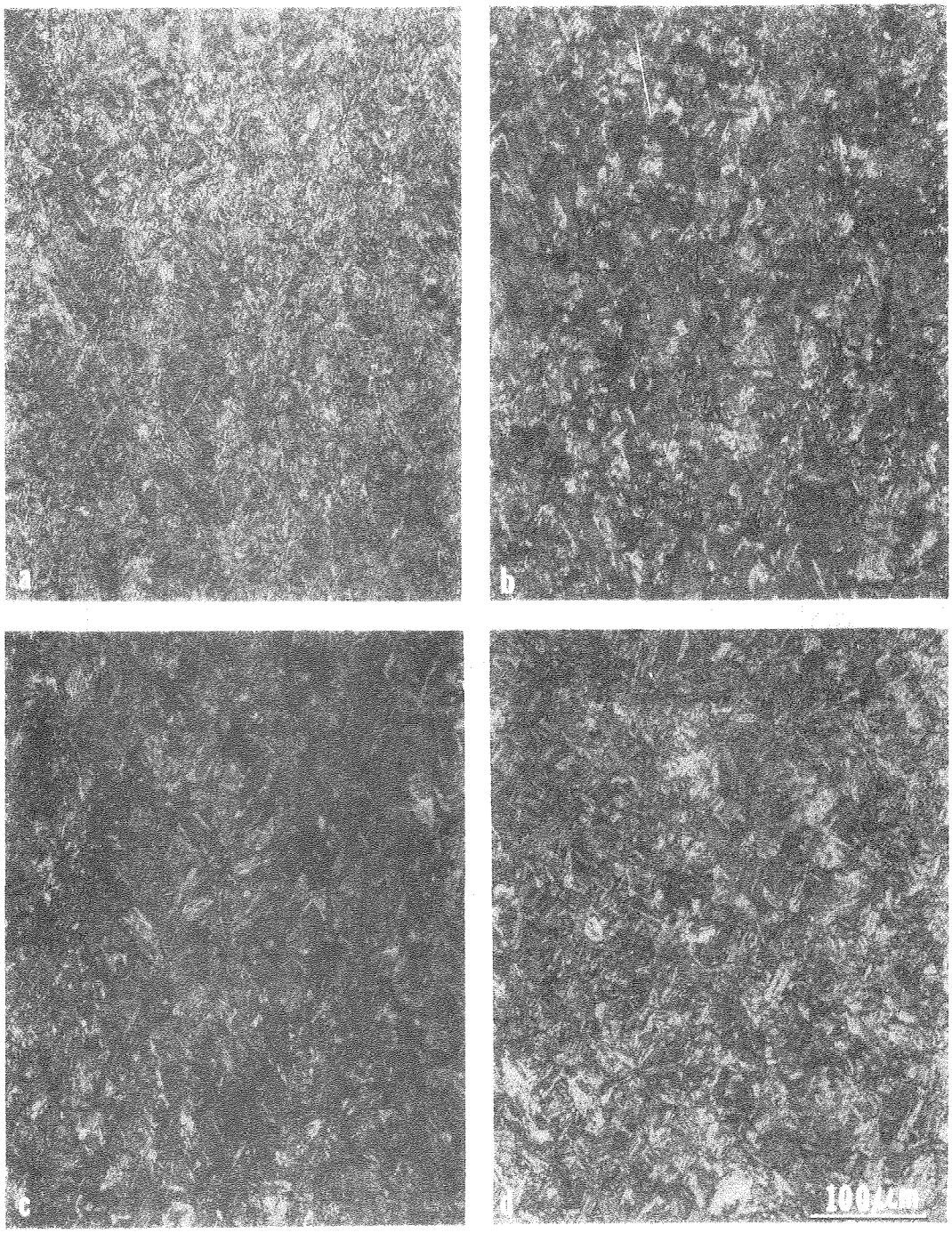

XBB 814-3887

Fig. 21

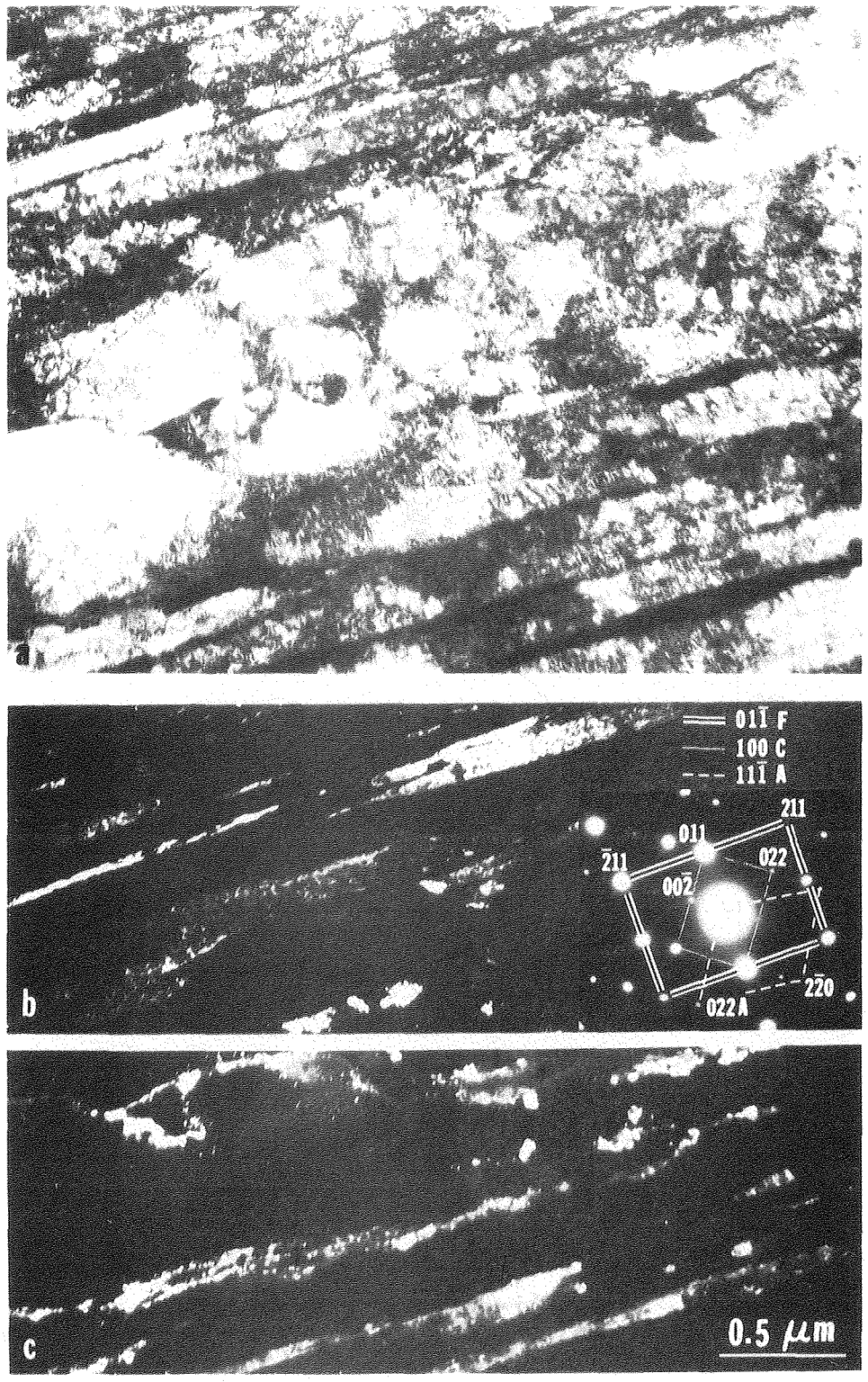

Fig. 22 XBB 814-3889

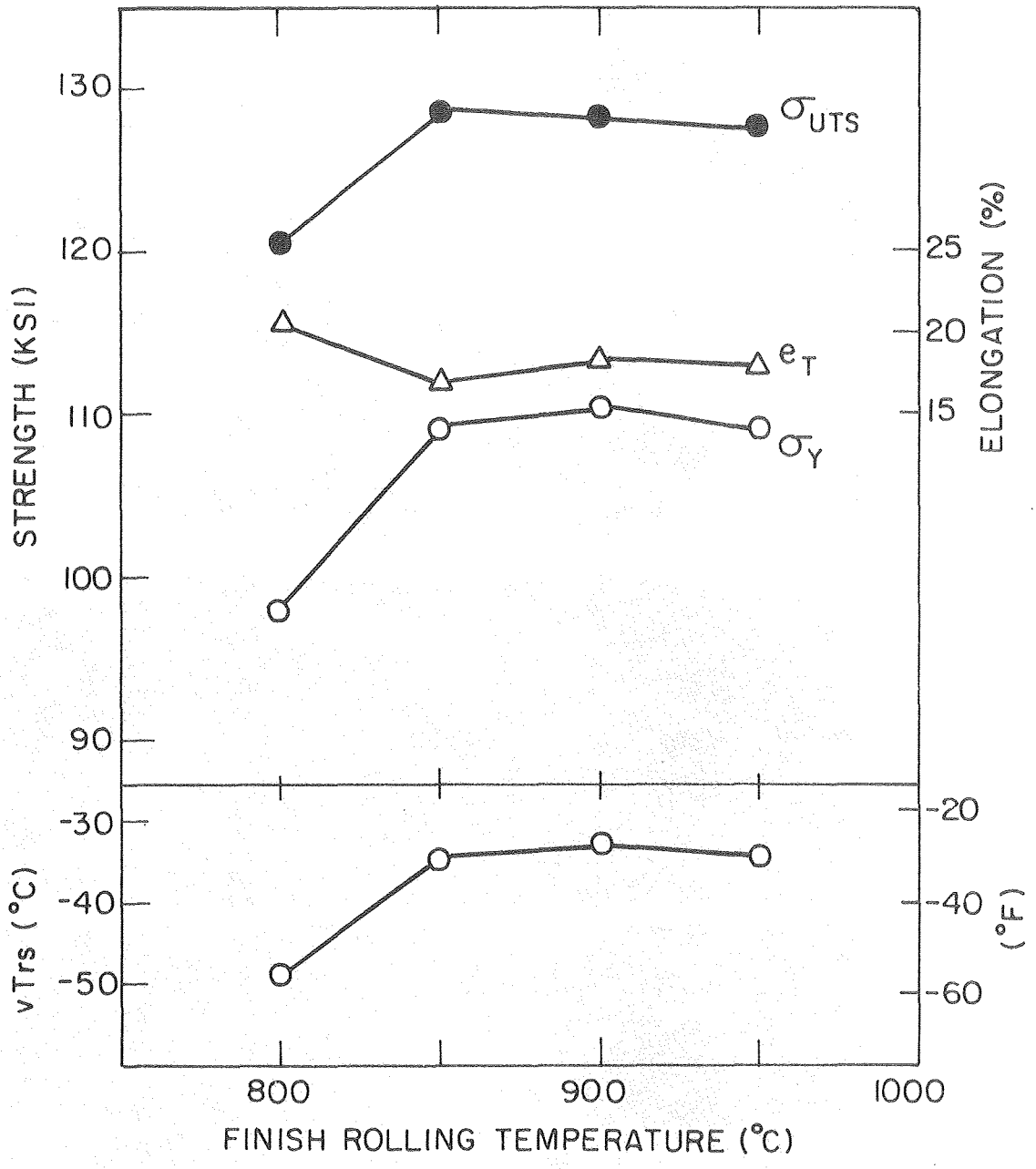
130
120
110
100
90
STRENGTH (KSI)
σ_{UTS}
e_T
σ_Y
25
20
15
ELONGATION (%)
-30
-40
-50
vTrs (°C)
-20
-40
-60
(°F)
800
900
1000
FINISH ROLLING TEMPERATURE (°C)
XBL813-5377

Fig. 23

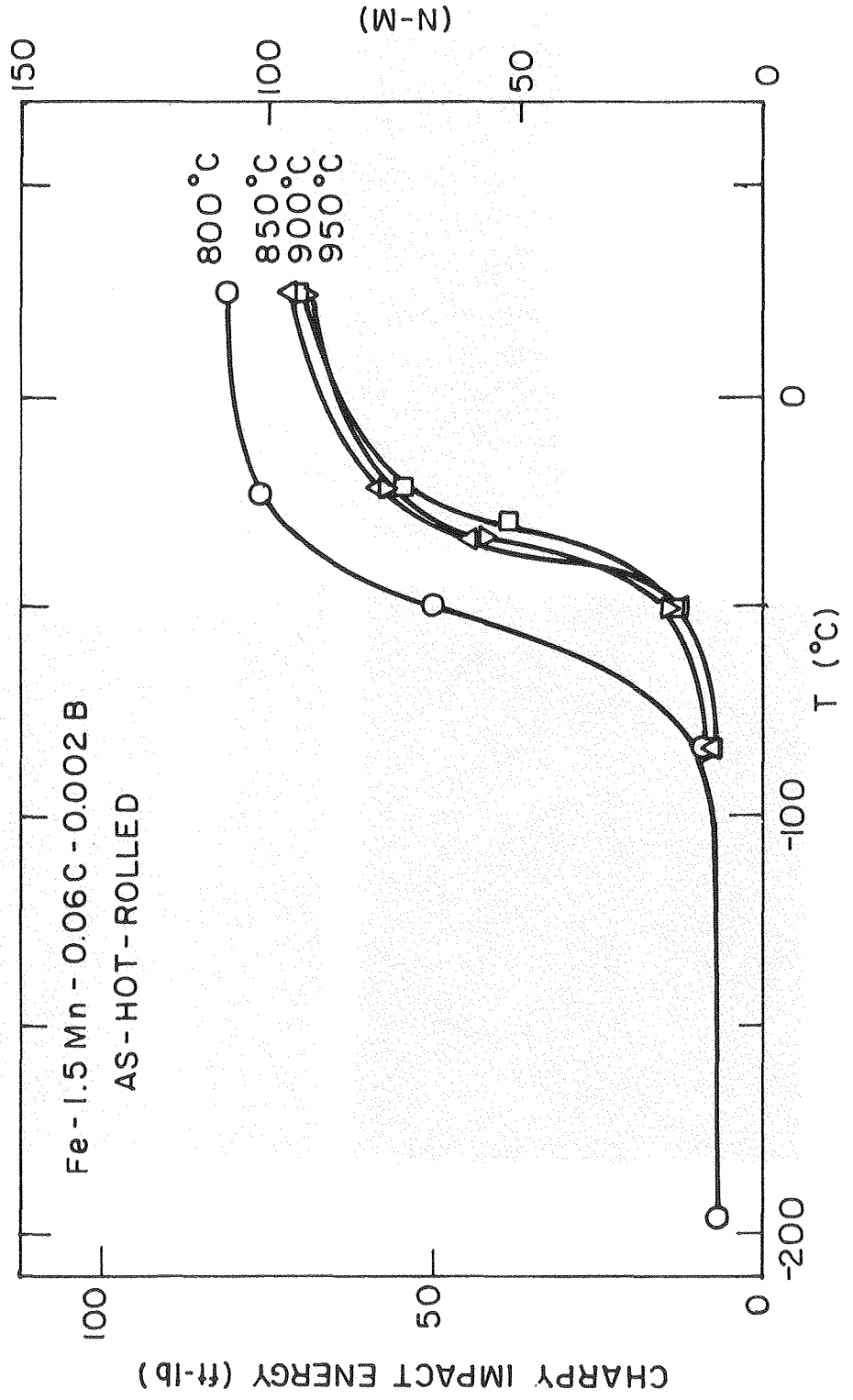
CHARPY IMPACT ENERGY (ft-lb)
100
50
0
-200
-100
0
T (°C)
50
100
150
(N-M)
800 °C
850 °C
900 °C
950 °C
Fe - 1.5 Mn - 0.06 C - 0.002 B
AS-HOT-ROLLED
XBL 813-5380

Fig. 24

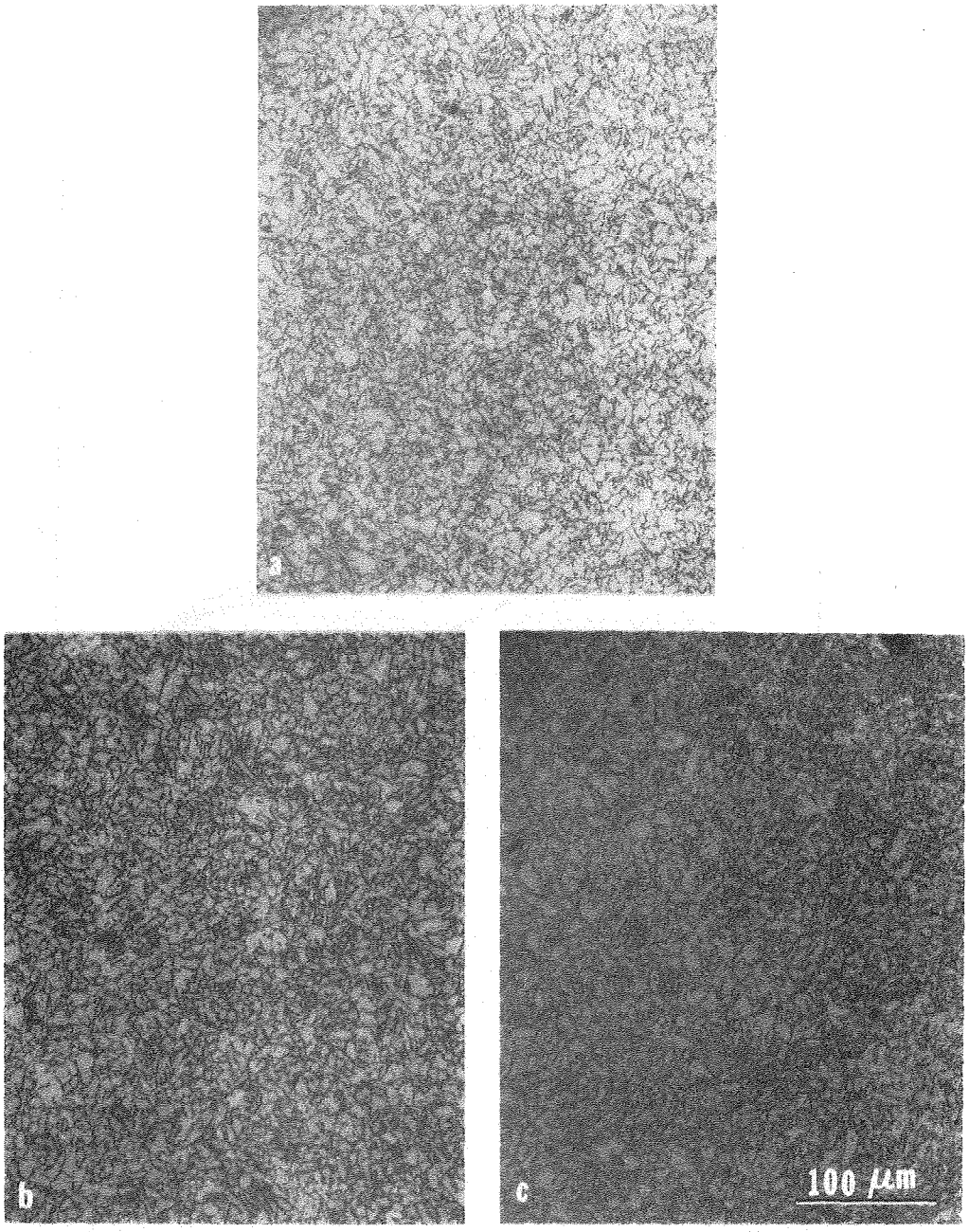

XBB 814-3212

Fig. 25

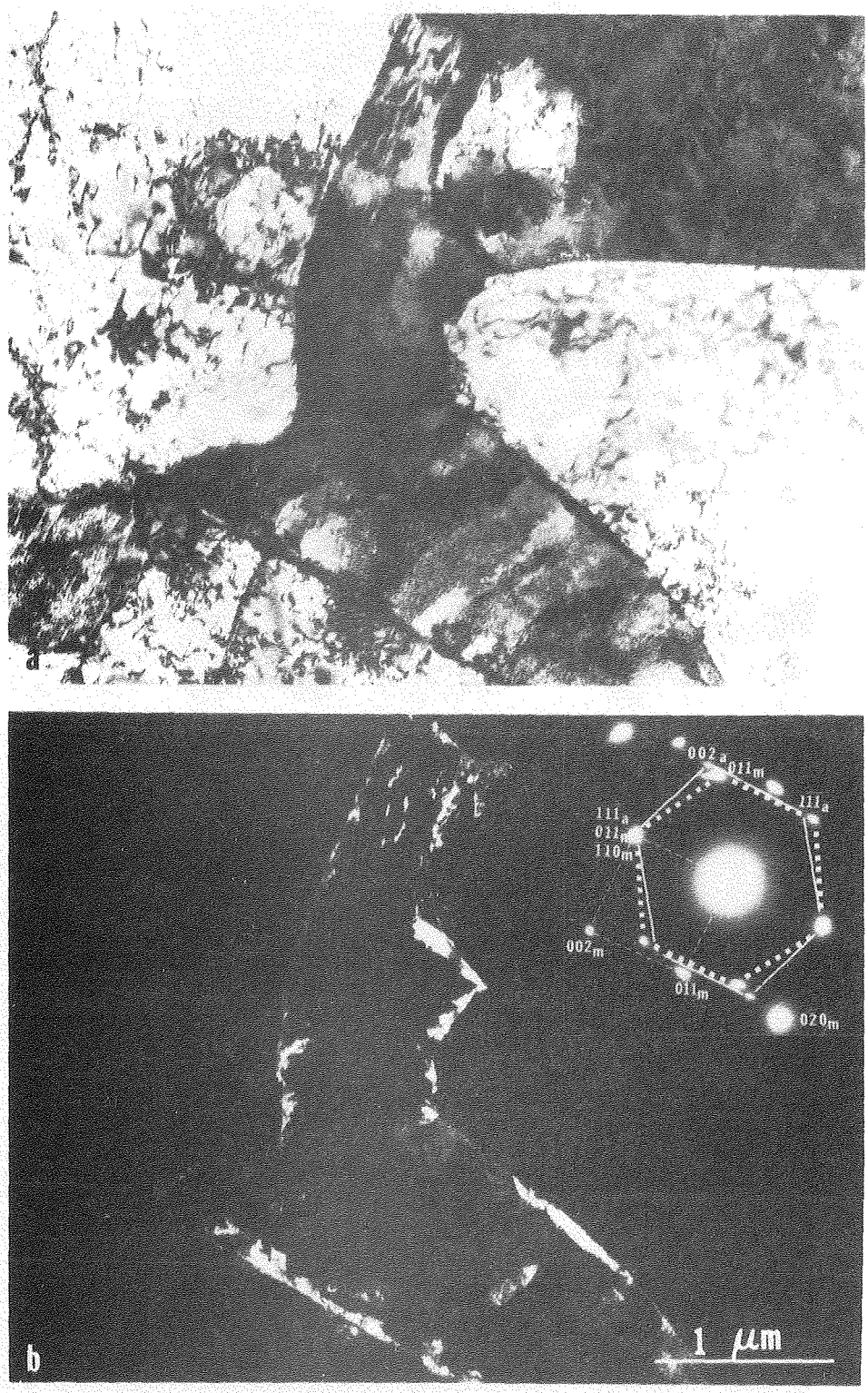

XBB 809-11373

Fig. 26

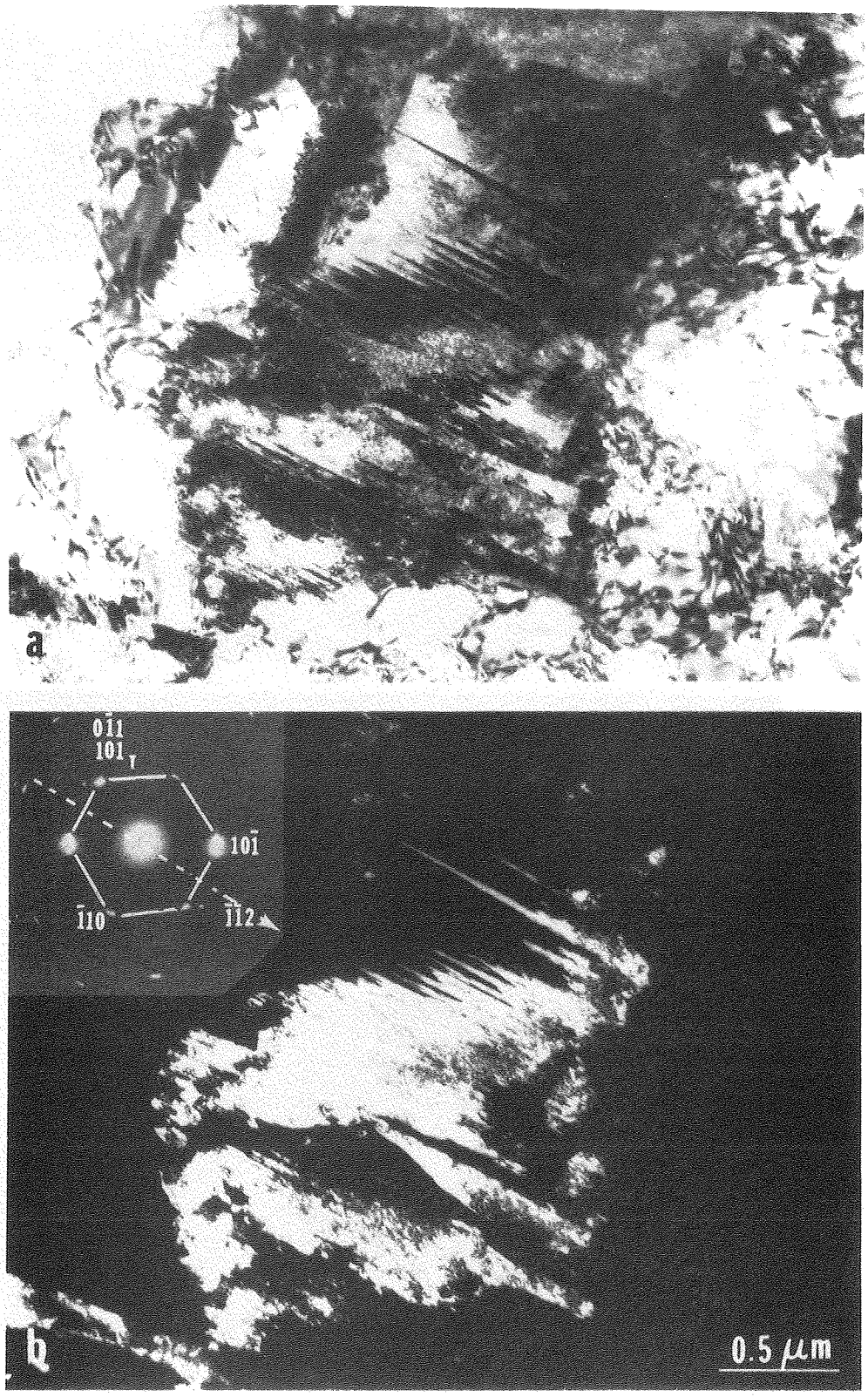

XBB 814-3888

Fig. 27

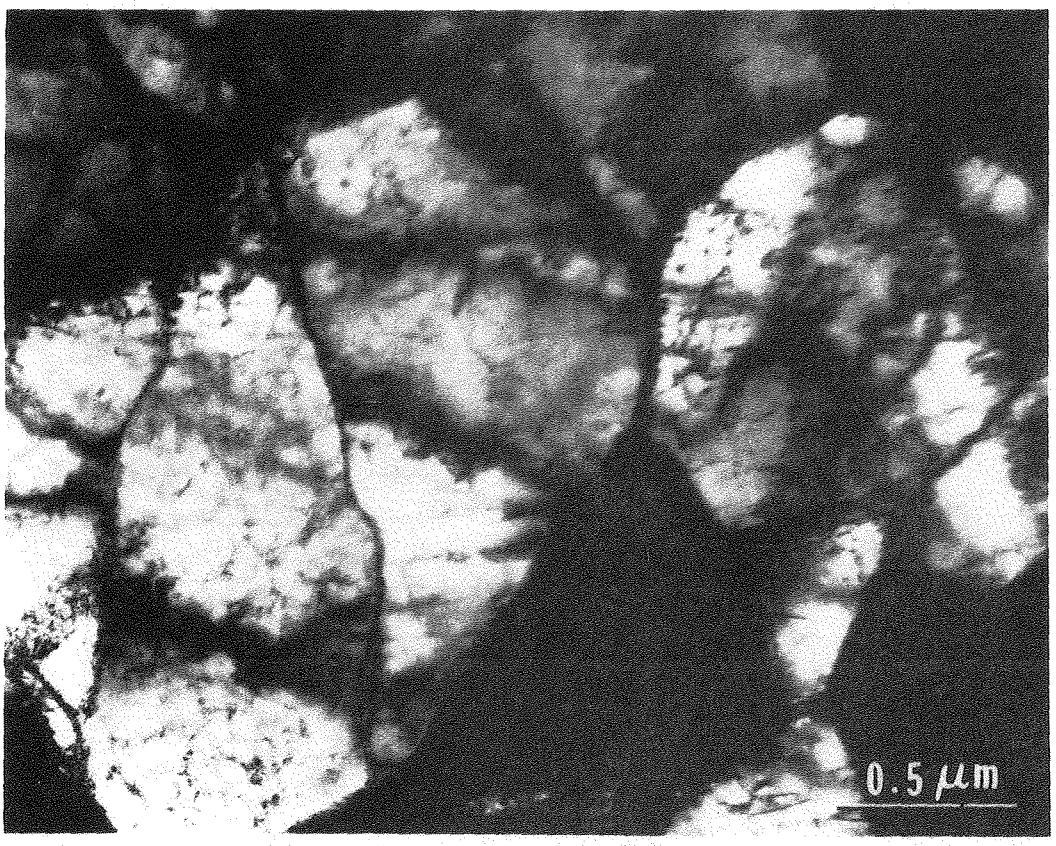

XBB 809-11367

Fig. 28

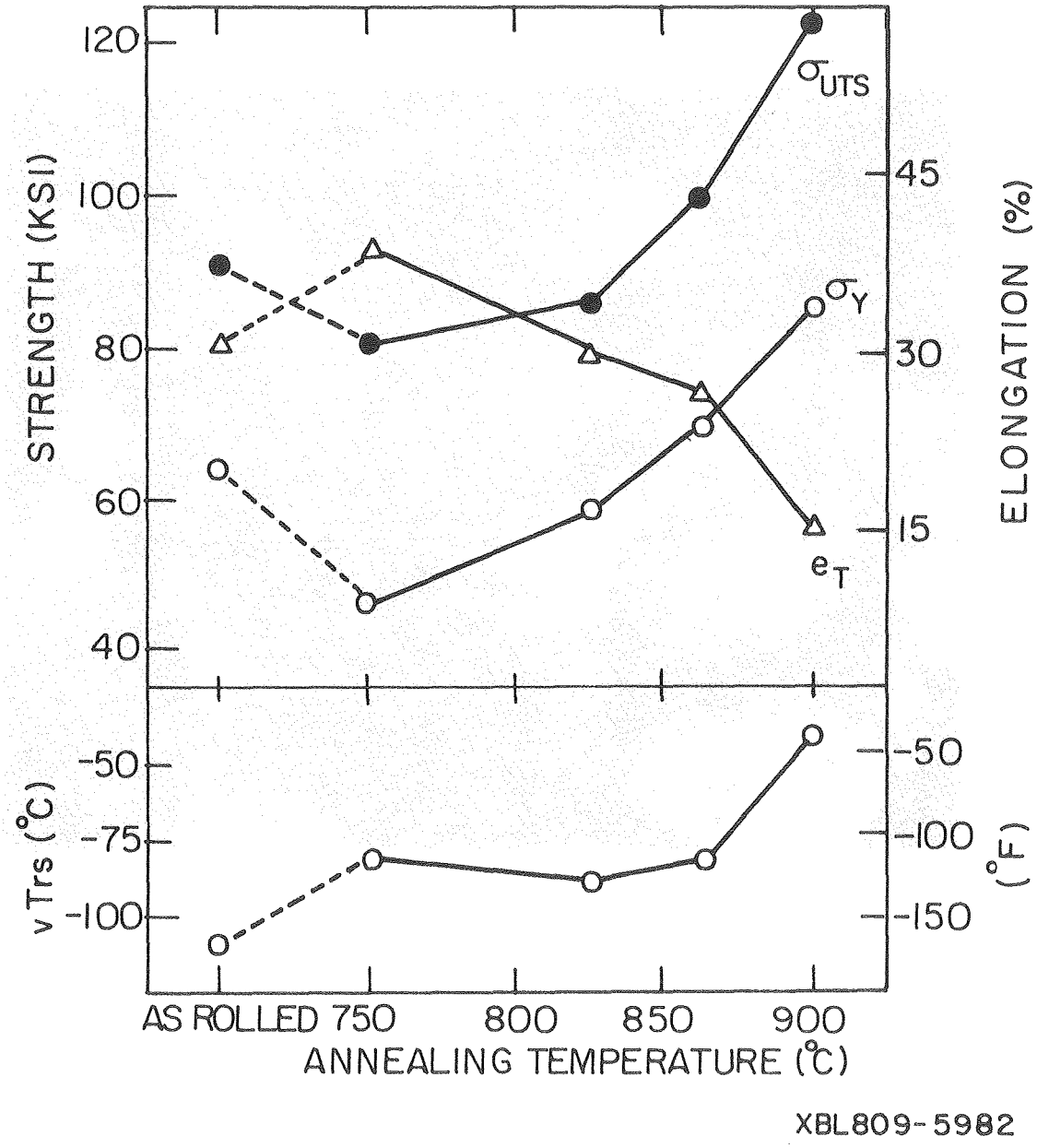
120
100
80
60
40
STRENGTH (KSI)
σ_{UTS}
σ_Y
e_T
45
30
15
ELONGATION (%)
-50
-75
-100
vTrs (°C)
-50
-100
-150
(°F)
AS ROLLED 750
800
850
900
ANNEALING TEMPERATURE (°C)
XBL809-5982

Fig. 29

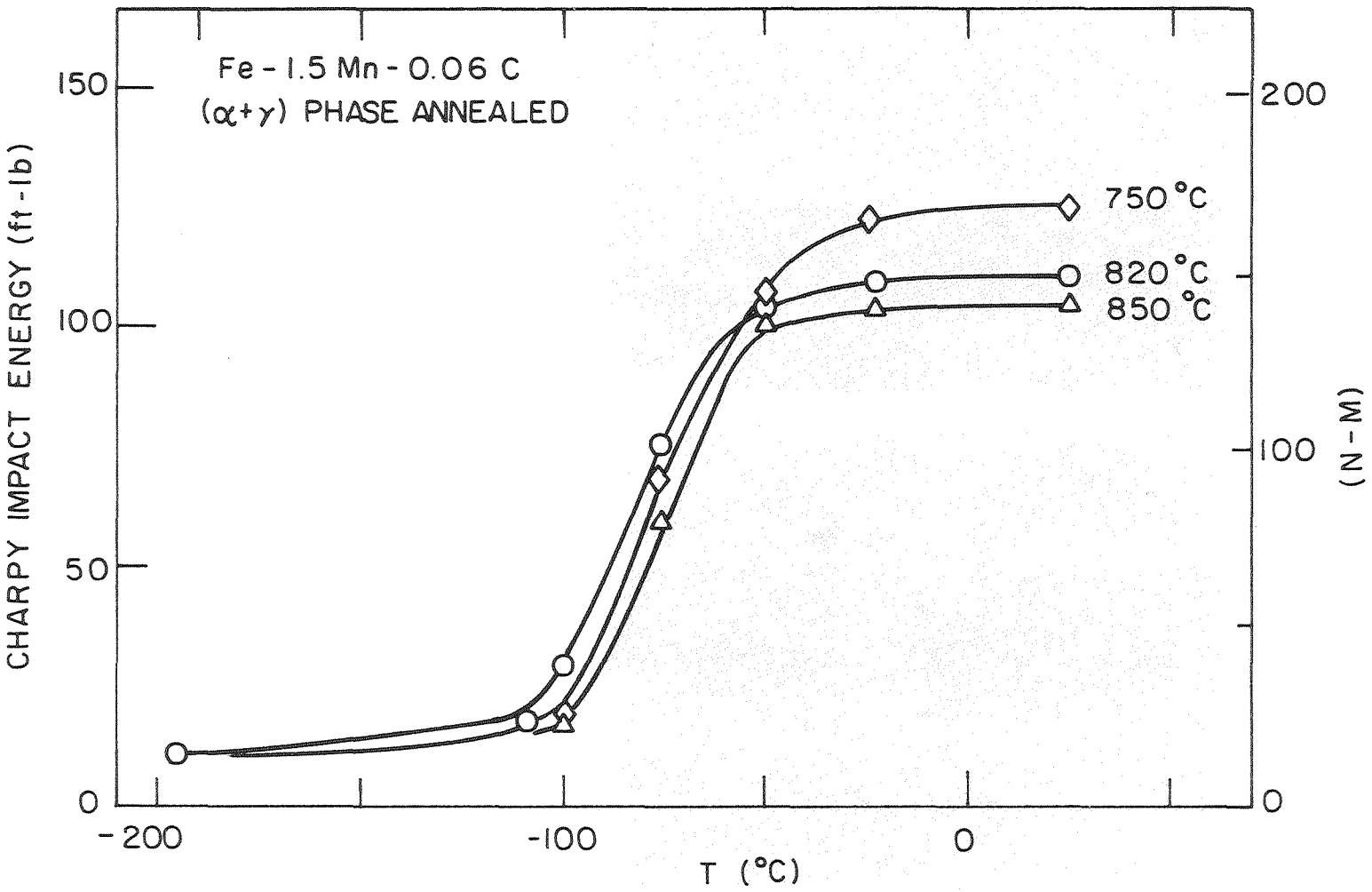

XBL 813-5382

Fig. 30

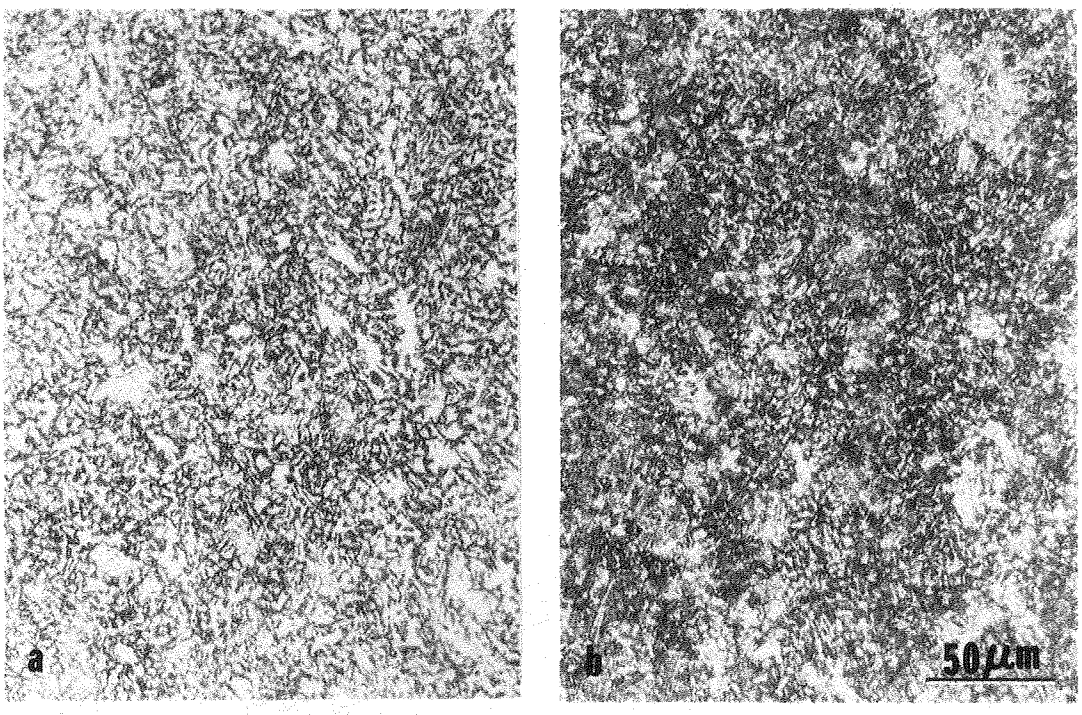

XBB 814-3211

Fig. 31

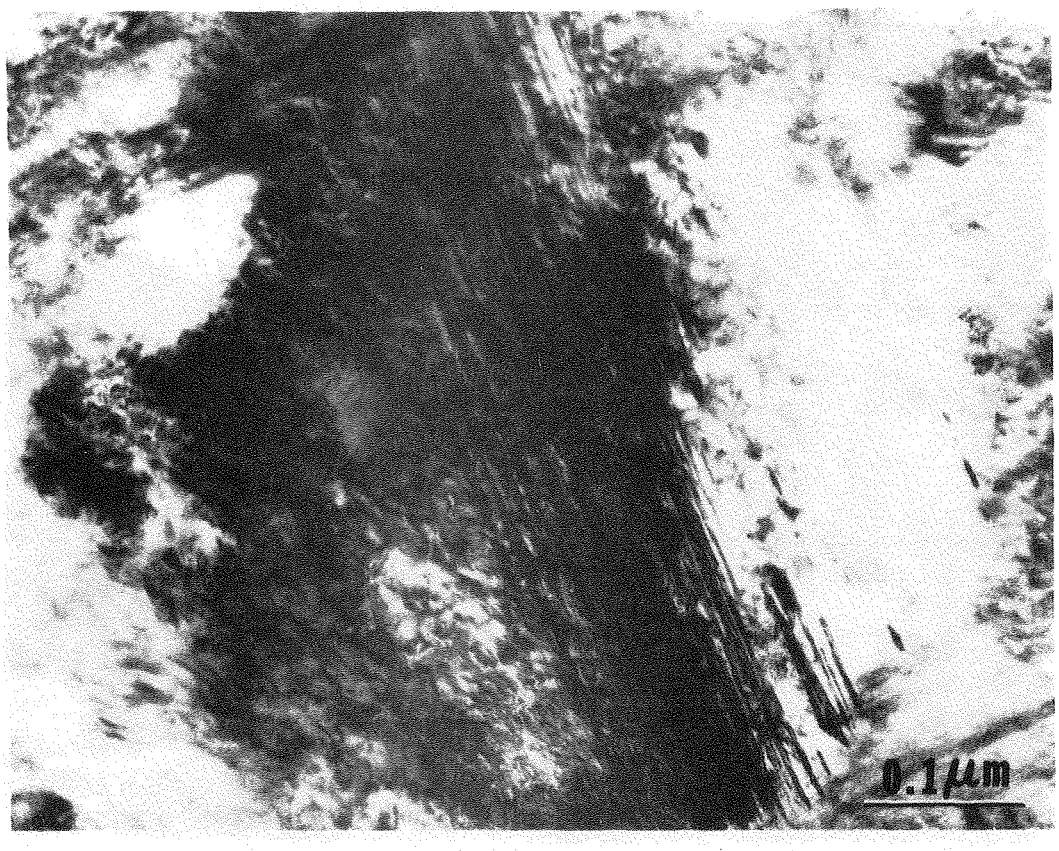

XBB 809-11369

Fig. 32

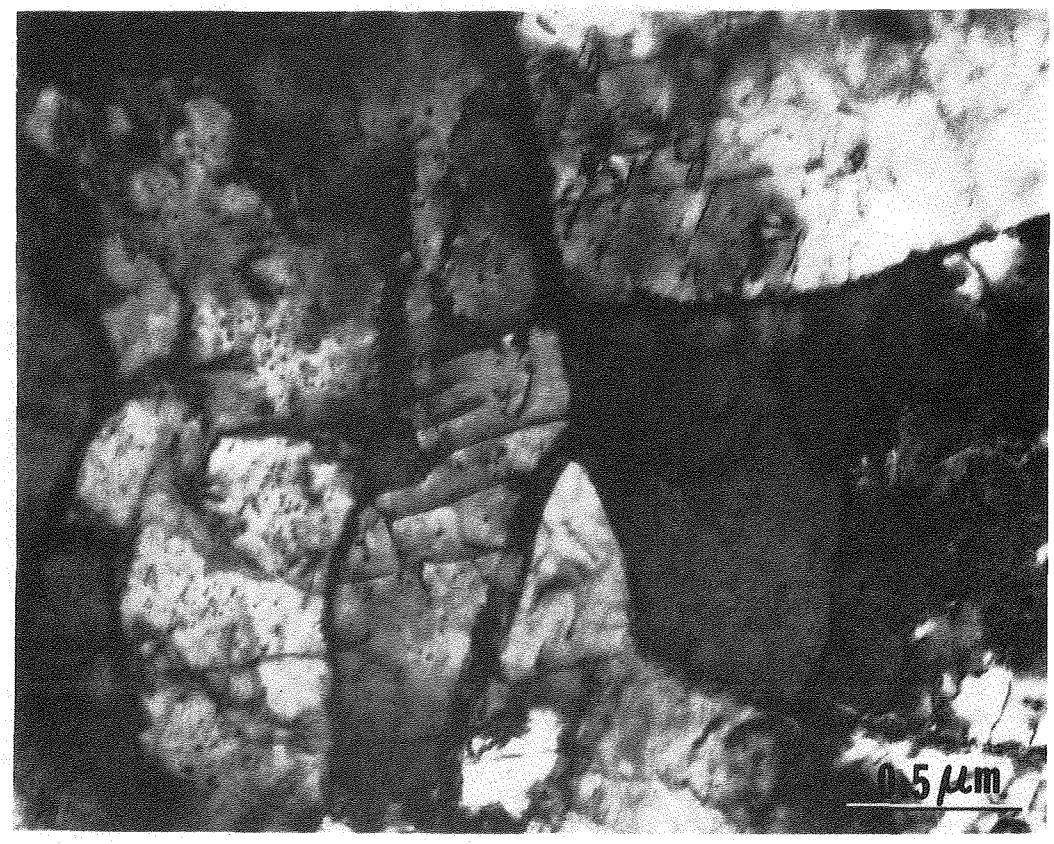

XBB 809-11374

Fig. 33

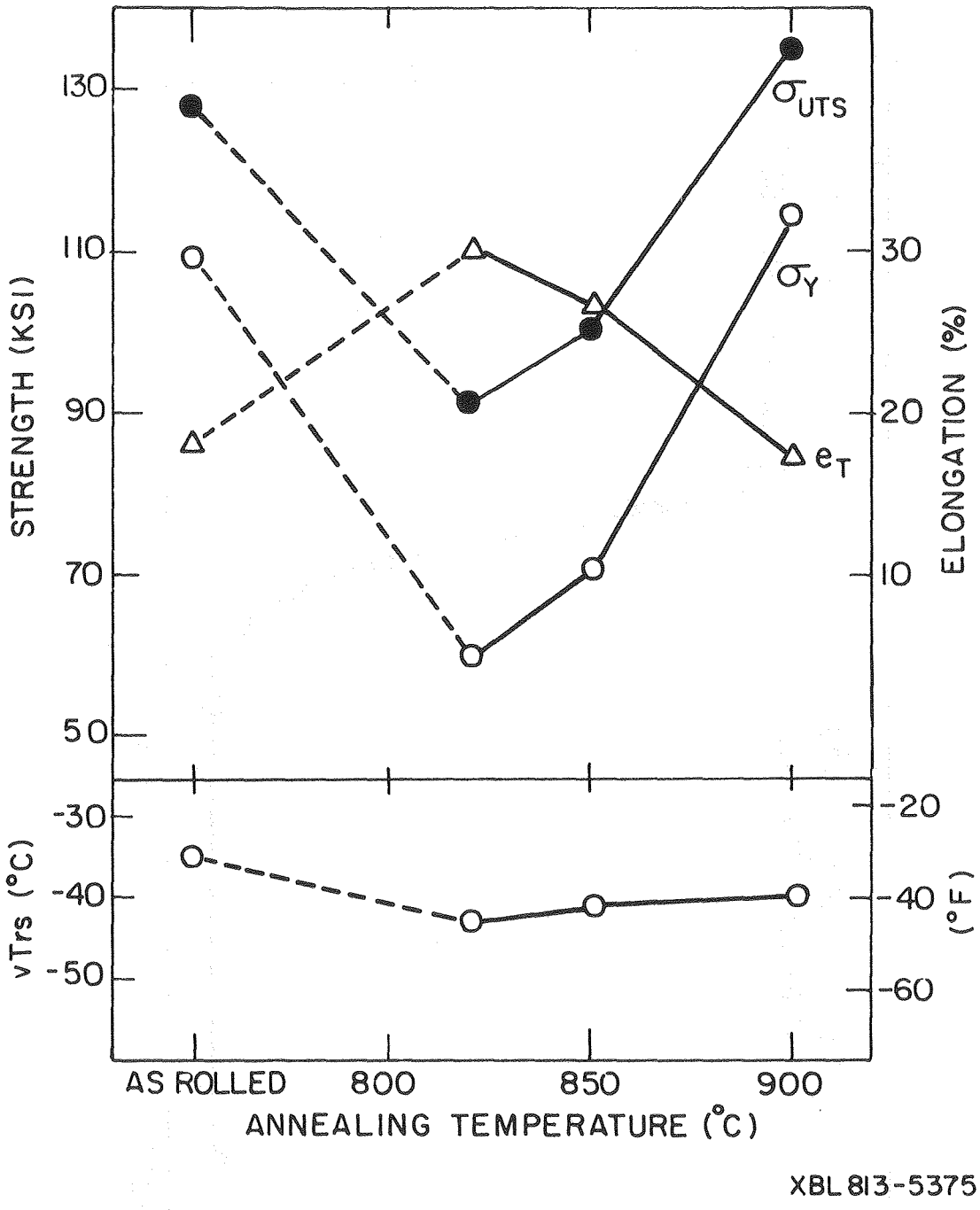
130
110
90
70
50
STRENGTH (KSI)
σ_{UTS}
σ_Y
e_T
30
20
10
ELONGATION (%)
-30
-40
-50
vTrs (°C)
-20
-40
-60
(°F)
AS ROLLED
800
850
900
ANNEALING TEMPERATURE (°C)
XBL 813-5375

Fig. 34

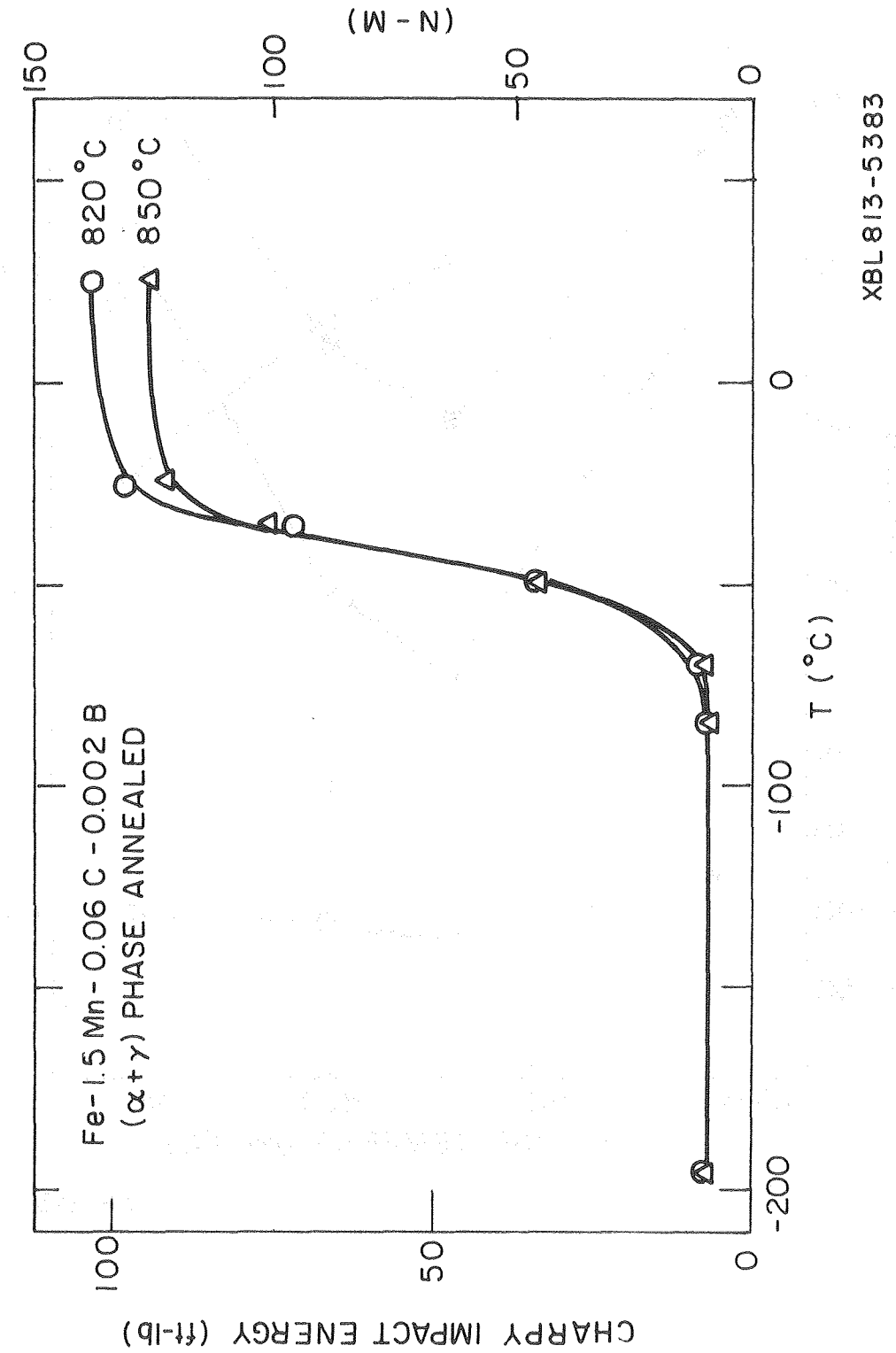
CHARPY IMPACT ENERGY (ft-lb)
100
50
0
-200
-100
0
T (°C)
150
100
50
0
(N - M)
Fe-1.5 Mn-0.06 C-0.002 B
(α+γ) PHASE ANNEALED
820 °C
850 °C
XBL 813-5383

Fig. 35

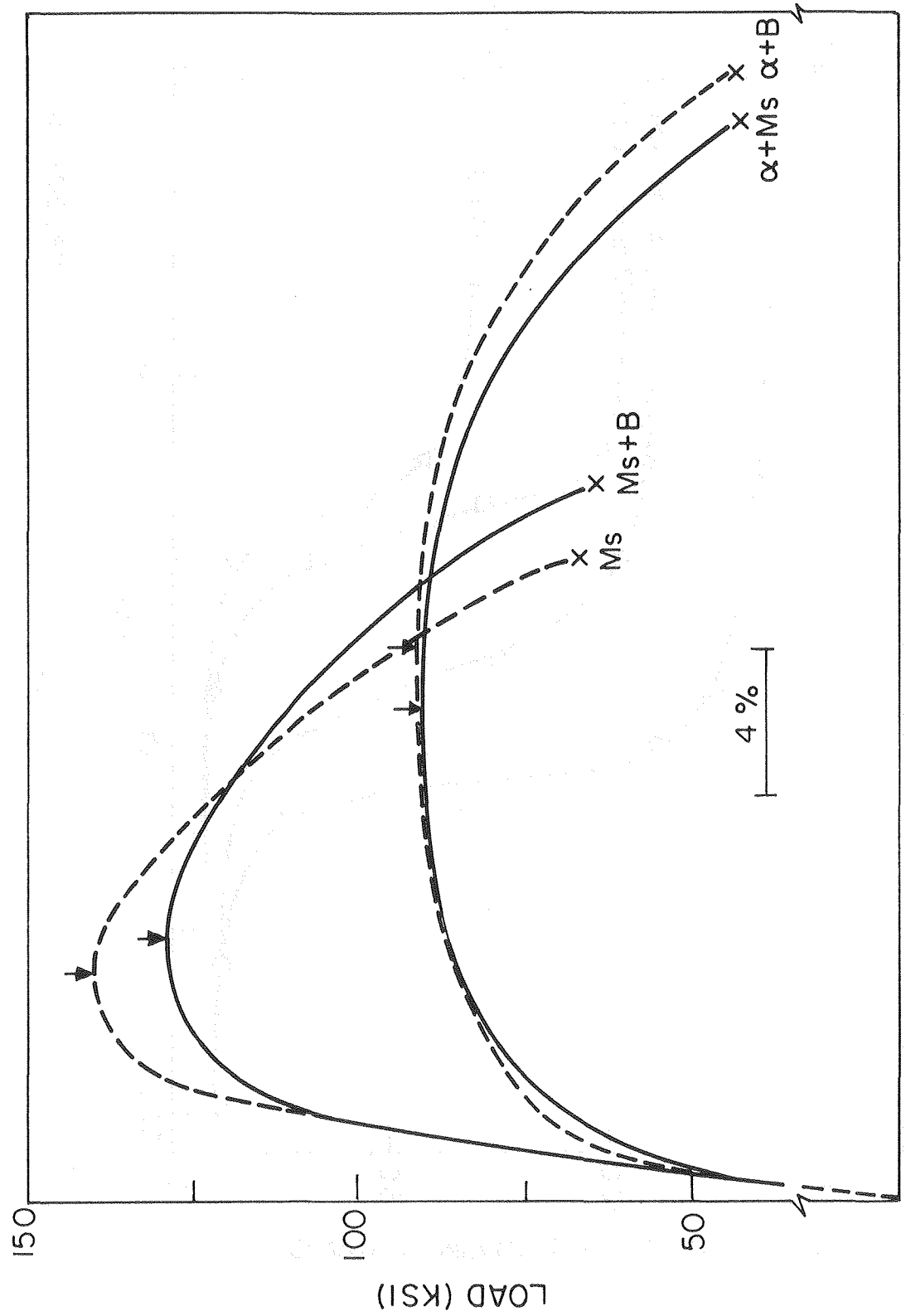

XBL 813-5379

Fig. 36

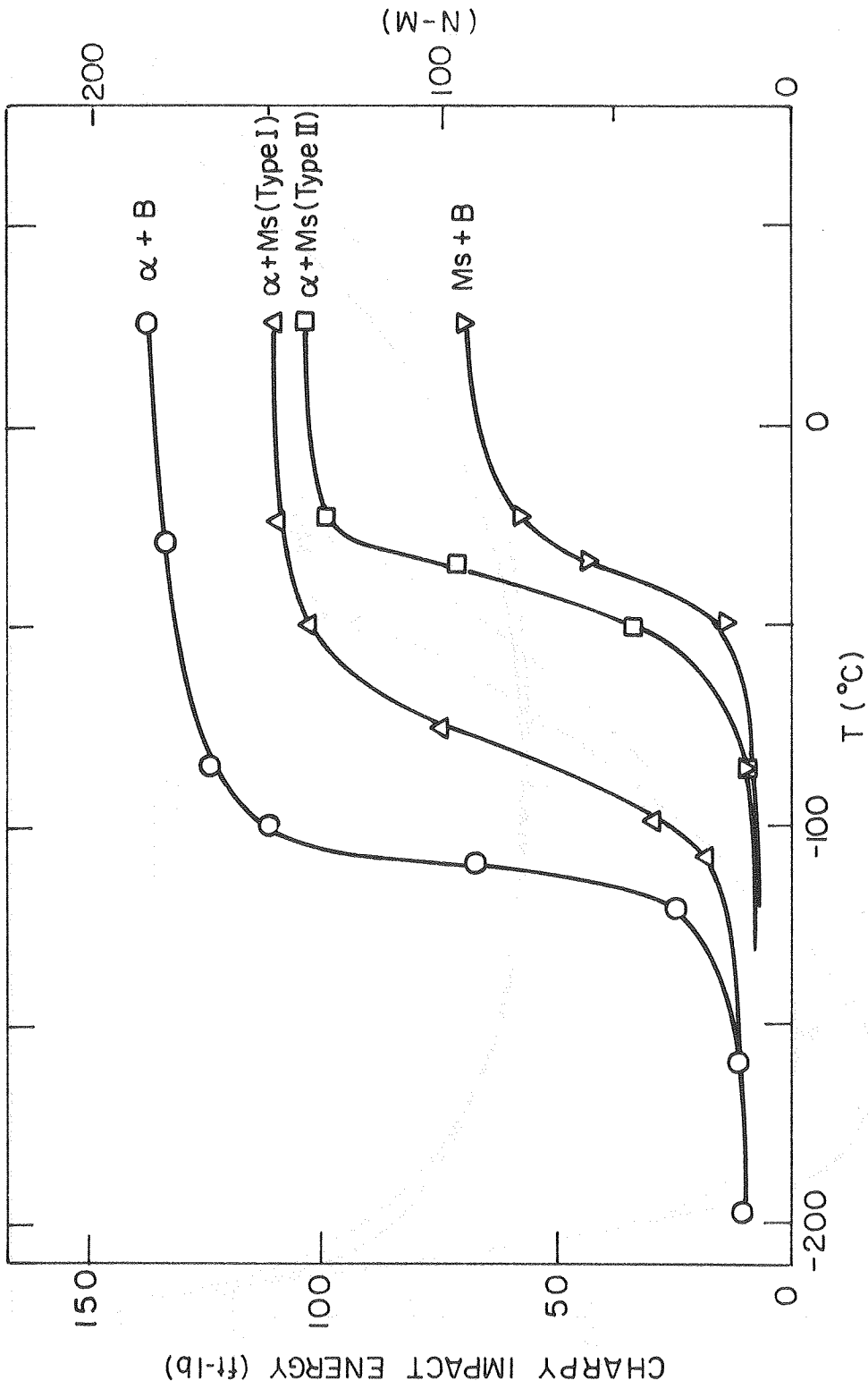
CHARPY IMPACT ENERGY (ft-lb)
150
100
50
0
-200
-100
0
T (°C)
200
100
0
(N-M)
α + B
α+Ms(Type I)
α+Ms(Type II)
Ms + B
XBL 813-5384

Fig. 37

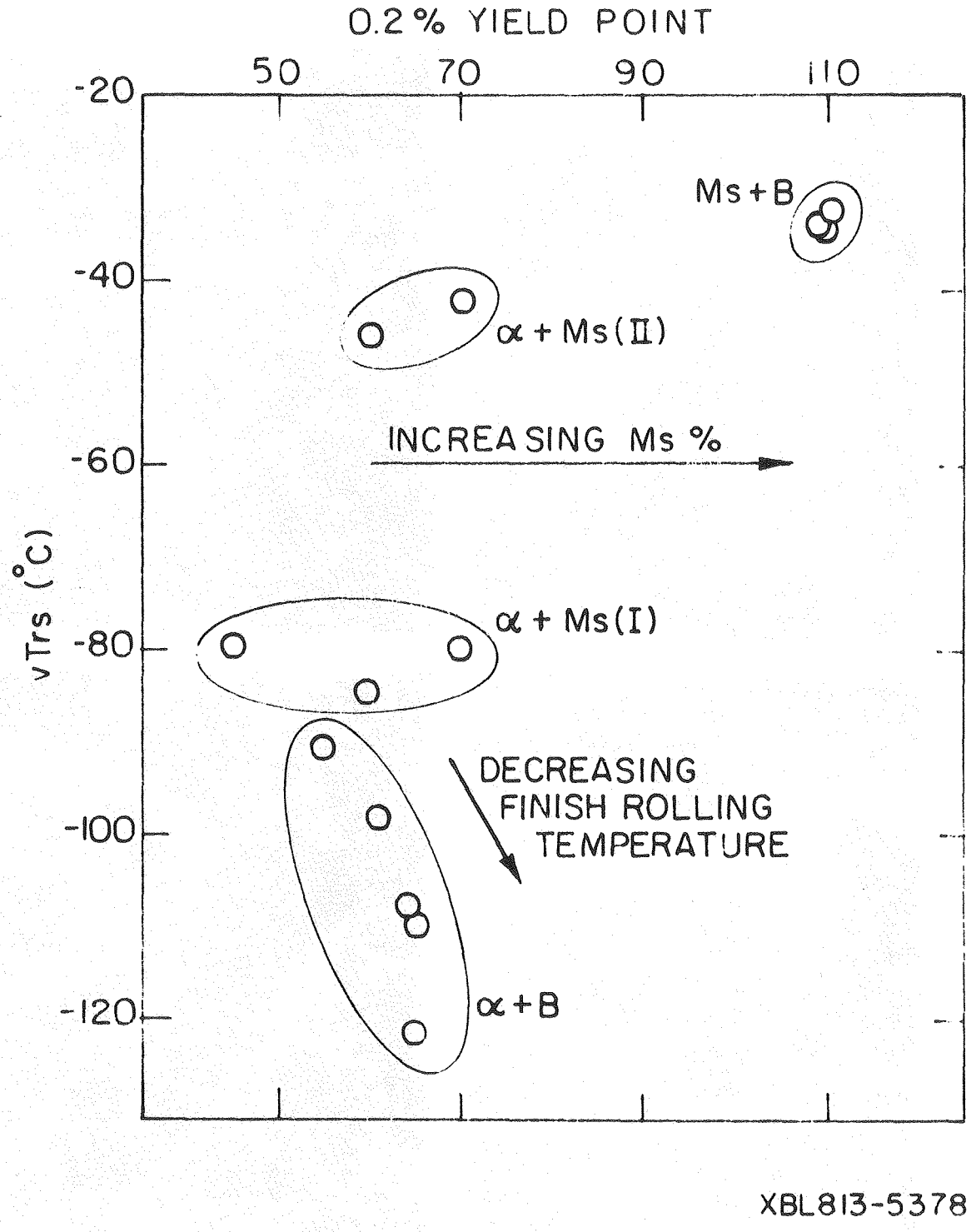
0.2% YIELD POINT
50
70
90
110
-20
-40
-60
-80
-100
-120
vTrs (°C)
Ms+B
α + Ms(II)
INCREASING Ms %
α + Ms(I)
DECREASING
FINISH ROLLING
TEMPERATURE
α+B
XBL813-5378

Fig. 38

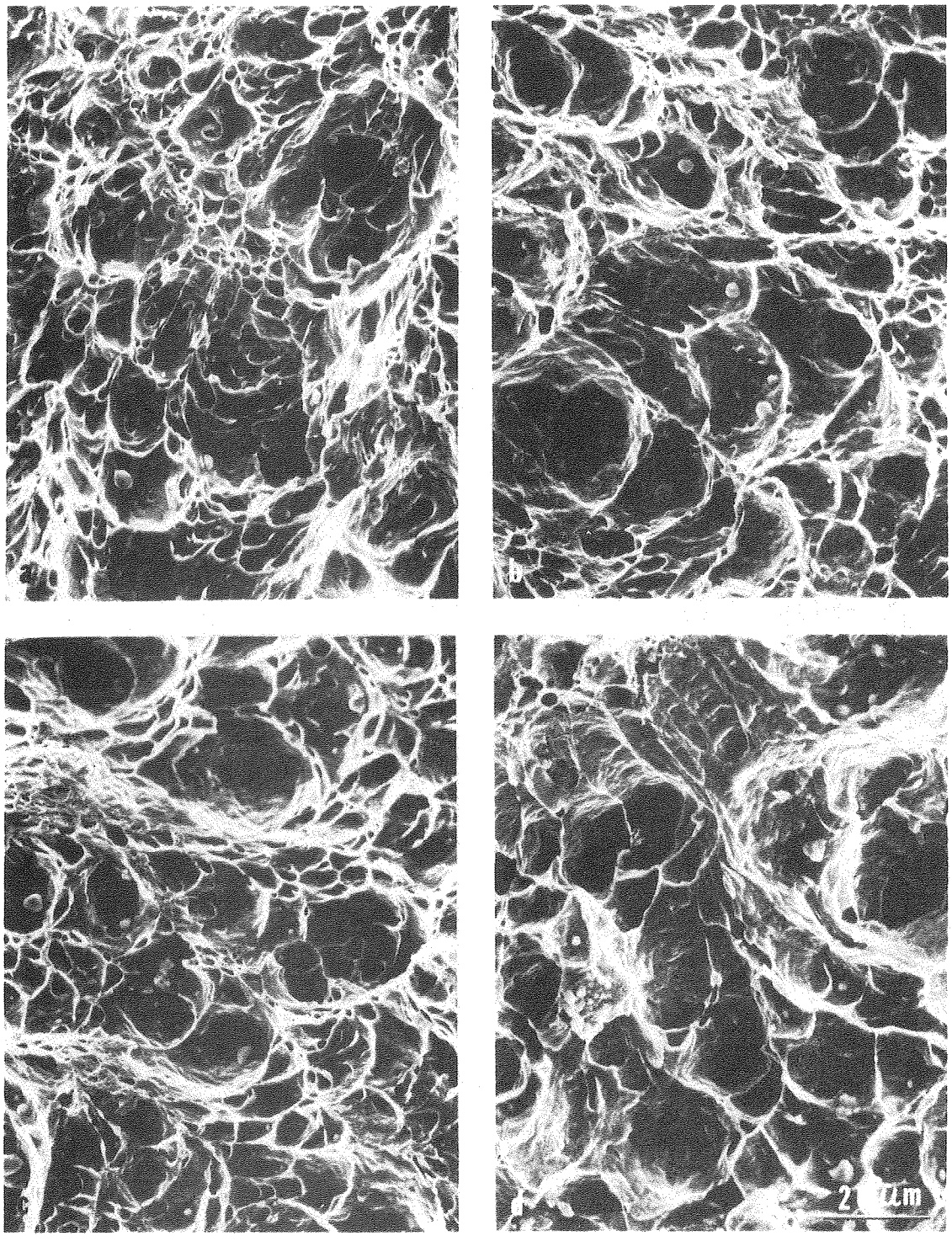

XBB 814-3202

Fig. 39

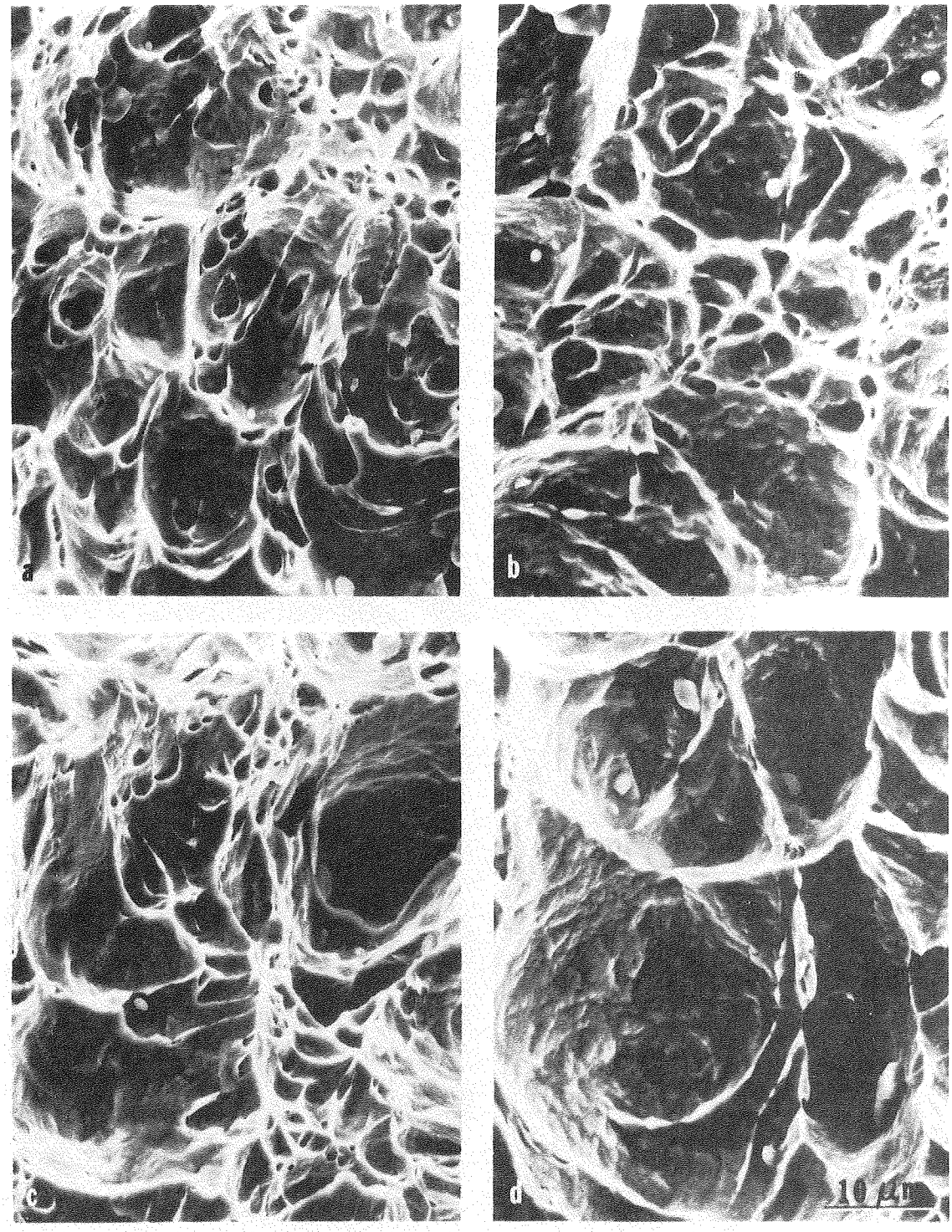

XBB 814-3201

Fig. 40

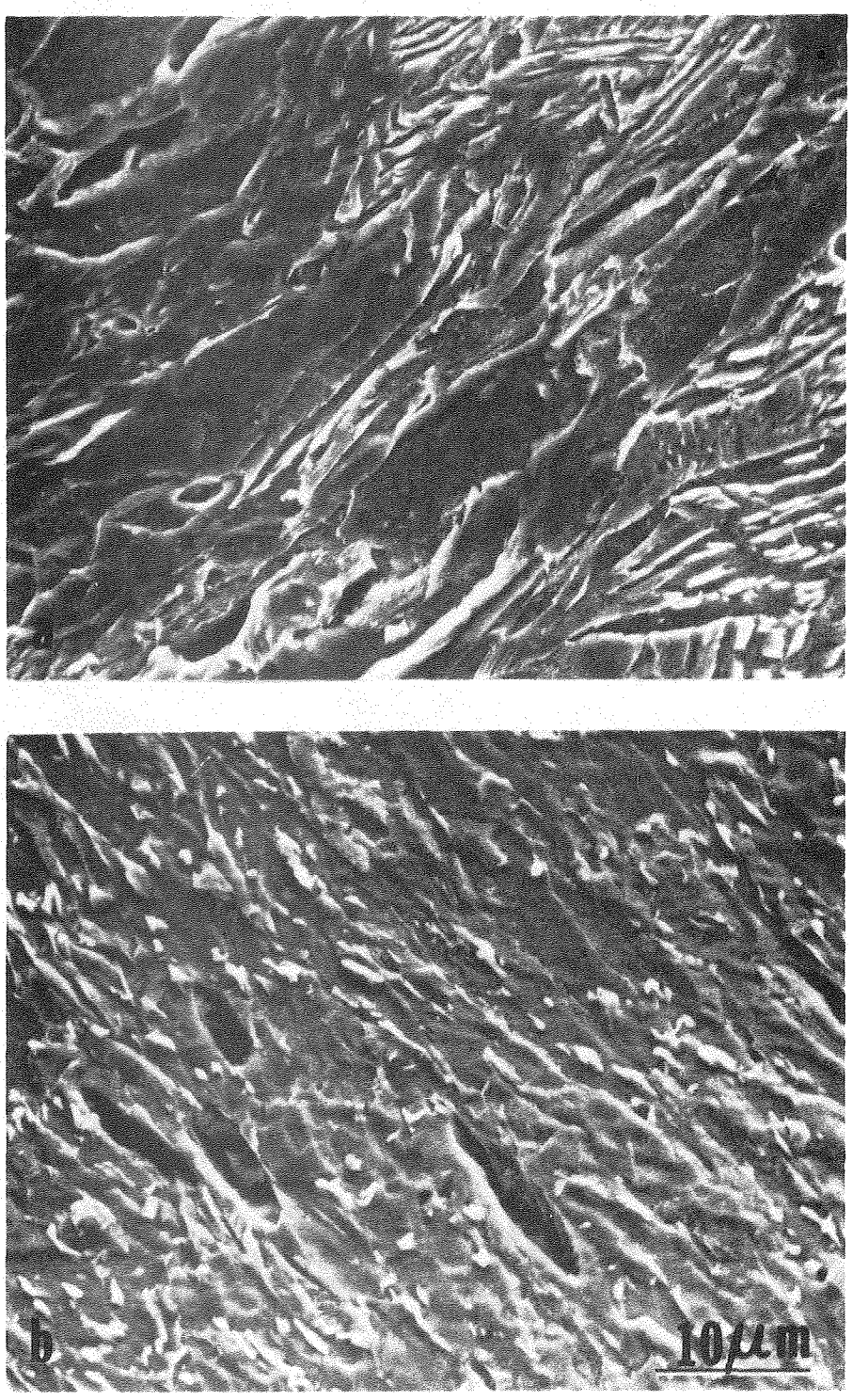

XBB 814-3210

Fig. 41

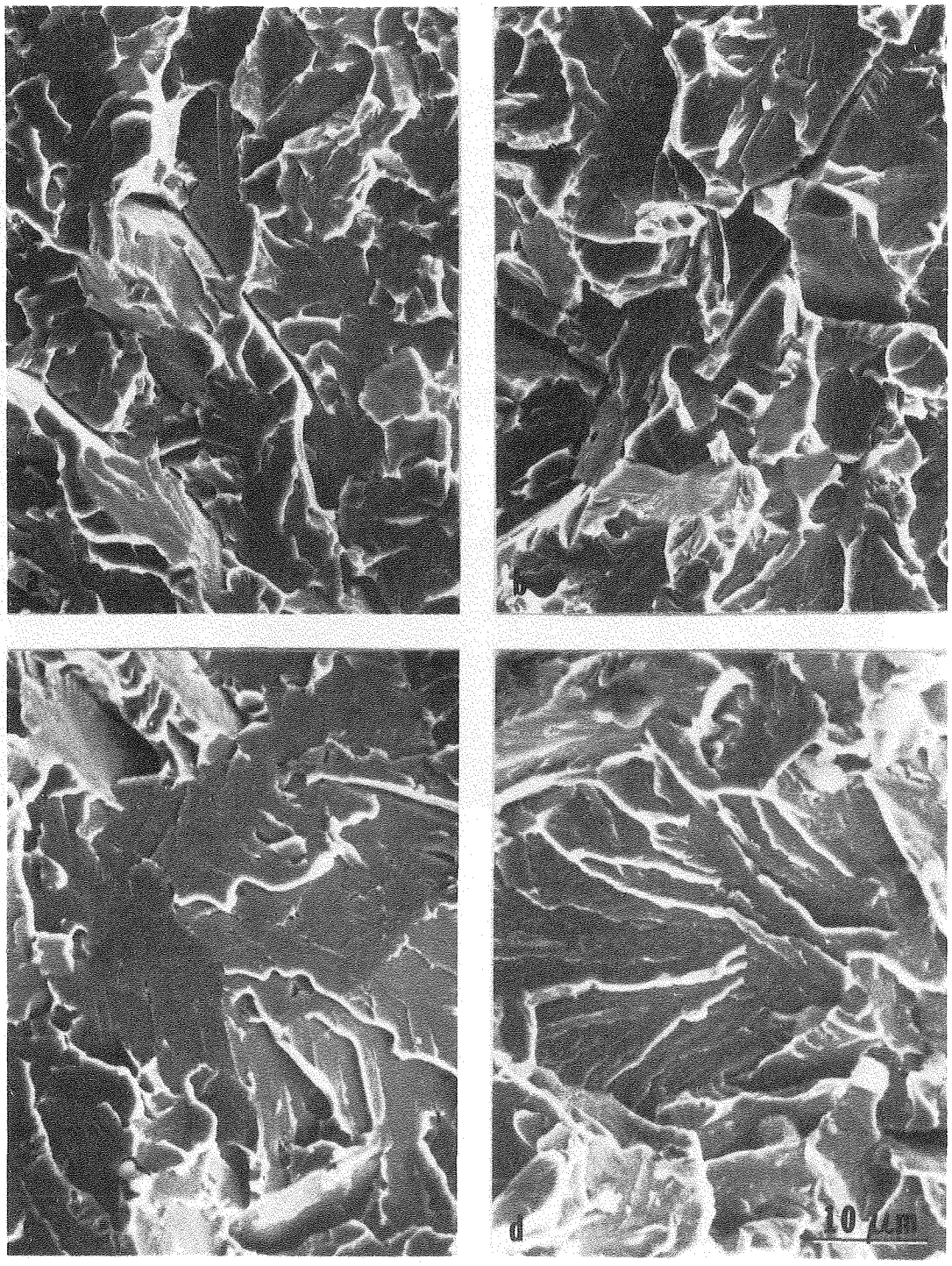

XBB 814-3200

Fig. 42

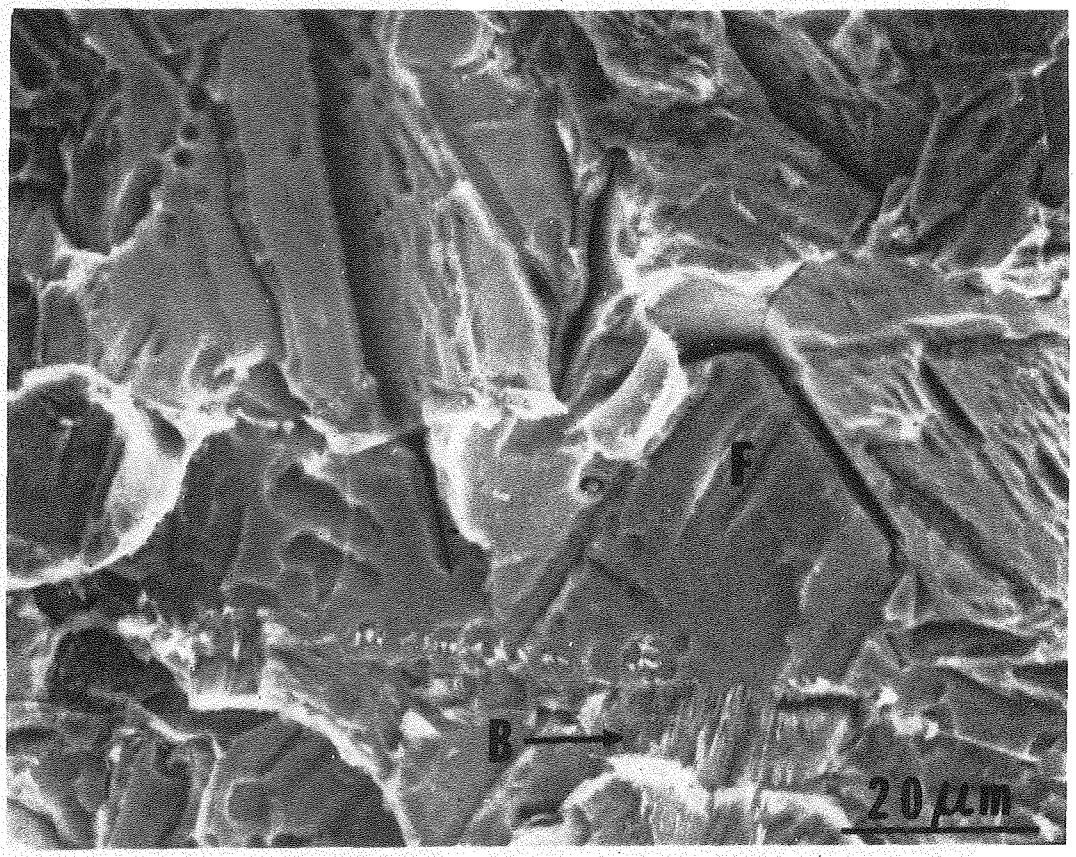

XBB 814-3215

Fig. 43

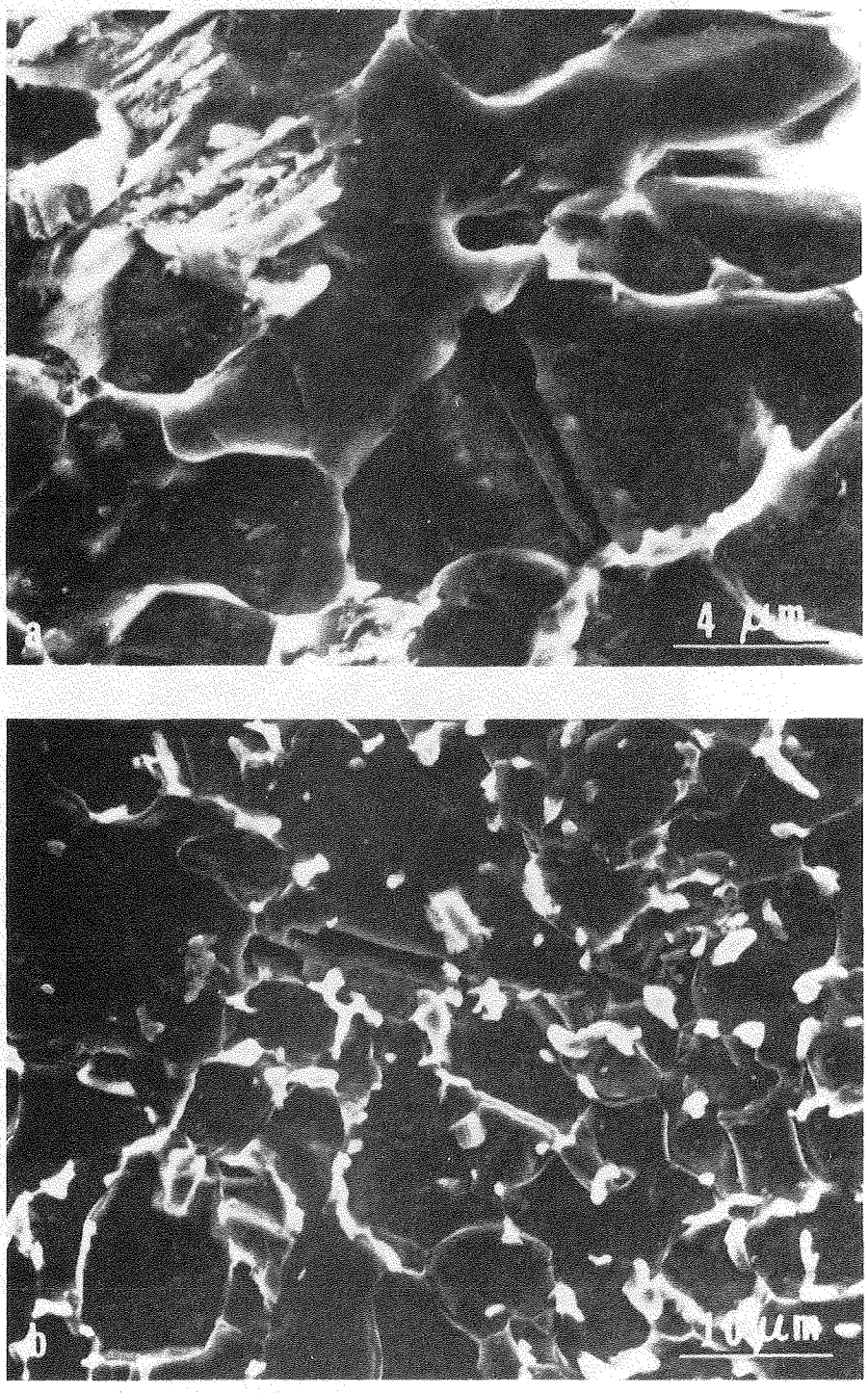

XBB 814-3207

Fig. 44(a,b)

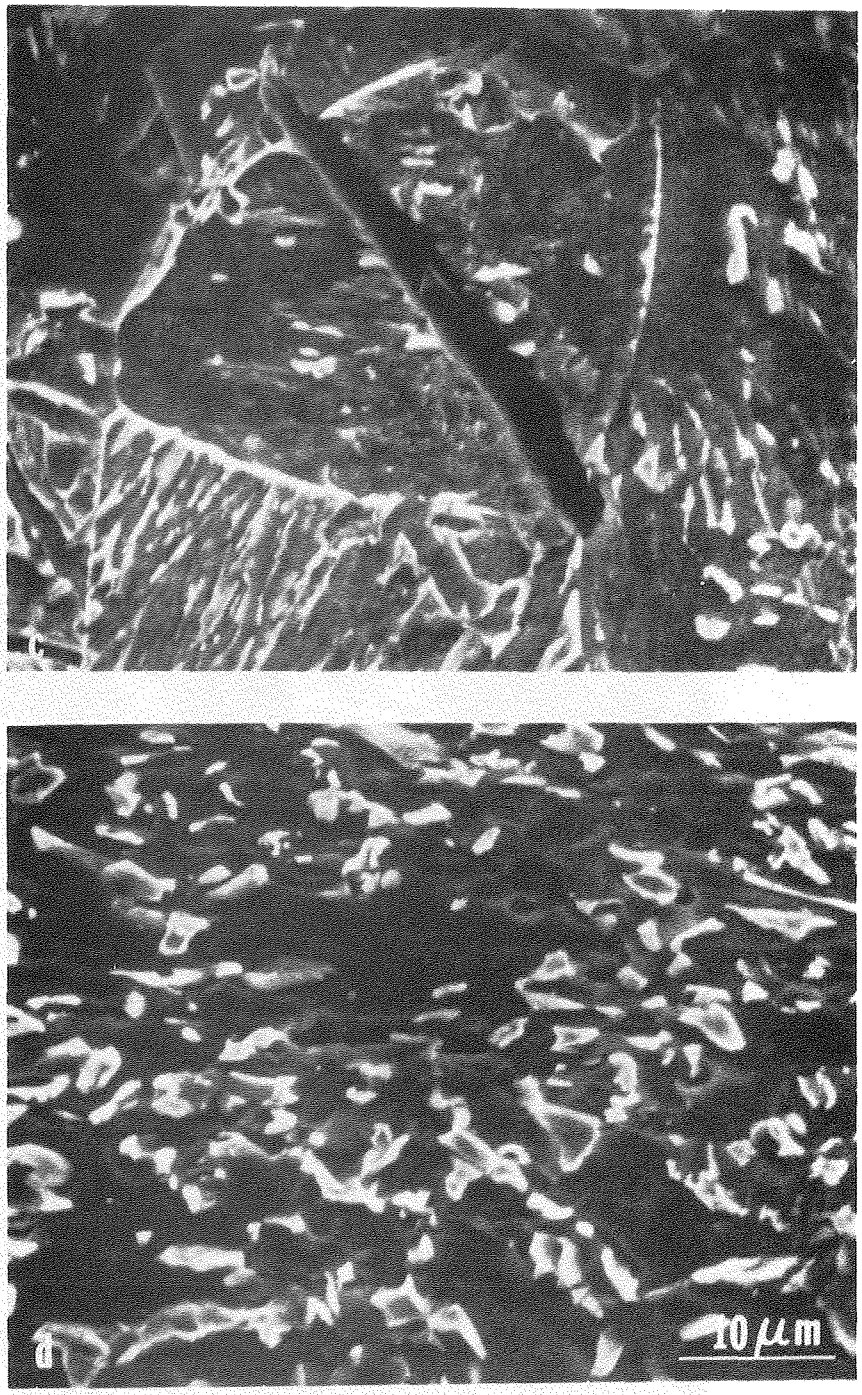

XBB 814-3214

Fig. 44(c,d)

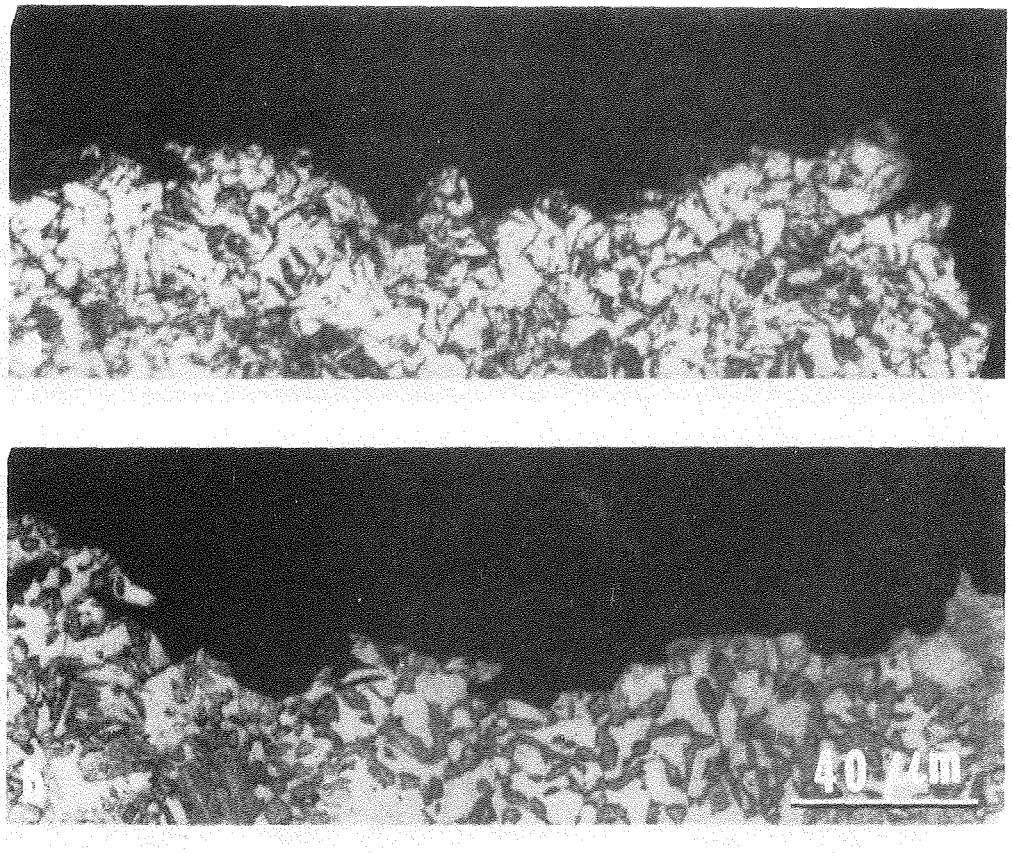

XBB 814-3209

Fig. 45(a,b)

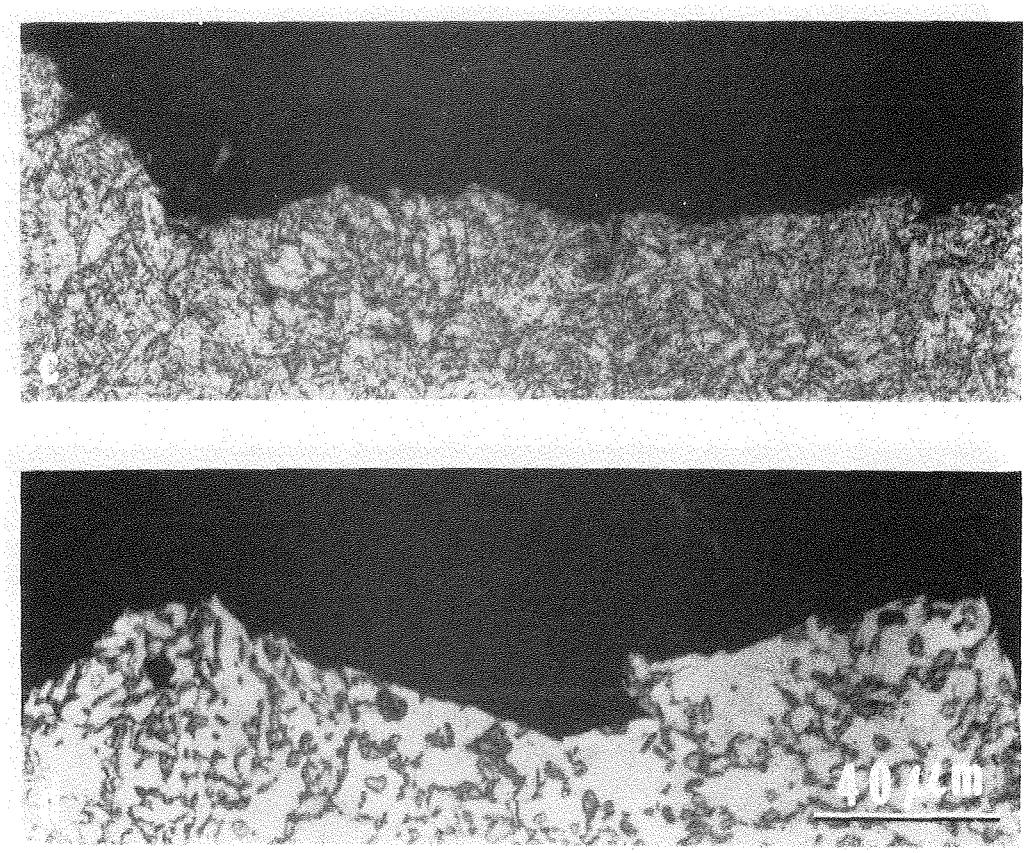

XBB 814-3208

Fig. 45(c,d)

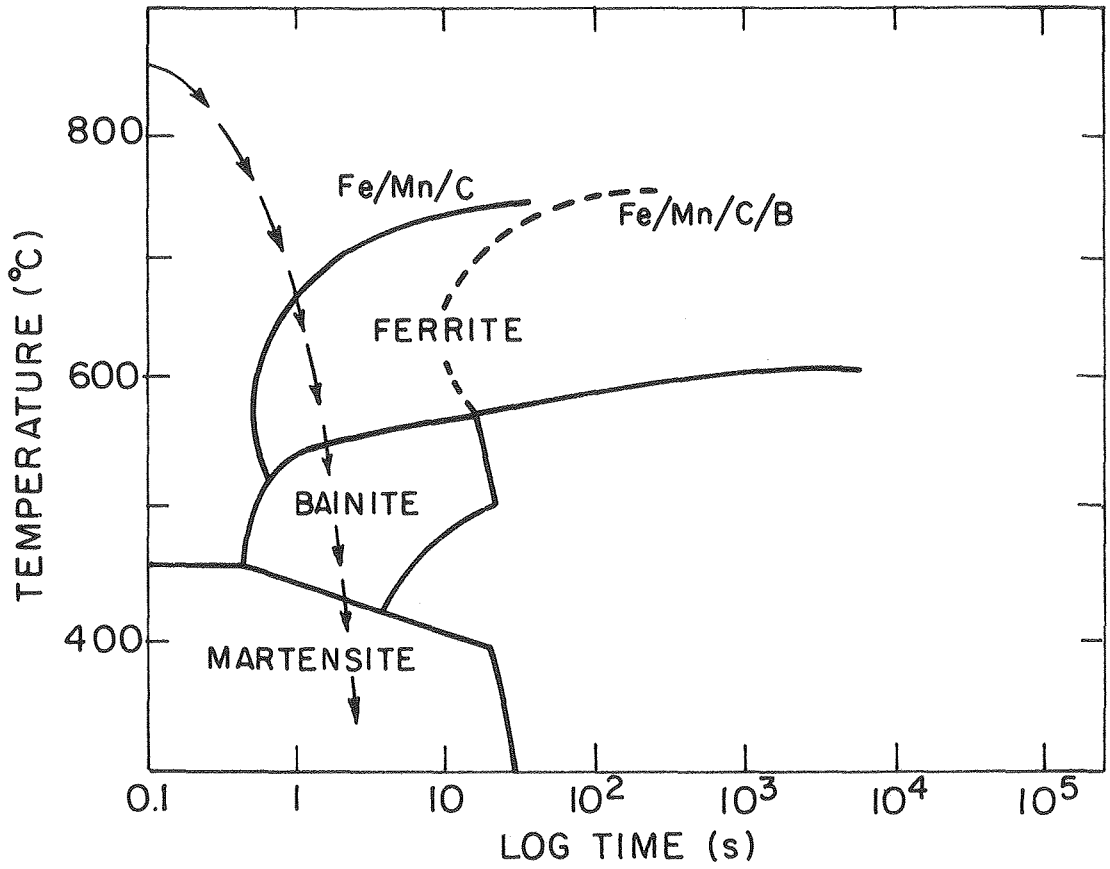
800
600
400
TEMPERATURE (°C)
Fe/Mn/C
Fe/Mn/C/B
FERRITE
BAINITE
MARTENSITE
0.1
1
10
10^2
10^3
10^4
10^5
LOG TIME (s)
XBL 813-5413

Fig. 46.